GLOBAL PHASE SEISMIC INTERFEROMETRY (GloPSI) AND BROADBAND SEISMIC
REFLECTION TECHNIQUES: AN INVESTIGATION OF THE SOUTHEASTERN SUTURE
OF THE APPALACHIAN MARGIN EXPERIMENT

by

ERIK ALBERTS

(Under the Direction of Robert Hawman)

ABSTRACT

Using Global Phase Seismic Interferometry (GloPSI) and methods originally formulated for active-source experiments, we develop a workflow for passive reflection profiling using PKIKP (range: 120°-180°) as a virtual seismic source. Instead of autocorrelation, we use estimates of the source-time function to deconvolve records for each earthquake prior to stacking. Array recordings for a given earthquake are windowed into overlapping subsets of traces and slant stacked to aid in the removal of PKP and PKiKP arrivals that interfere with PKIKP-generated reflections in the 140°-160° range. This greatly expands the inventory of events that can be used to construct a subsurface image. Coherency-filtered slant stacks for each spatial window then are migrated and the partial images stacked to construct a migrated section. Tests with single earthquakes recorded by the Southeastern Suture of the Appalachian Margin Experiment (SESAME) array show coherent reflections from the Moho (depths: 30-40 km) and sub crustal lithosphere (80-100 km).

INDEX WORDS: GloPSI, reflection profiling, seismic, SESAME, lithosphere

GLOBAL PHASE SEISMIC INTERFEROMETRY (GloPSI) AND BROADBAND SEISMIC REFLECTION TECHNIQUES: AN INVESTIGATION OF THE SOUTHEASTERN SUTURE OF THE APPALACHIAN MARGIN EXPERIMENT

by

ERIK ALBERTS

B.S., University of New Mexico, 2014

A Thesis Submitted to the Graduate Faculty of The University of Georgia in Partial Fulfillment of the Requirements for the Degree

MASTER OF SCIENCE

ATHENS, GEORGIA

2017

© 2017

Erik Alberts

All Rights Reserved

GLOBAL PHASE SEISMIC INTERFEROMETRY (GloPSI) AND BROADBAND SEISMIC REFLECTION TECHNIQUES: AN INVESTIGATION OF THE SOUTHEASTERN SUTURE OF THE APPALACHIAN MARGIN EXPERIMENT

by

ERIK ALBERTS

Major Professor: Robert Hawman

Committee: Doug Crowe

Christian Klimczak

Electronic Version Approved:

Suzanne Barbour Dean of the Graduate School The University of Georgia May 2017

ACKNOWLEDGEMENTS

I would like to thank Dr. Robert Hawman for his extensive work in developing the majority of the software packages used within this study. In addition, Dr. Hawman provided an un-calculable amount of guidance and help throughout my time at the University of Georgia. I would also like to recognize my committee members for taking the time to review this thesis, and offer advice. No student would be where they are without the conversations they share with their peers, thus, I would like to thank the University of Georgia Geology Department as a whole, for providing such a unique learning environment.

Additionally, this study (along with its related research) was funded by contributions from the Watts-Wheeler Fund, the Joseph W. Berg Fund, and NSF grants EAR-0844154 (R. Hawman), EAR-0884424 (K. M. Fischer, Brown University), and EAR-0844186 (L. S. Wagner, Carnegie Institution of Washington), for this, we are grateful.

Finally, I would like to thank the hundreds of un-named contributors who have worked over the past century to develop and implement the seismic techniques utilized within this study. Without their tireless work, this study would not have been possible.

TABLE OF CONTENTS

		Page
ACKNOV	VLEDGEMENTS	. iv
LIST OF	FIGURES	vii
СНАРТЕ	R	
1	INTRODUCTION AND LITERATURE REVIEW	1
2	GLOBAL PHASE SEISMIC INTERFEROMETRY (GloPSI) AND BROA	DBAND
	SEISMIC REFLECTION TECHNIQUES: AN INVESTIGATION OF THE	E
	SOUTHEASTERN SUTURE OF THE APPALACHIAN MARGIN	
	EXPERIMENT	.14
	ABSTRACT	.15
	INTRODUCTION	.16
	METHODS	.23
	RESULTS	.35
	DISCUSSION AND FUTURE WORK	.48
	CONCLUSIONS	.52
3	CONCLUSIONS	.89
REFERE	NCES	.91
APPEND	IX	
A	IN-HOUSE SOFTWARE	.95
R	EXAMPLE LINIX SHELL SCRIPTS	108

\sim	SUPPLEMENTARY MATERIAL	1 _	70	•
•		1 ' /	–	,
	JUEELINVIINI AK I WATIKIAL		, ,	1.

LIST OF FIGURES

	Page
Fig. 2.1: SESAME Array Map55	
Fig. 2.2: PKIKP / PKP Travel Time Curves	
Fig. 2.3: Schematic View of GloPSI	
Fig. 2.4: The Basis for Synthetic Modeling	
Fig. 2.5: Simple Synthetic Construction	
Fig. 2.6: Complex Synthetic Construction	
Fig. 2.7: Complex Synthetic Sub-Sectioning	
Fig. 2.8: Synthetic Slant Stacking and Coherency Filtering	
Fig. 2.9: Removal of Interfering Arrivals through Apparent Velocity Filtering63	
Fig. 2.10: Apparent Velocity Filtering	
Fig. 2.11: Synthetic Inverse Slant Stacking	
Fig. 2.12 a: Full Complex Synthetic	
Fig. 2.12 b: Full Recovered Complex Synthetic	
Fig. 2.13: 2-D Slant Stack Depth Migration of Filtered Synthetic Data68	
Fig. 2.14: Full Migrated Complex Synthetic	
Fig. 2.15: Estimated Source Time Functions	
Fig. 2.16 a: Line-D	
Fig. 2.16 b: Signal Deconvolved Line-D	
Fig. 2.16 c: Line F	

Fig. 2.16 d: Signal Deconvolved Line-E	74
Fig. 2.16 e: Line-W	75
Fig. 2.16 f: Signal Deconvolved Line-W	76
Fig. 2.17 a: Sub-Sectioned SESAME Line-W	77
Fig. 2.17 b: Sub-Sectioned SESAME Line-E.	78
Fig. 2.18 a: Selecting an Appropriate Slant Stacking Ray Parameter Range	79
Fig. 2.18 b: Slant Stacking and Coherency Filtering SESAME Line-W	80
Fig. 2.18 c: Slant Stacking and Coherency Filtering SESAME Line-E	81
Fig. 2.19 a: Apparent Velocity Filtering SESAME Line-W	82
Fig. 2.19 b: Apparent Velocity Filtering SESAME Line-E	83
Fig. 2.20: Recovered Time Sections	84
Fig. 2.21 a: 2-D Slant Stack Depth Migration of SESAME Line-W	85
Fig. 2.21 b: 2-D Slant Stack Depth Migration of SESAME Line-E	86
Fig. 2.21 c: SESAME Line-W Migrated	87
Fig. 2.21 d: SESAME Line-E Migrated	88

CHAPTER 1

INTRODUCTION AND LITERATURE REVIEW

This thesis is authored as a manuscript for submission to the Geophysical Research Letters (GRL), and thus, appears and is best read as a single chapter. The second chapter contains abstract, introduction, methods, results, discussion and future work, and conclusions. In chapter three, the conclusions of this thesis are summarized. Using the global seismic phase PKIKP (PKP_{df}) as a virtual seismic source to generate p-wave reflections to image the lithosphere, this study aims to retool active-source reflection seismology techniques for use within a passive-source experiment, and to create a useable and robust workflow / set of protocols for passive-source reflection profiling based in part on the relatively new global seismic technique known as Global Phase Seismic Interferometry (GloPSI) (Yang, et al. 2012; Ruigrok and Wapenaar 2012). The new protocols are applied to noisy earthquake waveforms recorded with broadband seismometers of the Southeastern Suture of the Appalachian Margin Experiment (SESAME) array. To this end, we adapt the techniques of brute stacking, static cross-correlation, signal deconvolution, apparent velocity filtering (through slant stacking), coherency filtering, band-pass filtering, and 2-D slant stack depth migration for use within an adapted GloPSI workflow.

Previous studies employing GloPSI have used many of these same techniques, demonstrating the effectiveness and adaptability of the GloPSI method. For example, Yang, et al. (2012) utilized a variation of the GloPSI method, taking advantage of the teleseismic wave phase PpPdp to image sedimentary basin structure of the Bighorn Mountains, north-central

Wyoming, USA. Ruigrok and Wapenaar (2012) used global seismic phases to image the subsurface structure of the Himalaya Mountains, Tibet. Yang et al. (2012) employed iterative deconvolution to remove source effects from recorded seismic waveforms, used a host of seismic filtering techniques (including bandpass filtering to enhance signal quality), and utilized a standard depth conversion technique to better interpret data. Ruigrok and Wapenaar (2012) used autocorrelation to identify reflections and performed a Kirchhoff time-migration (in addition to a standard depth conversion) to better interpret their data.

In this study we utilize many of the same techniques but combine them into a new workflow that differs from previous studies in several key ways. First, we attempt signal deconvolution as a means for removing source effects from the recorded seismic waveforms. This improves resolution of structure within the upper crust which is commonly obscured using autocorrelation as in previous studies.

Second, we greatly expanded the inventory of usable source events by employing apparent velocity filtering to remove interfering seismic arrivals. Previous studies have excluded recordings over distance ranges that include interfering seismic arrivals. This study offers the first treatment designed to utilize these recordings, thus greatly increasing the usability of the GloPSI method with respect to SESAME data, and to data sets worldwide. Additionally, apparent velocity filtering techniques may offer the opportunity to remove p-wave multiples from within the data, much like predictive deconvolution techniques employed by Yang, et al. (2012), especially when they are paired with predictive deconvolution (although this has not been attempted for this study).

Third, we implement a simple 2-D slant stack migration technique to better interpret reflectivity data. Previous studies utilized either a standard depth migration, as in the case of

Ruigrok and Wapenaar (2012), or a Kirchhoff time-migration, as in the case of Yang, et al. (2012). Fundamentally, this migration technique, an adaptation of an algorithm developed for wide-angle reflection data (Hawman, 2008) differs from those previously instituted, in that it does not require dense, evenly spaced traces, thus greatly simplifying the migration process, and eliminating the need to perform data projections and interpolations.

Finally, we include extensive semblance-based coherency filtering as a method for suppressing noise prior to migration. Performing this filtering while in the T-p (travel time –ray parameter) domain also allows for the removal of coherent noise such as interfering PKP arrivals. This treatment, in part, allows for the generation of meaningful seismic reflection profiles, even utilizing only a single earthquake source event.

Through this manuscript, we employ an array of synthetic and real world examples, outlining each process within our GloPSI workflow (as we have adapted and applied it). Geologic revelations, although not the focus of this study, are discussed as part of the real-world examples contained, thus, constraints are placed on the depths of the interpreted lithosphere / asthenosphere boundary, and Moho.

Conventional Active-Source Methods for Seismic Reflection Profiling

Traditionally, seismic reflection-profiles have been produced using active source experiments in which explosives, air cannons, or vibroseis have been employed to generate compressional seismic energy (Shearer, 2009). These experiments have been widely used by the petroleum industry as a method for hydrocarbon exploration over the past decades, and have been used with great success academically by many research groups, including (of interest to this study) the Consortium for Continental Reflection Profiling (COCORP), a group that has performed experiments in the southeastern United States, among other localities (Cook, et al.,

1979), and the Appalachian ultra-Deep Core Hole (ADCOH) experiment, a group that performed active source-profiling experiments to develop plans for the placement of a never drilled ultra-deep coring well. Active source seismic reflection profiling offers the investigator a well-constrained reflectivity image of the earths subsurface, in many cases providing an investigator with meter scale resolution of geologic features at depths of several kilometers (Shearer, 2009).

However, when considering academic investigations of deeper earth structure (for this study as deep as the lithosphere / asthenosphere boundary) active source techniques are limited. These limitations are three-fold. First, active source seismic surveys are expensive. Second, active source surveys are logistically complicated and man-power intensive. Finally, active source surveys are limited in their ability to resolve deep earth structure (Shearer, 2009).

Putting aside the logistical and financial limitations of active source seismic experiments, it is important to understand the scientific limitations of such surveys. Most seismic reflection profiles are generated using compressional seismic waves, logging two-way travel times of such waves as they travel from a seismic source to a set of seismic receivers (Shearer, 2009), the paths of these waves are described by seismic rays whose trajectories are governed by Snell's law (Robinson, 1984).

 $r \ u \ sin \theta = p_{sph}$ Where r = radius from the center of the earth to an interface, u = slowness, $\theta = incidence$ angle, and $p_{sph} = spherical$ ray parameter.

In the case of seismic reflection profiling, compressional waves decay (lose energy in terms of amplitude, and lose frequency content) along their respective ray paths from seismic source to seismic receiver for four main reasons: spherical spreading, intrinsic attenuation, scattering attenuation, and transmitted and converted energy loss (Shearer, 2009).

Spherical spreading: as compressional wave fronts move away from their respective source locations they expand. If it is assumed (incorrectly because of intrinsic attenuation, scattering attenuation, and transmitted and converted energy loss) the total amount of seismic energy contained along compressional wave fronts is constant, then as compressional wave fronts expand, the energy density of the seismic wave fronts decreases, thus decaying seismic amplitudes along any given ray path (Shearer, 2009). Changes in energy density due to spherical spreading are inversely proportional to the rate at which a spherical wave front expands, and can be calculated using the following equation (Shearer, 2009).

 $E(\Delta) = \frac{p_{sph}}{4 \pi u_1^2 r_1^2 r_2^2 sin\Delta cos\theta_1 cos\theta_2} \left| \frac{d p_{sph}}{d \Delta} \right| E_s$ Where $E(\Delta) =$ energy density of a radiated spherical wave front, $p_{sph} =$ spherical ray parameter, $u_1 =$ slowness, $r_1 =$ the initial radius of the spherical wave front, $r_2 =$ the new radius of the spherical wave front, $\Delta =$ source-receiver range in radians, $\theta_1 =$ is the source incidence angle, $\theta_2 =$ the receiver incidence angle, and $E_s =$ initial energy radiated from the source.

Therefore, the larger the sum of energy contained along the compressional wave front initially, the smaller the relative impact of spherical spreading. One of active source seismology's limitations is generating an energetic enough source to combat the effects of spherical spreading. This can be difficult when considering large target depths for reflection profiling, as source energies quickly become prohibitive.

Intrinsic attenuation: as seismic waves are transmitted through the earth there is an exchange between potential and kinetic energy, this exchange is the mechanism that allows elastic wave energy to be communicated from one location to another (i.e. from seismic source to seismic receiver) (Shearer, 2009). In the case of an ideal earth, this exchange would be a perfectly recoverable process, meaning there would be no energy lost, as potential energy becomes kinetic energy, and as the process is reversed (Shearer, 2009). However, in this sense, the earth is not ideal. As elastic waves propagate through the earth, energy is lost during the exchange between these two energy states; mostly converted to heat energy along mineral grain boundaries and dislocations (Shearer, 2009). Intrinsic attenuation can be described by calculating the percent amplitude reduction of a seismic wave (of a given frequency) as it travels through a medium with a given seismic velocity, quality factor, and thickness, using the following equation (Shearer, 2009).

 $A_r = \mathbf{1} - (A_0 e^{\frac{-\omega x}{2cQ}})$ Where $A_r =$ percent amplitude reduction, $A_0 = 1$, $\omega =$ angular frequency = $2\pi f$, x = medium thickness, c = seismic velocity, and Q = quality factor.

Examining this equation, it becomes clear that intrinsic attenuation is dependent on many factors, however, is most easily influenced by seismic frequency. As the frequency of a seismic wave increases, the percent amplitude reduction due to intrinsic attenuation also increases (Shearer, 2009). This means a seismic wave traveling through the exact same medium, at multiple frequencies, will decay much faster at the higher end of the frequency spectrum (Shearer, 2009).

The frequency dependency of intrinsic attenuation becomes one of the chief limiting factors of active source seismology when considering deep seismic targets. The clear majority of active source seismic techniques employ relatively high frequency sources (~30 Hz) (Robinson, 1984) for two main reasons. First, higher frequency seismic waves provide much higher vertical resolutions when performing reflection experiments (Robinson, 1983). Second, it is extremely difficult to generate a low frequency seismic source with enough energy to be useful (Robinson, 1983). Considering that most of reflection seismology has been developed for imaging targets within 10 or so km of the surface (mostly targets for oil and gas exploration) this limitation is generally not a problem. However, as seen with the COCORP studies (to which the SESAME experiment was developed to supplement) in which researchers developed beautiful upper lithosphere profiles but largely were unable to image targets as far down as the Moho, even with high quality crystalline rocks dominating the study area, this limitation becomes very real (Cook and Vasudevan, 2006).

Scattering attenuation: unlike intrinsic attenuation, where energy is removed from the seismic wave-field and converted to heat within the medium of propagation, scattering attenuation does not change the total energy balance of a seismic wavefield when integrated over the full wave-field (Shearer, 2009). Rather, scattering attenuation refers to energy that is lost from main seismic arrivals when they encounter small-scale heterogeneities, resulting in diminished seismic amplitudes for specific arrivals, but no loss of energy when considering the sum of all possible seismic arrivals (Shearer, 2009).

Scattering attenuation, along with all the mechanisms for decaying seismic arrivals discussed in this study, is not unique to active source experiments, and is the least limiting of the mechanisms discussed when considering active source reflection seismic studies (Shearer, 2009).

However, it is worth noting that shorter wavelength (high frequency) seismic waves are more likely to show the effects of small-scale heterogeneities, meaning one is more likely to experience complications due to scattering attenuation as the frequency content of their seismic wave-field shifts upward (Robinson, 1984). It is also worth noting, however, that these effects are generally low, and can be compensated for by employing three-dimensional migration and amplitude restoration techniques (Robinson, 1983).

Transmitted and converted energy loss: when a compressional seismic wave encounters a seismic impedance interface (most commonly defined by a change in seismic velocity), a portion of the seismic wave-field will be transmitted through the interface, reflected off the interface, mode converted and transmitted through the interface, and mode converted and transmitted off the interface (Shearer, 2009). This process conserves the total amount of energy contained within the seismic wave-field, however, when considering a single body wave arrival (in the case of reflection seismology the reflected p-wave) the amount of energy contained within that arrival is decayed at each seismic impedance interface (Shearer, 2009).

It is fortunate this process occurs, because it forms the technical basis for reflection seismology, measuring travel times of reflected compressional seismic waves as they encounter seismic impedance interfaces (Robinson, 1984). However, this process can quickly deplete the amplitude of a given seismic arrival. In the case of a non-vertically incident p-wave there will be a transmitted p-wave, transmitted sv-wave, a reflected p-wave, and a reflected sv-wave (Shearer, 2009). This means energy which was initially contained within one seismic wave, is distributed to four seismic waves at each seismic reflector. Considering there may be thousands to millions of seismic reflectors of varying impedance contrast along a given ray path, this process can quickly decay the amplitudes of seismic arrivals.

For simplicity, this point can be illustrated by calculating transmission and reflection coefficients for given seismic impedance boundaries using the example of a vertically incident p-wave, which does not encounter shear-wave mode conversions at impedance boundaries, the equations for calculating the compressional transmission and reflection coefficients are as follows (Shearer, 2009).

$$PP_{reflect} = -\frac{p_1\alpha_1 - p_2\alpha_2}{p_1\alpha_1 + p_2\alpha_2}$$

$$PP_{transmit} = \frac{2 p_1 \alpha_1}{p_1 \alpha_1 + p_2 \alpha_2} \text{ Where } p_1 = \text{slowness of layer 1, } p_2 = \text{slowness of layer 2, } \alpha_1 = p\text{-wave}$$

$$\text{velocity of layer 1, and } \alpha_2 = p\text{-wave velocity of layer 2.}$$

Again, the effects of transmitted and converted energy loss are not unique to active source seismology. However, these effects do contribute with respect to deep reflection targets such as the Moho or the lithosphere/asthenosphere boundary. The initial energy level of a seismic source is important in this respect because the magnitude of an active source is limited by many factors, and these issues disproportionately affect active source experiments. Simply put, the larger the magnitude of the initial source, the smaller the relative effect of losing energy to transmitted and converted seismic waves, and thus, the deeper the resolvable target (Shearer, 2009).

Given the main mechanisms for decaying both amplitude content and frequency content of a seismic wave-field, the true limitation of an active source seismic reflection experiment, with respect to deep reflection targets, becomes clear; and the potential value of passive source seismic reflection techniques is illuminated.

The true limiting factor of active source techniques, with respect to deep earth reflection targets, is they are both energy and frequency band limited (Robinson, 1984). Active source seismic techniques require the experimenter to generate a seismic source. For targets in the depth range of several km, this is not an issue. However, as targets exist at greater and greater depths, the energy levels required to preserve perceptible signal levels increases drastically. This presents an obvious issue, as experimenters cannot increase source size beyond a certain point, meaning, they cannot increase target depth beyond a certain point. In addition, these seismic sources most often generate only a narrow band of frequencies, with peak frequency centered somewhere on the higher end of the spectrum for seismic energy (example ~30 Hz) (Robinson, 1983). This is not only because of limitations in generating broadband seismic energy, but also because many important reflection targets are best imaged using high frequencies. Whatever the reason, because of the narrow band nature of most active source seismic studies, attenuation effects generally make it impossible to image deep earth reflection targets (Robinson, 1983).

Passive-Source Reflection Profiling

Passive source seismic techniques employ seismic energy generated by the natural earth. For this study, natural earthquakes with moment magnitudes between 6.0-7.0 are employed. Such events are ideal for applying and retooling techniques originally developed for active source seismic reflection profiling, using a passive source. These events generate large amounts of seismic energy, and they generate that energy at a variety of frequencies (i.e. they are broad band) (Shearer, 2009). The fact that these sources are broadband and initially energetic allows us to overcome the limitations of using an active source and produce images of deep earth reflection targets.

In this study we adapt and modify the relatively new global seismic technique global phase seismic interferometry (GloPSI) (Ruigrok and Wapenaar, 2012; Yang, et al., 2012) to generate passive source reflection profiles of the southeastern United States.

The method uses surface reflections of PKIKP (Figure. 2.2) as virtual seismic sources to generate zero-offset reflection profiles (Ruigrok and Wapenaar, 2012; Yang, et al., 2012). We choose these seismic phases for two main reasons. First, these phases contain only compressional seismic energy, and over many distance ranges represent the first seismic arrival recorded by our receiver array in the United States (Dzeiwonski and Anderson, 1981). This makes processing the data for these events relatively simple initially, because it is relatively easy to predict, within a reasonable range of error, when these seismic arrivals should be recorded, allowing us to more easily establish an equal time base. Second, over distance ranges between 110 and 180 degrees PKIKP corresponds to ray parameters less than 0.04 s/km, so the ray paths for incident waves (and their reflection from the surface as effective sources) are near vertical. Each station along a profile thus acts as a coincident source/receiver, so the seismograms recorded along the whole profile can be plotted together as a zero-offset section with each seismogram analogous to a trace in a conventional industry-style CDP-stacked section (Yang, et al., 2012).

Earthquakes are chosen based on distance (110-140 degrees / 160-180 degrees for interference free recordings, and 140-160 degrees for recordings containing interfering PKP arrivals (Figure. 2.2)) and signal level. The initial arrival of PKIKP or PKiKP for each station to be included along the profile line then is picked as time zero (i.e. the virtual source) and the traces are combined into a gather using this time base. Using additional events, a researcher could improve upon this process by stacking the resulting reflection profiles. The stacking

process would cause noise to trend towards zero as more events are added, due to deconstructive interference, and would cause real events to trend toward a non-zero value, due to constructive interference (Robinson, 1984). The rate at which profile quality would improve is assumed to follow a square root law (i.e. to make the signal twice as strong, one would require four times as many events) (Robinson, et al., 1986).

However, the process of employing GloPSI is more complex than just marking the arrivals of PKIKP and PKiKP as time zero and then seeing what reflections are recorded. This study identifies several main complexities with this process.

First, there is a wide range of distances over which PKIKP and PKiKP are observed, a significant portion of which is complicated by the interfering arrivals of the PKP family of bodywaves; in many cases PKP arrives almost simultaneously with reflections generated by PKIKP and PKiKP (Figure 2.2) (Kennett and Engdahl, 1991). Because PKP does not have an outer core segment along its ray path, PKP arrives with much larger absolute amplitude than PKIKP and PKiKP (Dzeiwonski and Anderson, 1981). This presents a very serious problem, as PKP can, in effect, wash out the visibility of PKIKP and PKiKP, and their reflections. In addition, other interfering seismic arrivals such as pPKIKP and pPKiKP (source-side free-surface reflections which arrive at a time equal to the TWT of PKIKP or PKiKP from source depth to source-side surface after the direct arrival of PKIKP or PKiKP is recorded) may be observed during critical windows, further complicating the process (Dzeiwonski and Anderson, 1981).

Second, this process assumes that the seismic source for reflection profiling (in this case the initial PKIKP or PKiKP arrival) is impulsive. Because we are employing natural earthquake signals, we know this assumption to be false (Robinson, 1984). Assuming a PKIKP or PKiKP waveform has a length roughly equivalent in seconds to the source earthquake's magnitude,

sources may be between 6 and 7 seconds long, far from impulsive (Shearer, 2009). The violation of this assumption means unprocessed reflection profiles collected using this technique will have real reflection events convolved with manifestations of the source wavelet, making interpretation of these data virtually impossible (Robinson, 1984).

Third, this technique is assumed to generate a zero-offset (i.e. coincident source-receiver) reflection profile (Yang, et al., 2012) analogous to a conventional industry common depth point (CDP) stacked section. Because this assumption is made, migration is required to account for the positions of subsurface impedance interfaces that may not occur horizontally (i.e. dipping interfaces).

Finally, station spacing can play a big role in data interpretation. Station spacing within the SESAME array is not uniform; this leads to difficulties interpreting data in places where stations are spaced far apart (Parker, et al., 2013).

For this study we find motivation in the desire to overcome these complications and present a reliable GloPSI workflow. We adapt and expand on previous GloPSI workflows (Yang, et al. 2012; Ruigrok and Wapenaar 2012), utilizing the most effective and meaningful advancements, and institute new protocols which offer the opportunity to employ GloPSI in an ever-expanding world of noisy broadband data. We then use the new protocols to form preliminary images of the lithosphere beneath the SESAME array, and demonstrate several interesting geologic results discovered while working with the single earthquake used in this development.

CHAPTER 2

GLOBAL PHASE SEISMIC INTERFEROMETRY (GloPSI) AND BROADBAND SEISMIC REFLECTION TECHNIQUES: AN INVESTIGATION OF THE SOUTHEASTERN SUTURE OF THE APPALACHIAN MARGIN EXPERIMENT $^{\rm 1}$

¹ Alberts, E.C., Verellen, D.N. and Hawman, R.B. To be submitted to *Geophysical Research Letters*.

ABSTRACT

The Southeastern suture of the Appalachian Margin Experiment (SESAME) consisted of a seismic broadband array containing approximately 85 stations deployed along three lines crosscutting the southeastern United States (Parker et al., 2013), and paralleling profiles of the older Consortium for Continental Reflection Profiling (COCORP) experiment (Cook et al., 1979). Two lines (line-W and line-E) trend N-S and one line (line-D) trends NW-SE, perpendicular to regional strike (Parker, et al., 2013). Using the relatively new global seismic technique Global Phase Seismic Interferometry (GloPSI) (Yang, et al. 2012; Ruigrok and Wapenaar 2012) and re-tooled reflection seismic techniques originally developed for active source experiments, we develop a reliable and robust passive source reflection profiling workflow via the use of a series of synthetic and real world (SESAME) data sets. Generation of reflection sections via deconvolution of the earthquake source-time function rather than by autocorrelation (as done in previous studies) improves the resolution of structure within the upper crust. Spatial windowing followed by slant stacking and coherency filtering is used to suppress artifacts and incoherent noise and to identify the most reliable events for interpretation. We then use apparent velocity filtering to suppress interfering arrivals such as PKP; this greatly expands the distance range for earthquakes that can be included in the analysis. Finally, the coherency-filtered slant stacks are migrated to build an image of subsurface structure. Partial migrated sections show coherent reflections for depths ranging from Moho (~35 km beneath the Coastal Plain) to the lower lithosphere (90-110 km).

INTRODUCTION

In the 1970's, the Consortium for Continental Reflection Profiling (COCORP) conducted a series of active source reflection profiling experiments along transects crosscutting the Appalachian Mountains of the United States (Cook, et al., 1979). Of interest to this study, COCORP generated a series of reflection profiles cutting across the southeastern United States (Cook, et al., 1979). These profiles produced high quality images of sub-surface structure down to depths approaching the continental Moho (Cook, et al., 1979). However, the COCORP experiments were largely unable to resolve reflection targets at the depth of the continental Moho and below due to the limitations of active source reflection profiling (Cook, et al., 1979). Additionally, in the 1980's the Appalachian ultra-Deep Core Hole (ADCOH) experiments were conducted, which included active-source profiling experiments which intended to develop plans for the placement of a never drilled ultra-deep coring well (Coruh et al., 1987). The ADCOH experiment produced clear images of structure to depths within the middle crust, but again was unable to resolve reflection targets at the depth of the continental Moho and greater (Hubbard et al., 1991).

Active source reflection profiling is primarily limited by several factors, it is expensive, it is logistically complicated and computer intensive, and target depths are fundamentally limited by how much energy is initially released by the seismic source, the frequency band of that energy, and the frequency band of seismic recording (Shearer, 2009). The limitations related to the initial energy of the source, and its frequency content are primarily a result of four main factors, which affect all types of seismic techniques. These factors are intrinsic attenuation, scattering attenuation, spherical spreading, and energy loss due to transmission and conversion at

impedance boundaries (Shearer, 2009). Although all seismic techniques are affected by these factors, active source techniques are disproportionately affected for three main reasons: their sources are limited in magnitude (they are manmade), they tend be narrow band in nature in terms of frequencies generated and in frequencies recorded, and those frequencies tend to be on the higher end of the seismic frequency spectrum (higher frequencies are easier to generate, and offer much better vertical resolution of shallower sub-surface targets) (Robinson, 1984).

The Southeastern Suture of the Appalachian Margin Experiment (SESAME) array (deployed 2010-2014) consisted of approximately 85 broadband seismic stations placed along three lines crosscutting the southeastern United States, and paralleling the positions of seismic transects of the older COCORP experiment (Parker, et al., 2013). Two lines (line-W and line-E) trend N-S and one line (line-D) trends NW-SE, perpendicular to regional strike (Parker, et al., 2013). Line-W extended from the Blue Ridge to the Atlantic Coastal Plain. Line-E was entirely situated within the Atlantic Coastal Plain. Line D crossed the Appalachian orogen perpendicular to strike, beginning in the Valley and Ridge and continuing southeastward across the Blue Ridge, Inner Piedmont, and Carolina Terrane.

The intent of the SESAME experiment was to use passive source broadband seismic techniques to investigate the lithospheric structure of the Appalachian orogen and a proposed suture zone marking the Alleghanian (Permian) collision of Laurentia and Gondwana (Parker et al., 2013).

Attempts to resolve deeper sub-surface structure using the SESAME array (using non-reflection seismic techniques) have proven highly successful for stations positioned within crystalline terrains (blue-ridge, line-D, portions of line-W), and have shown some success with stations positioned over the Atlantic Coastal Plain (portion of line-W and all of line-E) (Parker,

et al., 2016). The coastal plain has proven to complicate analysis due to p-wave multiples originating within the uppermost coastal plain sediments (Parker, et al., 2016).

To combat this issue, this study employs the relatively new passive source reflection profiling technique Global Phase Seismic Interferometry (GloPSI) (Yang, et al. 2012; Ruigrok and Wapenaar, 2012). GloPSI was chosen for this task because it was believed that the near vertical incidence of the seismic arrival PKIKP (the primary global wave phase employed under GloPSI), along with the broadband nature of earthquake seismic energy, would simplify the identification and removal of p-wave multiples generated within the Atlantic Coastal Plain sediments (Robinson, 1986).

In its simplest form the GloPSI method employs the global seismic phase PKIKP (Ruigrok and Wapenaar, 2012). We use earthquakes with moment magnitude between 6.0 and 7.0, at distances between 110 degrees and 180 degrees from the SESAME array. Over this distance range PKIKP corresponds to ray parameters less than 0.04 s/km, so the ray paths for incident waves (and their reflection from the surface as effective sources) are near vertical. Each station along a profile thus acts as a coincident source/receiver, so the seismograms recorded along the whole profile can be plotted together as a zero-offset section with each seismogram analogous to a trace in a conventional industry-style CDP-stacked section (Yang, et al., 2012)

Earthquakes are chosen based on distance (110-140 degrees / 160-180 degrees for interference-free recordings, and 140-160 degrees for recordings containing interfering PKP arrivals (Figure 2.2)) and signal level. The initial arrival of PKIKP for each station to be included along the profile line then is picked as time zero (i.e. the virtual source) and the traces are combined into a gather using this time base. Using additional events, a researcher could improve upon this process by stacking the resulting reflection profiles. The stacking process would cause

noise to trend towards zero as more events are added, due to deconstructive interference, and would cause real events to trend toward a non-zero value, due to constructive interference (Robinson, 1984). The rate at which the profiles quality would improve is assumed to follow a square root law (i.e. to make the signal twice as strong, one would require four times as many events) (Robinson, et al., 1986).

However, the process of employing GloPSI is more complex than just marking the arrivals of PKIKP and PKiKP as time zero and then seeing what reflections are recorded. This study identifies several main complexities with this process.

First, there is a wide range of distances over which PKIKP and PKiKP are observed, a significant portion of which is complicated by the interfering arrivals of the PKP family of bodywaves; in many cases PKP arrives almost simultaneously with reflections generated by PKIKP and PKiKP (Figure 2.2) (Kennett and Engdahl, 1991). Because PKP does not have an outer core segment along its ray path, PKP arrives with much larger absolute amplitude than PKIKP and PKiKP (Dzeiwonski and Anderson, 1981). This presents a very serious problem, as PKP can, in effect, wash out the visibility of PKIKP and PKiKP, and their reflections. In addition, other interfering seismic arrivals such as pPKIKP and pPKiKP (source-side free-surface reflections which arrive at a time equal to the TWT of PKIKP or PKiKP from source depth to source-side surface after the direct arrival of PKIKP or PKiKP is recorded) may be observed during critical windows, further complicating the process (Dzeiwonski and Anderson, 1981).

Second, this process assumes that the seismic source for reflection profiling (in this case the initial PKIKP or PKiKP arrival) is impulsive. Because we are employing natural earthquake signals, we know this assumption to be false (Robinson, 1984). Assuming a PKIKP or PKiKP waveform has a length roughly equivalent in seconds to the source earthquake's magnitude,

sources may be between 6 and 7 seconds long, far from impulsive (Shearer, 2009). The violation of this assumption means unprocessed reflection profiles collected using this technique will have real reflection events convolved with manifestations of the source wavelet, making interpretation of these data virtually impossible (Robinson, 1984).

Third, this technique is assumed to generate a zero-offset (i.e. coincident source-receiver) reflection profile (Yang, et al., 2012) analogous to a conventional industry common depth point (CDP) stacked section. Because this assumption is made, migration is required to account for the positions of subsurface impedance interfaces that may not occur horizontally (i.e. dipping interfaces).

Finally, station spacing can play a big role in data interpretation. Station spacing within the SESAME array is not uniform; this leads to difficulties interpreting data in places where stations are spaced far apart (Parker, et al., 2013).

For this study we find motivation in the desire to overcome these complications and present a reliable GloPSI workflow. We adapt and expand on previous GloPSI workflows (Yang, et al. 2012; Ruigrok and Wapenaar 2012), utilizing the most effective and meaningful advancements, and institute new protocols which offer the opportunity to employ GloPSI in an ever-expanding world of noisy broadband data. We then use the new protocols to form preliminary images of the lithosphere beneath the SESAME array, and demonstrate several interesting geologic results discovered while working with the single earthquake used in this development.

Using the global seismic phase PKIKP (PKP_{df}) as a virtual seismic source to generate pwave reflections to image the lithosphere, this study aims to retool active-source reflection seismology techniques for use within a passive-source experiment, and to create a useable and robust workflow for passive-source reflection profiling based in part on the relatively new global seismic technique known as Global Phase Seismic Interferometry (GloPSI) (Yang, et al. 2012; Ruigrok and Wapenaar 2012). The new protocols are applied to noisy earthquake waveforms recorded with broadband seismometers of the Southeastern Suture of the Appalachian Margin Experiment (SESAME) array. To this end, we adapt the techniques of brute stacking, static cross-correlation, signal deconvolution, apparent velocity filtering (through slant stacking), coherency filtering, band-pass filtering, and 2-D slant stack depth migration for use within an adapted GloPSI workflow.

Previous studies employing GloPSI have used many of these same techniques, demonstrating the effectiveness and adaptability of the GloPSI method. For example, Yang, et al. (2012) utilized a variation of the GloPSI method, taking advantage of the teleseismic wave phase PpPdp to image sedimentary basin structure of the Bighorn Mountains, north-central Wyoming, USA. Ruigrok and Wapenaar (2012) used global seismic phases to image the subsurface structure of the Himalaya Mountains, Tibet. Yang et al. (2012) employed iterative deconvolution to remove source effects from recorded seismic waveforms, used a host of seismic filtering techniques (including bandpass filtering to enhance signal quality), and utilized a standard depth conversion technique to better interpret data. Ruigrok and Wapenaar (2012) used autocorrelation to identify reflections, and performed a Kirchhoff time-migration (in addition to a standard depth conversion) to better interpret their data.

In this study we utilize many of the same techniques but combine them into a new workflow that differs from previous studies in several key ways. First, we attempt signal deconvolution as a means for removing source effects from the recorded seismic waveforms.

This improves resolution of structure within the upper crust which is commonly obscured using autocorrelation as in previous studies.

Second, we greatly expanded the inventory of usable source events by employing apparent velocity filtering to remove interfering seismic arrivals. Previous studies have excluded recordings over distance ranges that include interfering seismic arrivals. This study offers the first treatment designed to utilize these recordings, thus, greatly increasing the usability of the GloPSI method with respect to SESAME data, and to data sets worldwide. Additionally, apparent velocity filtering techniques may, much like predictive deconvolution techniques employed by Yang, et al. (2012), offer the opportunity to remove p-wave multiples from within the data, especially when they are paired with predictive deconvolution (although this has not been attempted for this study).

Third, we implement a simple 2-D slant stack migration technique to better interpret reflectivity data. Previous studies utilized either a standard depth migration, as in the case of Ruigrok and Wapenaar (2012), or a Kirchhoff time-migration, as in the case of Yang, et al. (2012). Fundamentally, this migration technique, an adaptation of an algorithm developed for wide-angle reflection data (Hawman, 2008), differs from those previously instituted, in that it does not require dense, evenly spaced traces, thus, greatly simplifying the migration process, and eliminating the need to perform data projections and interpolations.

Finally, we include extensive semblance-based coherency filtering as a method for suppressing noise prior to migration. Performing this filtering while in the T-p (travel time –ray parameter) domain, also allows for the removal of coherent noise such as interfering PKP arrivals. This treatment, in part, allows for the generation of meaningful seismic reflection profiles, even utilizing only a single earthquake source event.

Through this manuscript, we employ an array of synthetic and real world examples, outlining each process within our GloPSI workflow (as we have adapted and applied it). Geologic revelations, although not the focus of this study, are discussed as part of the real-world examples contained, thus, constraints are placed on the depth of the interpreted lithosphere / asthenosphere boundary, and Moho.

METHODS

A total of seven synthetic seismic reflection profiles, along with data from a single natural earthquake, were used in this study. Synthetic reflection profiles were modeled after the SESAME array line-D, and specifically, emulated a simplified version of the earthquake event 2014-01-25, a magnitude 6.1-earthquake occurring at a depth of 66 km, and 153 degrees from the SESAME array. Within Figure (2.2) the predicted travel times of PKIKP, PKiKP, and PKP_{bc} at a range 153 degrees may be observed. From this, it can be determined that this particular source event falls into the distance range (140-160 degrees) which includes complications arising from interfering PKP arrivals. Bearing this in mind, the synthetic reflection profiles generated included a simple full-line model, a complex full-line model, and five sub-section models of the full complex model.

The natural earthquake event was chosen based on several criteria. First, it had a magnitude of 6.1 and generated the global phase PKIKP (as observed on the SESAME array), and second, it included two interfering arrivals (interfering with PKIKP, in this case the interfering arrivals PKiKP / PKP_{bc} and PKP / PKP_{ab}). Interfering arrivals were desired as one of the main goals was to demonstrate the usability of earthquake events that previously would have been excluded from analysis (thus, greatly increasing the number of usable earthquake events when considering the SESAME array).

Synthetic Construction

Of the seven synthetic reflection profiles generated for this study, all were based on line-D event 2014-01-25. This event contained five arrivals, which were incorporated into all the synthetic models. These included the zero slowness arrival of PKIKP, two non-zero positive slowness arrivals representing PKiKP / PKP_{bc} and PKP_{ab}, and two near-zero slowness arrivals of un-interpreted mantle reflections. These events can be seen in Figure (2.4), and from this it can been seen that the relative amplitudes of these five events are as follows, PKIKP is roughly half as energetic as the PKP arrivals, and the un-interpreted mantle reflections are roughly the same relative amplitude as PKIKP. These relative amplitudes were carried through all the synthetic reflection profiles constructed. Finally, these five events (PKIKP, PKiKP / PKP_{bc}, PKP / PKP_{ab}, un-interpreted mantle 1, and un-interpreted mantle 2) are observed in Figure (2.4) to extend across the full length of line-D (although the un-interpreted mantle reflections may be difficult to discern without particularly careful inspection), this too was incorporated into all seven synthetic sections.

Simple Full-Line Section

A simple full-line section, seen in Figure (2.5), was constructed using nine synthetic arrivals. These arrivals included the zero slowness initial arrival of PKIKP, four simulated positive slowness dipping reflectors (all positive in the case of the simple full-line section to more easily verify the non-existence of dipping artifacts, because only positive slowness arrivals were included, any negative slowness arrival appearing after inverse slant stacking would be an artifact, had negative slowness arrivals been included initially this conformation would have been needlessly more complex), two simulated near zero-slowness upper mantle reflectors, and the positive slowness interfering arrivals PKP / PKP_{ab} and PKiKP / PKP_{bc}.

These arrivals were first generated as a series of spikes with given amplitudes and zero trace (furthest left position on profile) intercept times. Generation of synthetic sections and processing of real and synthetic data were carried out using the Seismic Unix software package (Cohen and Stockwell, 1999) and software developed in-house by R. Hawman (e.g., Hawman, 2008). A brief description of each program used is given in Appendix (A). These spikes then were convolved with a simple synthetic wavelet to emulate a nearly impulsive seismic source (roughly the expected result after signal deconvolution of real earthquake data) using the publicly available software suite seismic Unix (suconv) (Cohen and Stockwell, 2016). Finally, using the clock as a seed, random noise was added over the entire synthetic section with a signal to noise ratio of 10, again employing seismic Unix (suaddnoise) (Cohen and Stockwell, 2016). The construction of this simple full-line section is seen from start to finish in Figure (2.5), and the result is a simplified synthetic version of the real earthquake event 2014-01-25 with six simulated sub-surface reflections (generated by virtual source PKIKP), and two interfering PKP arrivals (PKP_{ab} and PKP_{bc}).

Complex Full-Line Section

A complex full-line section (Figure 2.6) was constructed using fifteen synthetic arrivals. Included among these fifteen synthetic arrivals were the five arrivals common to all the constructed synthetic sections previously discussed above and a variety of simulated positive and negative slowness dipping reflectors. The primary differences between this complex full-line section and the previously discussed simple full-line section are as follows: the complex model includes simulated reflectors with both positive and negative apparent slownesses (in contrast with the simple model, which contains simulated reflectors with positive slownesses only), and the complex section includes simulated reflectors which do not span the entire length of the

synthetic section (the simple section includes only arrivals which span the entire length of the section), instead each simulated reflector spans a variable length of the section to simulate reflecting interfaces of limited lateral extent (Figure 2.6).

Spatially Windowed Sub-Sections

Five sub-sections of the complex full-line profile were constructed, and can be seen in Figure (2.7). These trace gathers were generated by partitioning the complex full-line section into five equal sub-sections. Boundaries were chosen to match breaks in the continuity of individual reflections.

Global Phase Seismic Interferometry and Associated Seismic Techniques

Adapted Global Phase Seismic Interferometry

Understanding the complications associated with applying GloPSI in its simplest form, we present a usable and robust workflow, which addresses these complications, and allows for the application of an adapted GloPSI workflow. The primary seismic techniques within this workflow (many of which have been re-tooled for this purpose) include band-pass filtering, static cross-correlation, signal deconvolution, slant stacking, coherency filtering based on semblance (Neidell and Tanner, 1971), 2-D slant-stack migration, and brute stacking. Each of these techniques is described within the adapted GloPSI workflow below, and the full results of applying this workflow (with respect to synthetic and real world data cases) are demonstrated within this studie's results section.

The adapted GloPSI workflow outlined below can be broken down into thirteen primary steps, with two additional optional steps, ranging from identifying the initial arrival of PKIKP, to stacking fully processed time sections / 2-D slant stack migrated depth sections to generate a

final reflection imaging product. Adapted GloPSI has been presented within this study's methods section using the generalized processing case of a natural earthquake.

It is crucial to note that the parameters of these steps will vary greatly depending on the input seismic data. In addition, several of the preliminary steps (steps 1-8) are not necessary when working with synthetic data because the latter were generated using an impulsive sourcetime function from the start, thus eliminating the need for signal deconvolution. The fork in the GloPSI processing workflow that occurs at the start of step 9 represents the split between two main processing streams. The first is performed entirely in the time domain and results in unmigrated time-domain sections. The second is performed between the time and depth domains and results in 2-D slant-stack depth-migrated seismic sections. Throughout the time-domain analysis, a 20-second noise window preceding PKIKP was preserved as a means of verifying the reliability and robustness of the processing techniques, as many seismic artifacts are more easily seen in the pre-event section, which should, without artifacts, appear random or nearly blank. Steps 1-6 (Obtaining Data, Stripping the SAC Headers, Assembling Line Gathers, Time Windowing, Removal of Linear Trends and Trace Mean, and Static Corrections)

Obtaining Data, Time Windowing, and the Removal of Linear Trends and the Trace Mean

Usage of the adapted GloPSI workflow begins with obtaining seismic data, and manipulating that data into a more useful form. For this study, we employed the publicly available IRIS software suite JWEED, which provides a user-friendly environment designed for seismic data storage and access. From JWEED, we obtained a set of single-station verticalcomponent earthquake event traces of the SESAME array (must be Z-component only, these are downloaded in the standard SAC format; see Appendix B). In our case, traces were initially 300 seconds long (50 seconds before the keyed event, and 250 seconds after), using first recorded p

arrival time as a reference time. Using the publicly available IRIS software suite SAC (Goldstein and Snoke, 2005), these single-station event traces then were further windowed to a more appropriate length, in the case of SESAME data, 180 seconds of recording (30 seconds before first p, and 150 seconds after), and any linear trend in the waveforms was removed, along with the trace mean.

Stripping the SAC Headers and Assembling Line Gathers

Using University of Georgia Geophysics Lab in-house software sacheaderstrip (Appendix A), the header information attached to each single station event trace is removed, allowing for the generation of single event line-gathers (using standard Unix concatenation commands). Single event line-gathers are then duplicated, one copy used to calculate the appropriate static corrections, and the other stored for later use.

Static Corrections

To extract an estimate of the source-time function of the earthquake, the traces were first shifted in time to align the PKIKP arrival. This was done after first combining traces from all three lines (W, E, and D) to ensure a common time base. Shifts were determined by cross-correlation (Robinson, 1986). Appropriate static corrections were calculated by first band-pass filtering the single event line-gathers to relatively high frequency narrow-band data. This reduced noise and greatly sharpened the arrival of PKIKP. The traces then were cross-correlated and static-corrected to align PKIKP across each respective single event line-gather. Through this cross-correlation routine, the total number of time samples each trace within each gather must be shifted up or down to maximize cross-correlation is stored in a series of separate outputs. These static shifts, along with one last time windowing to 50 seconds (20 seconds before PKIKP, and

30 seconds after), were then applied to the set aside single event line-gathers, resulting in statically corrected, broad-band, and appropriately time windowed, single event line gathers.

Steps 7-8 (Estimating the Source Time Function and Signal Deconvolution)

Estimating the Source Time Function

Utilizing relatively high moment magnitude earthquake events (6.0 - 7.0) as seismic sources for reflection profiling requires the removal of source wavelet manifestations from within single event line-gathers. This study accomplishes this using signal deconvolution, a technique widely used by active-source seismologists for removing the signatures of seismic sources from within recordings, while reducing the recordings to zero-phase (Robinson, 1984). Creating the source wavelet, and therefore, knowing the source wavelet, allows active-source seismologists to perform signal deconvolution with relative ease. However, in the case of natural earthquake sources, the source wavelet is not known from the start, because it was not artificially created and designed. If signal deconvolution is to be performed using natural earthquake derived data, this necessitates estimation of the source wavelet (Robinson, 1984).

The source wavelet, also known as the source-time function, was (in our case) estimated by utilizing several key assumptions. First, it was assumed that stations within the SESAME array were sufficiently spaced that sub-surface geologic structure was not the same beneath any two stations (i.e. sub-surface reflectors do not appear at identical two-way travel times). Second, it was assumed that the recorded seismic wavelet was a result of only the wavelet contributions of the seismic source, and the sub-surface structure between the seismic source and receiver (Robinson, 1984). If these assumptions hold, to estimate the source time function, simply stacking all the static-corrected traces within each respective single event line gather will provide

an estimate of the source-time function. The stacking process will attenuate features related to earth structure and constructively stack the seismic source wavelet.

These assumptions were observed to be sound, however, this process was slightly modified to avoid contamination of the source-time function with energy from PKiKP and PKP. For small-magnitude events, (M < approximately 7.0), the source-time function will be roughly equal in duration in seconds to the moment magnitude of the source event (Shearer, 2009). For this study, we stacked the traces within each single event line gather to form a stacked source time function trace, and then zeroed out the stacked source time function trace preceding the first kick, and proceeding a number of seconds equal to the moment magnitude of the event after the first kick.

Signal Deconvolution

We then performed signal deconvolution using this newly estimated source time function. We performed signal deconvolution in the frequency domain, where deconvolution is equivalent to division (Robinson, 1984). The results of this process were single event line gathers in which the effects of the source wavelet have been removed and have been reduced to zero-phase.

Step 9 (Sub-Sectioning and Slant Stacking)

Sub-Sectioning and Slant Stacking

Following deconvolution, the traces were slant stacked to obtain objective measures of arrival time and apparent slowness (apparent dip) of reflections (Phinney et al., 1981). The slant stacks were carried out by summing amplitudes of waveforms along linear trajectories over a range of slopes (slownesses p) and times T (using the center of the gather as a time reference).

The single event line-gathers were first sub-sectioned into five smaller (sometimes overlapping) line-gathers based on apparent continuity of possible sub-surface reflectors and

then were tapered to minimize artifacts during slant stacking. Following this, the sub-sectioned single event line-gathers were slant stacked into the T-p domain.

Caution was taken during this process to ensure that the resulting slant stacks were symmetric with respect to p (meaning they included an equal range of positive and negative apparent velocities), ensuring dipping artifacts would not be introduced during inverse slant stacking into the time-distance domain. The range in p included in this transformation (and thus the range of apparent dips) was determined by the distribution of coherent energy in the slant stack.

<u>Steps 10-11</u> (Semblance Based Coherency Filtering and the Removal of Interfering Seismic Arrivals)

Semblance Based Coherency Filtering

Following the slant stacking process, sub-sectioned single event slant stacks were then ready to be filtered via a modified semblance filtering technique. Semblance is a measure of coherence that represents, for a given slant trajectory and time window, the power in the beam (stack) normalized by the power in the traces (Neidell and Taner, 1971; Phinney et al., 1981). As part of the forward slant stacking process a series of semblance spectra were generated (using a time-gate of one); these spectra were utilized to generate a semblance based coherency filter for each of the sub-sectioned single event slant stacks.

We designed a series of binary matrices that assigned a value of one to any semblance value above a specified cutoff and a value of zero to any semblance value below a specified cutoff. The cutoff value was determined by scaling the entire semblance plot so that the maximum value of semblance was equal to one, and then setting the cutoff value to 0.75, in

effect allowing the top 25 percent of semblance values to pass as a one, while reducing the bottom 75 percent of semblance values to a zero.

Next, we multiplied the original sub-sectioned single event slant stacks by their corresponding binary semblance filtering matrices resulting in coherency filtered sub-sectioned single event slant stacks. The coherency filtering process greatly reduced the amount of random noise, and served as a robust technique for eliminating many of the prominent alias-fans generated during the slant stacking process (Stoffa et al., 1981).

The Removal of Interfering Seismic Arrivals

With alias-fan free, noise-reduced, coherency filtered sub-sectioned single event slant stacks; removal of interfering or unwanted arrivals was then possible. For this study, we removed the interfering arrivals PKP / PKP_{ab} and PKiKP / PKP_{bc}. These arrivals were relatively easy to recognize within the coherency filtered sub-sectioned slant stacks as they arrived at predictable and easily observed times and apparent slownesses and were much larger in amplitude compared to any other observed arrivals.

To remove PKP / PKP_{ab} and PKiKP / PKP_{bc} we first identified the interfering arrivals within each of the coherency filtered sub-sectioned single event slant stacks, and then isolated them for removal. Next, we subtracted the isolated interfering arrivals from each of the coherency filtered sub-sectioned single event slant stacks, resulting in fully filtered sub-sectioned single event slant stacks, which were then ready for 2-D slant-stack migration (to produce a depth section), and inverse slant stacking back to the time domain. The migration and inverse slant stacking process was then accomplished without the worry of introducing slant-stacking artifacts, with drastically reduced random noise, and with no identified interfering seismic arrivals.

Steps 12-13 (Inverse Slant Stacking and Brute Stacking)

Inverse Slant Stacking

Following coherency filtering, inverse slant stacking offered the opportunity to interpret seismic data in its simplest form (in the time-domain). This was critical for several reasons, first, these data consisted of filtered sub-sectioned single event slant stacks, each with 20 seconds of a quiet (signal-free) window preceding PKIKP, which allowed for verification that significant artifacts had not been introduced while performing the previous seismic processing steps (these artifacts would have been most visible in the pre PKIKP window). Second, having a reasonable time-domain interpretation of the fully processed data, allowed for simple ground-truthing of the proceeding 2-D slant stack depth migration.

Inverse slant stacking was performed on the filtered sub-sectioned single event slant stacks that had been set aside for time-domain only analysis. The results of this process were time-domain sub-sectioned single event line gathers (with coherency filtering having been applied, and interfering seismic arrivals removed). At this stage of processing, lower frequencies in the waveform spectrum will be amplified. To correct for this effect, the traces were modified by computing the first derivative of the Hilbert transform (Phinney et al., 1981). An additional filter was then applied to suppress noise at higher frequencies not represented by significant energy in the original spectrum.

The final step in this process was to recombine the sub-sectioned line-gathers into fully processed time-domain single event line gathers, which were then ready for interpretation, and for comparison to the proceeding depth migrated line gathers.

Brute Stacking (optional)

Utilizing multiple seismic events, this interpretation of the sub-surface structure of the Southeastern United States could be improved via the concept of stacking waveforms for multiple earthquakes. It is assumed that the reliability of this interpretation would improve following a square root law, e.g., doubling the signal to noise ratio would require four earthquakes (Shearer, 2009).

Steps 14-15 (2-D Slant Stack Migration and Brute Stacking)

2-D Slant Stack Migration

The final step in our workflow was to perform 2-D slant stack migration. Using a modification of an approach developed for wide-angle reflection data (Hawman, 2008), each sample in the slant stack was treated as a reflector from an interface at depth, arriving as a plane wave across the input subsection. The samples were downward continued through an assumed velocity model along a ray defined by the appropriate ray parameter p. A reflector segment then was constructed with a dip determined by the ray parameter and layer velocity and a width controlled by the subsection aperture. The process then was repeated for neighboring (and perhaps overlapping) subsections to build a subsurface image. The edges of individual reflection segments sometimes show concave upward curvature; these "smiles" are measures of the degree of smearing of individual peaks in the slant stack, and thus serve as useful measures of the resolving power of the component subsections (Hawman, 2008). Subsurface velocities were based on models derived from sparse wide-angle reflection data (Hawman et al., 2012) and broadband SsPmp data (Parker et al., 2016). It is worth noting that this migration technique is best employed with inherently noisy seismic data recorded with sparse arrays of unevenly spaced receivers and is not the best migration technique for high-quality industry-style surveys.

The migrations were performed with distance allowances made within each sub-sectioned gather, which allowed data to be migrated outside the original horizontal extent of the sub-sectioned gathers. For this, we used a distance allowance of 100 kilometers on either side of each sub-sectioned gather. Finally, we combined the results of 2-D slant stack migration from each fully filtered sub-sectioned single event slant stack, and generated migrated full-line single event gathers for SESAME lines E and W, resulting in a robust broadband interpretation of the sub-surface of the Southeastern United States.

Brute Stacking (optional)

Utilizing multiple seismic events, this interpretation of the sub-surface structure of the Southeastern United States could be improved via the concept of stacking waveforms for multiple earthquakes. It is assumed that the reliability of this interpretation would improve following a square root law, e.g., doubling the signal to noise ratio would require four earthquakes (Shearer, 2009).

RESULTS

Synthetic Results

For this study, a total of seven synthetic reflection profiles were generated, including a simple full-line profile, a complex full-line profile, and five sub-section lines (which were generated by sub-sectioning the complex full-line profile). The simple full-line profile was created primarily as a tool for verifying the functionality of shell scripts during their development; consequently the simple full-line profile is not further discussed within this text. The complex full-line profile was generated as a tool for developing the presented adapted GloPSI workflow. The synthetic results presented here are centered on the use of the five sub-sectioned lines, which were derived from the complex full-line profile. These five sub-sectioned

lines most closely represent the reality of natural data within this study, and offered the most useful insights, as the adapted GloPSI method presented was being developed, and fine-tuned. Specifically, these lines best simulated the observation of reflections of limited spatial extent, and as a result of partitioning, allowed for maximization of resolution within the migrated section. Steps 1-6 of the adapted GloPSI workflow, although essential to its functionality, are relatively trivial and are primarily concerned with preparing seismic data for more advanced processing, thus, the results of steps 1-6 are not further discussed within this text.

Step 9 (Slant Stacking and Sub-sectioning)

Slant Stacking and Sub-sectioning

We begin by demonstrating the results of sub-sectioning the complex full-line gather, seen in Figure (2.6), into five sub-sectioned gathers, seen in Figure (2.7), and then slant stacking each of the five sub-sectioned gathers into the T-p domain (Figure 2.8).

Examining Figure (2.7), which illustrates the results of sub-sectioning the complex full-line model, it becomes clear that sub-sectioning has resulted in one primary improvement.

Simulated seismic arrivals which previously did not span a significant length of the complex full-line gather, Figure (2.6), do extend across a significant length of their respective sub-sectioned gathers, Figure (2.7). This partitioning was crucial during semblance based coherency filtering, otherwise, simulated arrivals which did not span a significant length of the input gather, would have been greatly diminished during the slant stacking process, and would have been at great risk of being removed during coherency filtering due to artificially low local coherency values. The width of each subsection is chosen to span but not exceed the width of individual reflection branches. This ensures a maximum coherency measure when each subsection is slant stacked.

Figure (2.8) illustrates the results of slant stacking the five sub-sectioned synthetic line gathers to the T-p domain. Notice the reduction of each simulated arrival from a line in the time-distance domain to a concentrated region in the T-p domain. Because time is referenced to the center of the subwindow, the slope of each region is horizontal. Due to the broadband nature of the input synthetic sections, we see in Figure (2.8) that slant stacking does not completely reduce the synthetic arrivals to concentrated points, rather, the stack results in a somewhat smeared region in the T-p domain. Notice also the development of subtle alias fans (Phinney et al., 1981; Stoffa et al., 1981), emanating from each arrival's concentrated region in the T-p domain (Figure 2.8).

These alias fans, along with some of the broadband energy smearing, were addressed through coherency filtering, and are considered workable because of large separations between separate arrivals (Figure 2.8). Due to this treatment, it was considered unlikely that meaningful energy would be removed from one arrival because of filtering for another arrival, and even more unlikely that meaningful energy from one arrival would be removed because of isolating and removing an interfering arrival. Thus, the slant stacks generated during this process were considered robust, because 1) they preserved the most important energy corresponding to each simulated arrival, 2) they allowed for the removal of both alias fans and random noise via semblance based coherency filtering, and 3) they allowed for the complete removal of interfering arrivals (with both semblance based coherency filtering and the removal of interfering arrivals occurring in subsequent processing steps).

<u>Steps 10-11</u> (Semblance Based Coherency Filtering and the Removal of Interfering Seismic Arrivals)

Semblance Based Coherency Filtering

Semblance based coherency filters were designed by scaling the maximum value of semblance from each sub-sectioned slant stack to one, assigning a lower cutoff value of 0.75, and generating a binary matrix of pass (1) and fail (0) values. Multiplication of the slant stack by the coherency filter largely eliminates the alias fans that previously emanated from each simulated arrival and greatly reduces random noise (Figure 2.8). The width of each peak along the p axis can be reduced further by raising the cutoff. Coherent energy is now better focused, paving the way for identifying and removing interfering seismic arrivals.

The Removal of Interfering Seismic Arrivals

The simulated interfering seismic arrivals PKP / PKP_{ab} and PKiKP / PKP_{bc} were identified within each of the five semblance filtered sub-sectioned slant stacks (based on their given apparent slownesses (p) and center-trace intercept times (T)), and then were isolated by forming tapered rectangles (with dimensions time (T) and apparent slowness (p)) around the concentrated areas of energy corresponding to each simulated interfering arrival within the coherency filtered sub-sectioned slant stacks. The results of one of these isolations in the T-p domain can be seen in Figure (2.9), in which the simulated PKP arrivals have clearly been isolated from all other seismic arrivals. Note the clear outlining of the PKP arrivals, and the lack of any other non-PKP energy within the isolated rectangular regions.

Within Figure (2.10), the results of removing the simulated PKP arrivals (by taking the difference between the coherence filtered sub-sectioned slant stacks and the isolated PKP slant stacks) are illustrated. From this, the quality of this removal is observed. Comparing the before

image Figure (2.8), which illustrates the semblance filtered sub-sectioned slant stacks, and the after-image seen in Figure (2.10), it becomes evident that the PKP removal was highly successful. There is no evidence that any other arrivals have been removed inadvertently, and is no sign that the process has affected energy from other arrivals.

Demonstrating the effective removal of simulated interfering seismic arrivals, without doing damage to other arrivals, is an important result. This allows investigators the opportunity to employ natural earthquakes that previously were excluded from analysis, and allows for the implementation of 2-D slant stack migration techniques (without the worry of misinterpreting known interfering seismic arrivals as possible sub-surface seismic reflectors). However, it is important to realize (with respect to real earth data) that any seismic arrival appearing after the TWT of the interfering arrival must be treated with some caution, even after removing the interfering arrivals. Particularly, this is the case if the arrival appears at a similar apparent velocity (p) to the interfering arrival itself, as there still exists the potential for the interfering arrival's reflections to be present within the data.

Step 12 (Inverse Slant Stacking)

Inverse Slant Stacking

Following the removal of interfering arrivals, inverse slant stacking was performed on the five-filtered sub-sectioned slant stacks (on the set which contained pre PKIKP data), resulting in the time-domain sub-sectioned gathers seen in Figure (2.11).

The resulting time-domain sub-sectioned gathers were then recombined to form a full time-domain gather, seen in Figure (2.12). Comparing this result with the original complex full-line gather, seen in Figure (2.6), we confirm the reliability and robustness of the adapted GloPSI workflow, as all the original simulated reflectors have been preserved, random noise has been

drastically reduced, and we no longer have the effects of interfering seismic arrivals present within the data. In addition (Figure 2.12), no noticeable artifacts are observed within the window preceding the arrival of PKIKP, indicating there are likely no major artifacts contained within the time window after.

Step 14 (2-D Slant Stack Migration)

2-D Slant Stack Migration

Utilizing the coherency and apparent velocity filtered sub-sectioned slant stacks, 2-D slant stack migration was performed (employing simple two-layer velocity model which assumed an average crustal velocity of 6.4 km/s to 55 km and an average upper-mantle velocity of 7.8 km/s to 110 km). The results were five depth migrated sections (Figure 2.13). The input synthetic data for this migration consisted of arrivals with a relatively narrow range of apparent slownesses (-0.01 to 0.01), simulating the flat nature of major subsurface interfaces. Because of this relatively narrow apparent slowness range migrated images, seen in Figure (2.13), appear nearly flat (the characteristic "smile" is absent). Additionally, migrated reflectors are generally migrated to positions which are nearly directly beneath the sub-arrays from which they are derived (an un-expected result with real data).

Within the migrated sub-sections (Figure 2.13) we observe migrated reflectors located in their appropriate locations (given the input synthetic section) (Figure 2.12 a). Note that the width of migrated reflection segments is directly controlled by the aperture of their corresponding arrays (which in this case is small compared to the length of the full array). Because of this, reflection segments within Figure (2.13) are seen to be narrow. This treatment provides a conservative interpretation of reflector positions, however, may make interpolation

between migrated segments difficult (it would be possible to expand this limit; however, it should be noted that confidence in the actual position of reflectors drops as this limit increases).

Figure (2.14) yields the results of combining the five-migrated synthetic sub-sections back to a single full-line gather. From this we see that all the input simulated reflectors have been recovered. However, because of the narrow length of the utilized sub-arrays compared to the total length of the array and the relatively narrow range of migrated apparent slownesses, we observe relatively large spaces between migrated reflectors. This result (and the interpolation difficulties that come with it) was considered when selecting sub-arrays involving real world data (the aim being to have enough closely spaced sub-arrays such that some of the risk involved with interpolating reflector lengths is reduced), and the migrated apparent ray parameter range was increased to allow reflectors to be migrated further from their corresponding sub-arrays, thus increasing lateral resolution of migrated data.

Natural Earthquake Results

For this study, a single natural earthquake was employed to test the reliability and robustness of the presented adapted GloPSI workflow. The event, a moment magnitude 6.1, occurred on 01/25/2014 along the Philippine subduction zone, at a depth of 66 km and an average distance of 153 degrees from the SESAME array. From this, three passive-source time-domain seismic reflection profiles were generated, and two depth-domain migrated sections were created. These included line-D, line-W and line-E, and line-W and line-E respectively. The results of each step of the adapted GloPSI workflow are presented here.

Steps 7-8 (Estimating the Source Time Function and Signal Deconvolution)

Estimating the Source Time Function

Estimation of the source time function was done for each single event line gather (line-D, line-W, and line-E) by stacking the static-corrected traces within each gather, and then zeroing out the resulting trace before the initial kick of PKIKP and after a number of seconds equal to the moment magnitude of the event after PKIKP (approximately 6 seconds for this study). The resulting source time functions can be seen in Figure (2.15). Notice that all three resulting source-time functions show a relatively long / energetic waveform representing PKIKP, and are otherwise empty. Notice too that all three-source time functions are relatively smooth, and include a variety of frequency contents, indicating that they likely represent reasonable interpretations of the actual source time functions.

Signal Deconvolution

Signal deconvolution was performed for each line gathers (Figures 2.16 a-f) utilizing the appropriate source-time function generated during estimation of the source-time function (step 7). Deconvolution compresses the initial arrival of PKIKP to a single (relatively impulsive) arrival, indicating that the effects of the source function have been sufficiently removed. At this point, the start of what may be real structure is visible within the deconvolved line gathers, however, it is important to note that the effects of interfering arrivals have not yet been removed, as can be seen with the very energetic arrivals of PKP / PKP_{ab} and PKiKP / PKP_{bc} (Figures 2.16 a-f). We observe no notable artifacts within the time window preceding PKIKP, suggesting the deconvolution has not imparted any undesirable signals onto the data. The results of signal deconvolution appear to be stable, an absolute necessity moving forward into the proceeding steps in the adapted GloPSI workflow.

Step 9 (Slant Stacking and Sub-sectioning)

Slant Stacking and Sub-sectioning

Figure (2.17 a-b) illustrates the results of sub-sectioning SESAME lines W and E.

Figures (2.18 b-c) demonstrate the results of slant stacking sub-section gathers of SESAME lines W and E to the T-p domain. An appropriate apparent ray parameter range for slant stacking was determined by slant stacking first with a large apparent ray parameter range (-0.2 to 0.2) to visually determine the range which would include the majority of meaningful arrivals. This range was determined to be -0.075 to 0.075 s/km (Figure 2.18 a). Notice the reduction of each simulated arrival from a line in the time-distance domain to a concentrated region in the T-p domain. Because time is referenced to the center of the subwindow, the slope of each region is horizontal. Due to the broadband nature of the input synthetic sections, we see in Figures (2.18 b-c) that slant stacking does not completely reduce the arrivals to concentrated points, rather, the stack results in a somewhat smeared regions in the T-p domain. Notice also the development of subtle alias fans (Phinney et al., 1981; Stoffa et al., 1981), emanating from each arrival's concentrated region in the T-p domain (Figure 2.18 b-c).

The slant stacks generated during this process 1) preserved the most important energy corresponding to each primary arrival (PKIKP, PKiKP, and PKP), 2) generated enough separation between arrivals to allow for the removal of both alias fans and random noise via semblance based coherency filtering, and 3) generated enough separation between arrivals to allow for the removal of interfering arrivals (with both semblance based coherency filtering and the removal of interfering arrivals occurring in subsequent processing steps).

<u>Steps 10-11</u> (Semblance Based Coherency Filtering and the Removal of Interfering Seismic Arrivals)

Semblance Based Coherency Filtering

Again, as with the synthetic examples, by employing semblance based coherency filters, the images seen in Figure (2.18 b-c) are generated; notice the elimination of alias fans, which previously emanated from each arrival. Also, notice the great reduction in random noise, and the increased concentration of energy with respect to each arrival. Finally, the outline of each concentrated point of energy within the slant stacks has become clearer, once again, paving the way for identifying and removing interfering seismic arrivals.

The Removal of Interfering Seismic Arrivals

The interfering seismic arrivals PKP / PKP_{ab} and PKiKP / PKP_{bc} were identified within each of the semblance filtered sub-sectioned slant stacks for each of the full-line gathers (line-D, line-W, and line-E) based on their given apparent slownesses (p) and center-trace times (T), and were then isolated by forming tapered rectangles (with dimensions of time and apparent slowness) around the concentrated areas of energy corresponding to each interfering arrival within the semblance filtered sub-sectioned slant stacks.

Within Figure (2.19 a-b), the results of removing PKP arrivals from SESAME line W and E are illustrated. From this, the quality of these removals is observed. Comparing the before images at the top of the figures, which illustrates the coherence-filtered sub-sectioned slant stacks, and the after-images at the bottom of the figures, which shows the coherence-filtered sub-sectioned slant stacks with the PKP arrivals removed, it becomes evident that PKP removal was highly successful. There is no evidence that any other arrivals have been removed inadvertently, and is no sign that the process has affected even a portion of the energy from other arrivals.

As in the synthetic case, demonstrating the effective removal of interfering seismic arrivals, without doing damage to other arrivals, allows investigators the opportunity to take advantage of earthquakes that previously were excluded from analysis. However, again, it is important to realize that any seismic arrival appearing after the TWT of the interfering arrival must be treated with some caution, even after removing interfering arrivals. Particularly, this is the case if the arrival appears at a similar apparent velocity (p) to the interfering arrival itself, as there still exists the potential for the interfering arrival's reflections to be present within the data.

Step 12 (Inverse Slant Stacking)

Inverse Slant Stacking

Once again, as in the synthetic case, following the removal of interfering seismic arrivals, inverse slant stacking was performed on each of the filtered sub-sectioned slant stacks, resulting in the time-domain sub-sectioned gathers.

Again, the resulting time-domain sub-sectioned gathers were then recombined to form full time-domain gathers for each of the three profile lines (line-D, line-W, and line-E), seen in Figure (2.20). However, in the case of real data, there are no reference lines to which to compare these results. In this case, based on the reliability and robustness of the preceding synthetic case, these profiles were assumed to represent accurate zero-offset time-domain reflection profiles (with potential errors in the location of reflected energy, because no migration has been applied). Direct interpretation of these time-domain images is not performed; rather these profiles are employed primarily as a ground-truthing tool for the proceeding depth migrated sections.

Step 14 (2-D Slant Stack Migration)

2-D Slant Stack Migration

Again, as in the synthetic case we migrated the coherence-filtered / apparent velocity filtered sub-sectioned slant stacks to produce a preliminary cross-section that represents our best-resolved interpretation of the broadband sub-surface structure of the southeastern United States. Once again, during the migration process care is taken to ensure that data is allowed migrate to its proper position by employing distance allowances on each side of the migrated gathers. Migration was performed for the SESAME lines W and E only because poor velocity constraint made migration of the D line inappropriate.

Figures (2.21 a-b) demonstrate the results of migrating the sub-section gathers of SESAME lines W and E. Examining Figure (2.21 a) we see that the migration of the W line has resulted in many reflectors (real and non-real) being placed at a number of depths. Sub-section 1 of line-W is further complicated by noise, which we were unable to fully remove from slant stacks. Sub-sections 2-7 show migrated reflectors, which are most likely the result of interfering arrivals which were not fully removed from the slant stacks, highlighting the possible dangers involved with utilizing earthquakes with distance ranges between 140 and 160 degrees.

However, we do observe the appearance of what may be real migrated reflectors at depths of ~20 km, ~30 km, and ~90 km (Figure 2.21 a).

Figure (2.21 b) demonstrates the results of migrating sub-sections of SESAME line-E. This migration produces very favorable results. We observe a drastic reduction of noise, and what appears to be a complete removal of interfering arrivals. We are left with migrated subsections that illuminate what are interpreted as real subsurface interfaces. We observe strong

reflection interfaces at depths of ~35 km and ~90-110 km which we interpret as the Moho and possible LAB / upper-mantle lithospheric reflectors respectively.

The resulting migrated sub-sectioned gathers (for lines W and E) were recombined to form full-migrated sections, seen in Figures (2.21 c-d). Though geologic insight was not the specific goal of this study, several interesting geologic reflectors were illuminated within the final 2-D depth migrated sections (especially so for line-E) even with this study only employed a single natural earthquake. Examining Figure (2.21 d), two reflectors are of particular interest. The first, appearing at approximately 40 km depth, is interpreted as the Moho. The second, appearing much deeper, around 90 km to 110 km depth, is interpreted as structure within the lower sub-crustal lithosphere, possibly the base of the lithosphere (LAB), in agreement with results from previous Sp receiver-function studies (Abt et al., 2010). The Moho depths are somewhat greater than previously observed (Parker, et al., 2016). For the purposes of this study, resolving targets at the same depths as have been resolved using alternate techniques is very encouraging, as this lends itself to the idea that this adapted GloPSI workflow has been able to resolve deep-reflection profiling targets that were previously not imaged using reflection seismic techniques. In addition, because these two reflectors are interpreted to be located at depths consistent with previous studies, we can to an extent feel safe in the assumption that data processed through this adapted GloPSI workflow is reliable and robust. Thus, this adapted GloPSI workflow is offered as a means for performing reliable and robust broadband passivesource seismic reflection profiling, using data derived from ultra-long traveled global phase natural earthquake seismic waves.

DISCUSSION AND FUTURE WORK

The primary focus of this study was to generate a usable, reliable, and robust workflow, which would allow for the generation of broadband reflection profiles using global phase seismic recordings of natural earthquakes over a broader distance range than previously employed.

Specifically, we focused on the use of data recorded by the SESAME broadband array, which was deployed in the southeastern United States from 2010 to 2014 (Parker, et al., 2013). To this end, the relatively new global seismic technique GloPSI (Yang, et al. 2012; Ruigrok and Wapenaar, 2012) was adapted using a host of reflection profiling techniques, of which many were originally designed for active-source seismic experimenting. Specifically, signal deconvolution, slant stacking, 2-D slant stack depth migration, and many of the seismic filtering techniques presented in this text, either have not been used within a GloPSI workflow, or have been used to a varying extent, and / or application. This study provides a framework in which these techniques and others can be used together, to overcome challenges associated with employing less than ideal, passive source seismic energy, to image a range of the earth's crust and mantle that is almost untouchable with ideal, active-source seismic energy.

However, parameters and techniques involved with maximizing the results of the 2-D slant stack depth migration process have not yet been fully determined and applied. Future work should focus on the determination and application of parameters used for migration, as well as the implementation of this adapted GloPSI workflow to seismic recordings of many natural earthquakes. With the results of approximately 16-25 natural earthquakes, brute stacking could be performed in both the time and depth domains, greatly increasing the quality of seismic reflection profiles. An improvement in profile quality of this magnitude would allow for much

more detailed interpretations of the sub-surface geology of the southeastern United States, especially within the sub-crustal lithosphere.

Along with fine-tuning the 2-D slant stack depth migration process, and using many more natural earthquake events, future work should include detailed examinations into the effects of earthquake magnitude and depth, as they are concerned with the results of our adapted GloPSI workflow. Utilizing much deeper earthquake events may allow for resolution of sub-surface structures at far deeper depths than what is presented in this study. Larger magnitude earthquake events may also generate seismic sources, which have much higher initial signal to noise ratios than signals used in the present study. On the other hand, larger magnitude sources may make signal deconvolution much more difficult, because of an increase in the duration of the source time function. These relationships, and more, should be addressed to maximize the final reflection imaging products.

Underside reflections have not been removed for this study, although, in the future this will be done through apparent velocity filtering. Arrival times and apparent ray parameters of underside reflections are predictable, permitting their isolation and removal. For this study, it is important to note that predicted underside reflections first arrive after ~17 seconds TWT and have apparent ray parameters that are greater than or equal to zero and closely match the apparent ray parameters of their respective parent arrivals. Energy arriving after ~17 seconds TWT with a negative apparent ray parameter therefore does not represent an underside reflection but rather likely represents a true mantle reflection. Within this study, reflections observed at depths of 90-110 km (line-E) are thus interpreted as real subcrustal lithospheric reflections. This interpretation may be further supported by evidence from migrated images showing the same reflections (90-110 km) but employing earthquake events that occurred at much greater depths

(therefore avoiding underside reflections). The inclusion of earthquake events that occur at much greater depths will be a focus of future GloPSI research.

Interpreted by this study (even using a single earthquake event), are a set of seismic reflections appearing at depths between 90 and 110 km. There are two main interpretations for the origin of these reflections, 1) reflections at these depths are generated by a drop in seismic velocity occurring at the lithosphere / asthenosphere boundary (LAB), and 2) reflections at these depths do not represent the LAB, but rather represent seismic velocity anomalies occurring within the middle to lower subcrustal lithosphere (Abt et al., 2010; Deschamps et al., 2008; Fischer et al., 2010; Yuan and Levin, 2014).

If these reflections represent a seismic velocity drop occurring at the LAB there are several possible geologic interpretations available to explain their origin. Priestly and McKenzie (2006) believe a combination of thermal contrast and grainsize variation occurring at the LAB (hotter / smaller grained asthenosphere and colder / larger grained lithosphere) possibly generates a sufficient reduction in seismic velocity to generate these reflections. Others (Abt et al., 2010) contend that the asthenosphere is highly water saturated when compared to a dry (water depleted) lithosphere and that some amount of partial melt may occur at the LAB. This interpretation considers the LAB as a possible "damp" solidus, trapping partial melt in the upper-asthenosphere (Abt et al., 2010). Partial melt and a rapid change in water saturation at the LAB could possibly generate a sufficient seismic velocity reduction to generate the observed reflections (Abt et al., 2010). Finally, some (Gung et al., 2003) contend that rapid variations in anisotropy at the LAB may be the origin of these reflections.

However, if these reflections are the result of seismic velocity anomalies within the subcrustal lithosphere there too are several possible geologic interpretations available to explain

their origin. Layers of partial melt within the subcrustal lithosphere are called on as a possible explanation; however, questions concerning water emplacement (required to produce partial melt within a relatively cold lithosphere) remain largely unanswered (Abt et al., 2010). Layers of melt cumulate (now solid) held over from a time when the subcrustal lithosphere was at a higher temperature are evoked as an explanation (Abt et al., 2010). These layers of melt cumulate have been hypothesized as having been enriched in pyroxene minerals which eventually cooled to form pyroxenite the lower seismic velocity of which may generate the observed seismic reflections (Abt et al., 2010). Rapid shifts in anisotropy may produce the observed reflections as mineral's seismic fast directions and slow directions are preferentially oriented by possible subcrustal lithospheric flow (Abt et al., 2010). Finally, it has been hypothesized that stacking of subducted slabs within the subcrustal lithosphere may account for the observed reflections (Abt et al., 2010).

Further investigation into the origin of these seismic reflections (observed between 90 and 110 km) and the nature of what is producing them will be key as work with GloPSI progresses. Understanding the subcrustal lithosphere / possible LAB beneath the SESAME array in the southeastern United States will have implications globally as researchers progress in unraveling the complex nature of this depth range.

Not interpreted by this study, are a whole host of seismic reflectors within the middle to upper crust. One interesting path of research would be to examine the results of many natural earthquakes, and attempt to match these uninterpreted reflectors to know features. In addition, reflectors that may not match to known features should be examined carefully, and some interpretation as to their origin should be made. Digital models could also be generated to

approximate the results of many natural earthquakes, helping to nail down specifics of the makeup of the sub-surface beneath the SESAME array.

The future of the GloPSI method in general, as well as the future of the adapted GloPSI method presented within this text, are only truly limited by the imaginations of the people working to utilize them. There are an endless number of seismic techniques waiting to be retooled and plugged into the process. If there is a problem that presents itself, there is also a solution ready to be called upon. With continued work, and continued interest, the GloPSI method, and its adaptation within this study, could be applied along with any number of different methods and / or modeling techniques, to better understand the earth beneath our feet, and to continue to see the un-seeable.

CONCLUSIONS

Through the development of an adapted GloPSI workflow, which intended to employ passive-source global phase broadband seismic recordings derived from natural earthquakes, to produce broadband reflection profiles of the southeastern United States, beneath the former location of the SESAME seismic array, we come to five major conclusions.

First, the adapted GloPSI workflow presented within this text offers a set of reliable and robust seismic methods which allow for reflection imaging of the earth using broadband earthquake derived seismic waves. Particularly, this method generates meaningful reflection images even using a single natural earthquake event, meaning with the addition of many more earthquake events, this method will likely allow for the generation of images which permit very high quality interpretations of sub-surface structure, even making many types of digital modeling possible, including rock physics modeling.

Second, signal deconvolution as it is employed within this study is a viable method for removing the effects of seismic sources from broadband reflection profiles. Previous studies employing the general GloPSI method, have utilized the method of auto-correlation to accomplish this processing task. Signal deconvolution offers an alternative to the auto-correlation method that provides better resolution of structure within the upper crust.

Third, the slant stacking processes employed within this study, along with the processes for removing interfering seismic arrivals, offer huge advantages in terms of the number of usable earthquake source events for GloPSI processing. Previous work suggested that distance ranges from seismic source to receiver between 135 degrees and 150 degrees were unusable, because interfering seismic arrivals hampered the identification of PKIKP and associated reflections (Ruigrok and Wapenaar, 2012). However, slant stacking and the removal of interfering arrivals deals with both issues, greatly increasing the number of usable earthquake source events.

Fourth, 2-D slant stack depth migration offers a meaningful and reliable method for migrating data within the T-p domain into the seismic depth domain. Previously, GloPSI was almost exclusively performed only in the time-domain. This improvement, along with future work, will allow for far more detailed analysis and modeling of the sub-surface of the southeastern United States, and will permit more direct comparisons of future results with previous work, including the results of the COCORP experiments (Cook and Vasudivan, 1979).

Fifth and finally, the adapted GloPSI method presented here offers further interpreted constraints on the depth of the continental Moho and is the first reflection profiling technique to image what is interpreted to be structure within the sub-crustal lithosphere of the southeastern United States. We image the continental Moho beneath the Atlantic Coastal Plain at depths of roughly 35-40 km, and we place deeper lithospheric structure at depths between 90 km and 110

km, a similar depth to what was interpreted (using Sp receiver functions) by Abt et al. (2010) as the base of the lithosphere (LAB). Future studies, which will employ many natural earthquake events, will be able to further constrain these depths, and better interpret the sub-surface geometries of these features, as well as many other geologic features, which will likely be revealed with brute stacking of reflection profiles.

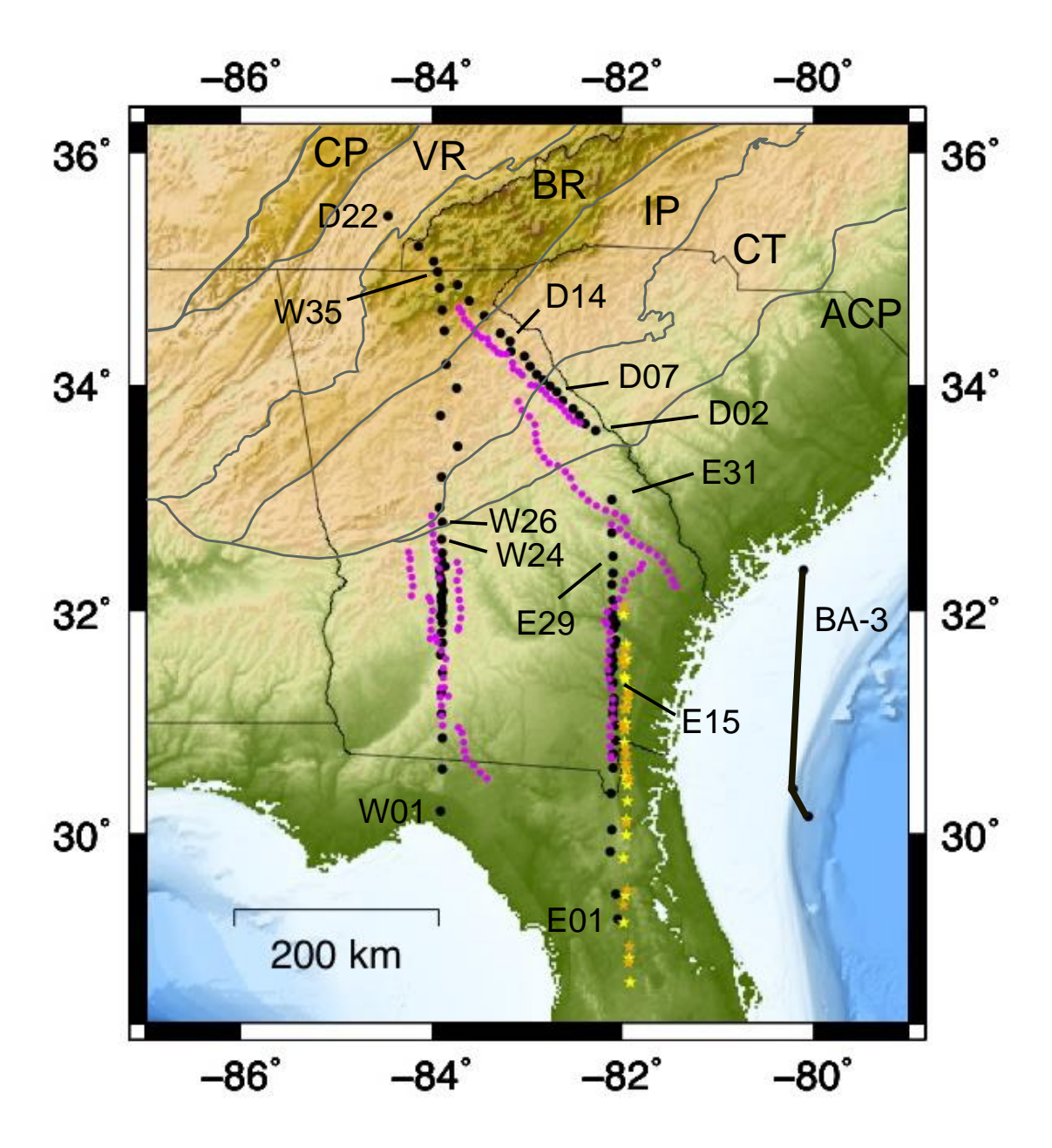
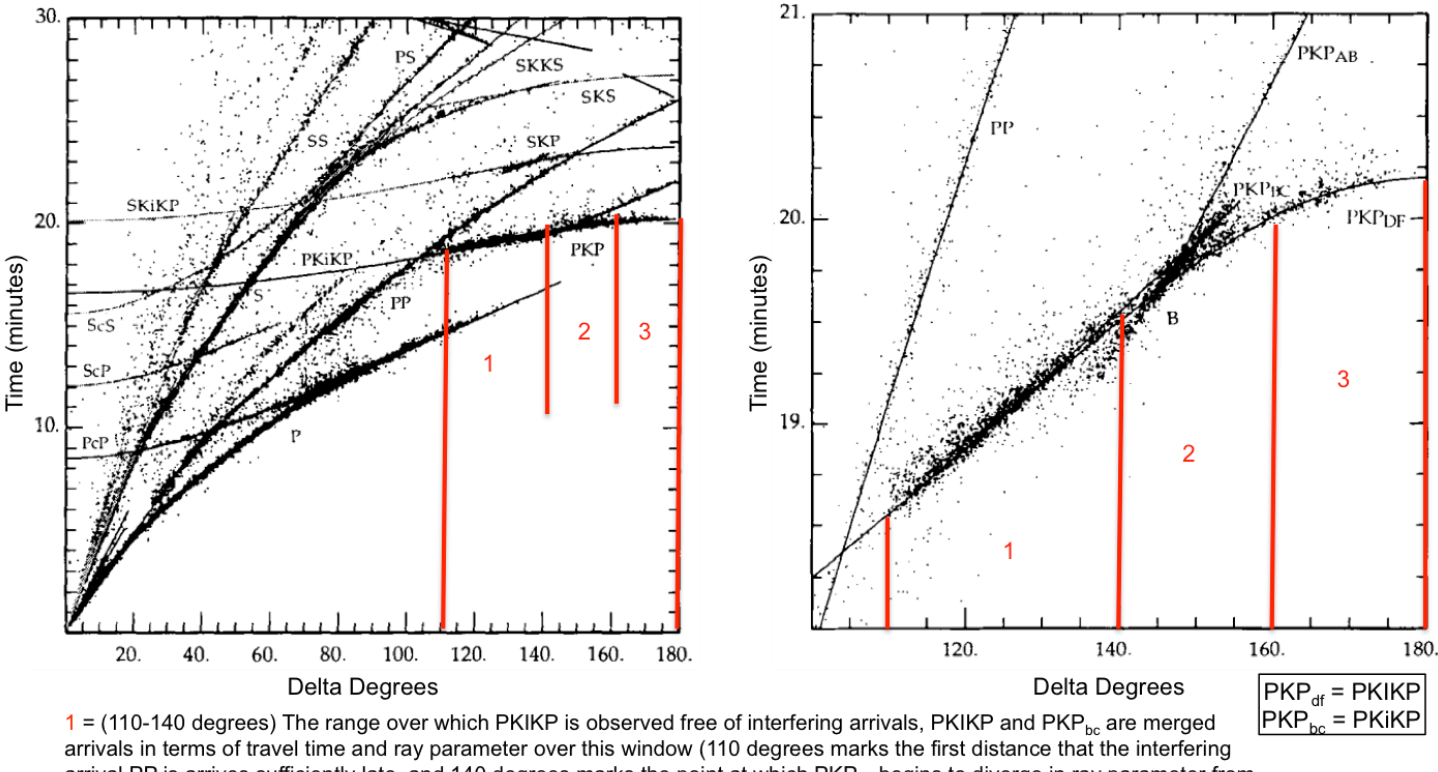


Fig. 2.1 Map of a portion of the southern Appalachians and Atlantic Coastal Plain (from Parker et al., 2016) showing stations of the SESAME array. The black dots indicate the locations of SESAME stations, and the pink dots show the former locations of COCORP stations in 100 station intervals.

PKIKP / PKP Travel Time Curves



arrival PP is arrives sufficiently late, and 140 degrees marks the point at which PKP_{bc} begins to diverge in ray parameter from PKIKP)

 2 = (140-160 degrees) The range over which PKIKP and PKP_{bc} have diverged in terms of travel time and ray parameter sufficiently that PKP_{bc} appears as an interfering arrival, and over which PKP_{ab} appears as a high ray parameter interfering arrival.

3 = (160-180 degrees) The range over which PKIKP is observed as the first seismic arrival, with all other seismic arrivals appearing sufficiently late, leaving an interference free window featuring only PKIKP.

Fig. 2.2 Travel time figures modified from Kennett and Engdahl (1991), showing travel times for seismic phases (real earth data plotted as points, and iasp91 modeled data plotted as lines). Note that real earth data has been corrected to surface focus depths (Kennett and Engdahl, 1991).

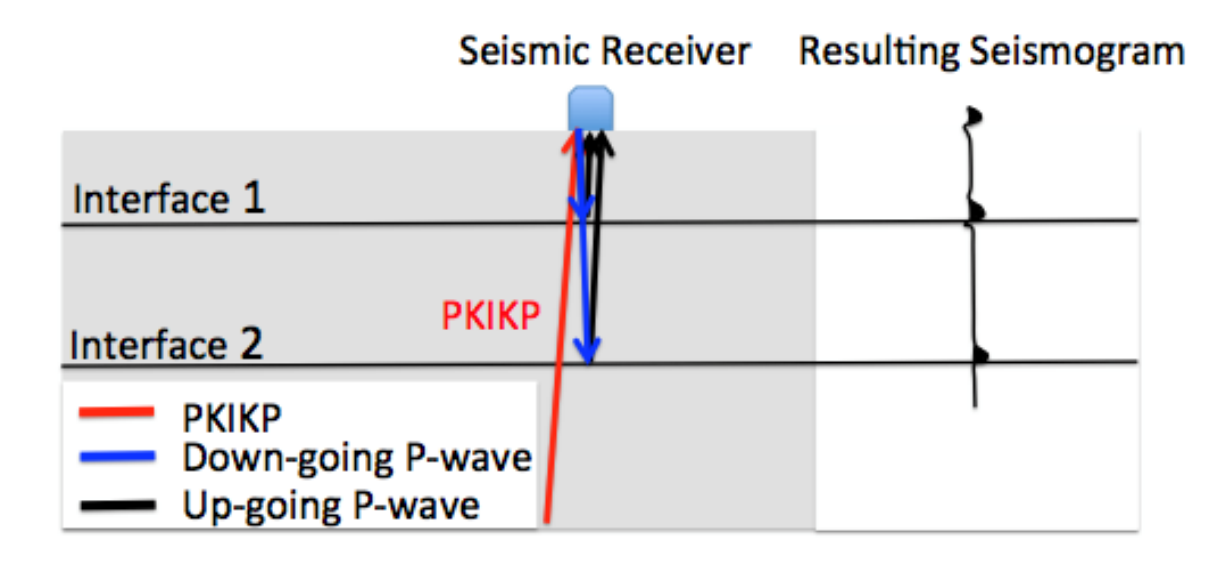


Fig 2.3 Simplified cross-sectional model showing the basics behind the global-phase seismic interferometry method. PKIKP strikes the underside of the array at near-vertical incidence acting as a virtual seismic source for near-vertical p-wave reflections.

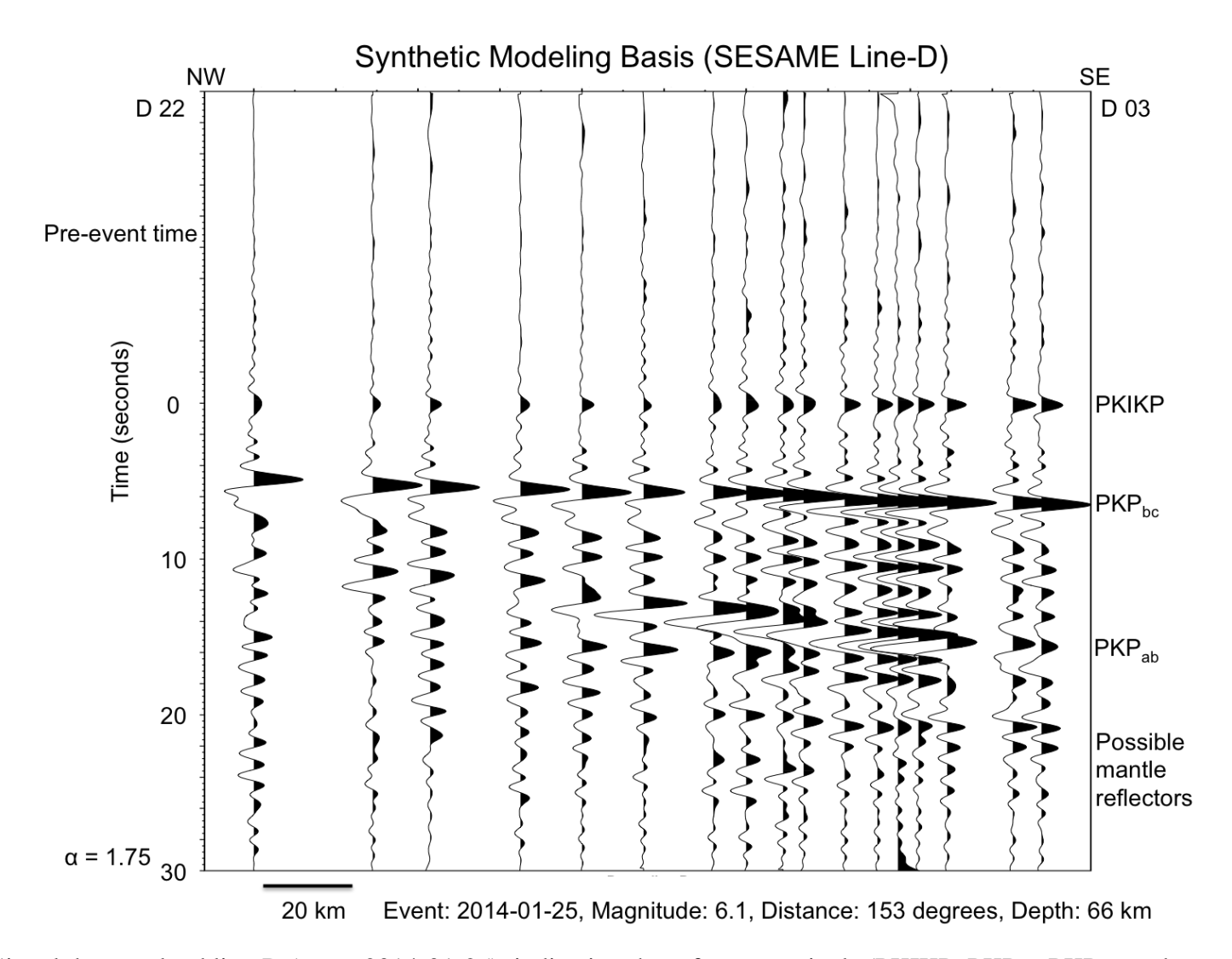


Fig. 2.4 Signal deconvolved line-D (event 2014-01-25), indicating the reference arrivals (PKIKP, PKP_{ab}, PKP_{bc}, and two possible mantle reflectors) common to the generation of the seven synthetic seismic sections utilized by this study. Note the apparent velocities of the events, the arrival's relative amplitudes, and that all five events extend the length of the gather, as these features were incorporated through the full extent of the presented synthetics.

Simple Synthetic Construction

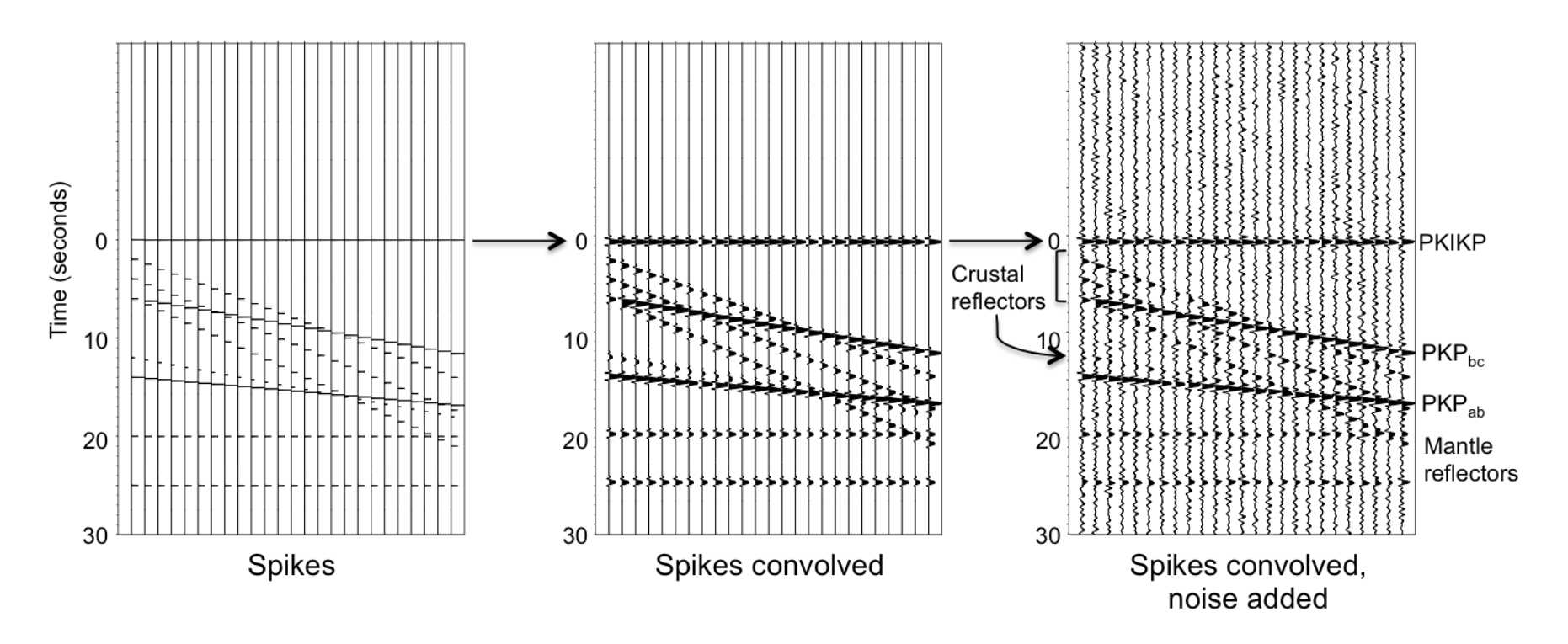


Fig. 2.5 Incremental construction of a synthetic profile, starting with a series of arrivals represented as spikes (furthest left), moving to those spikes convolved with a simple simulated waveform (center), and finishing with the addition of random noise (furthest right).

Complex Synthetic Construction

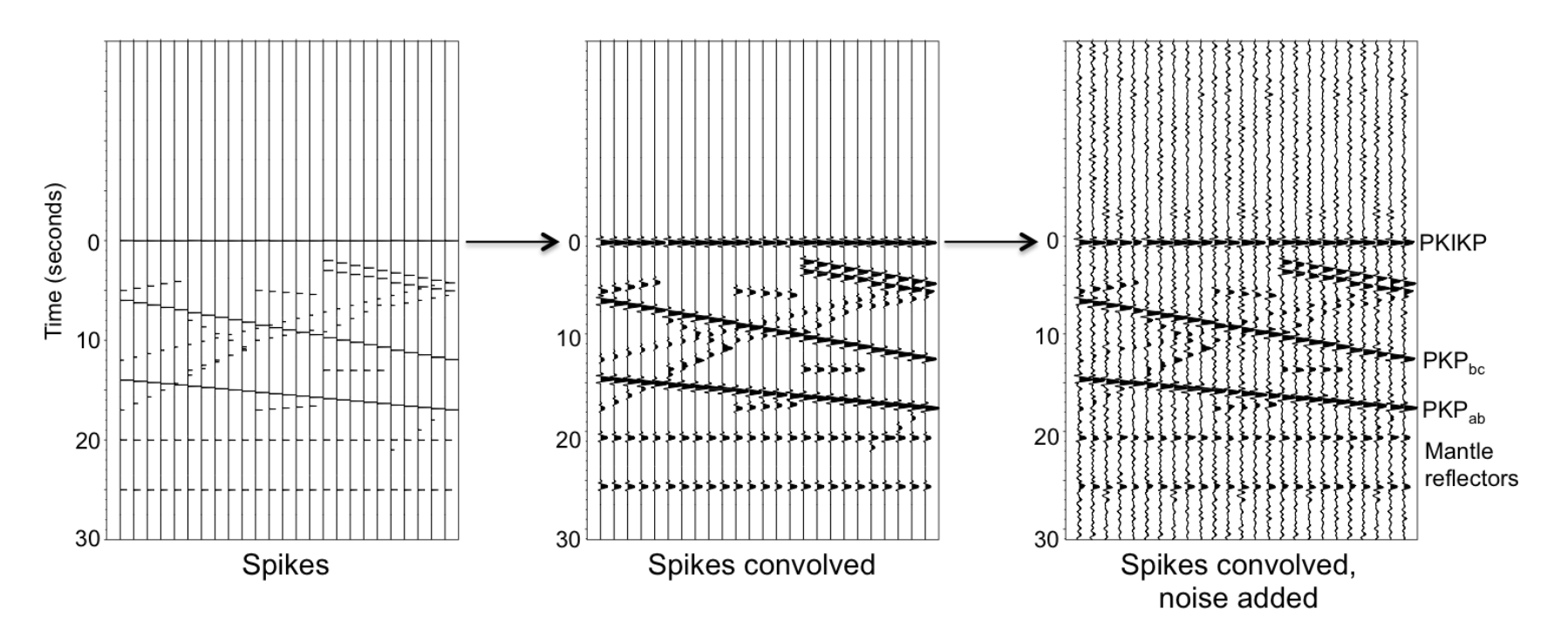


Fig. 2.6 Incremental construction of a synthetic profile, starting with a series of arrivals represented as spikes (furthest left), moving to those spikes convolved with a simple simulated waveform (center), and finishing with the addition of random noise (furthest right). To more realistically simulate real earth structure, the unlabeled reflectors represent crustal reflectors of varying apparent velocities and horizontal extents, i.e. many of the reflectors do not span the length of the gather.

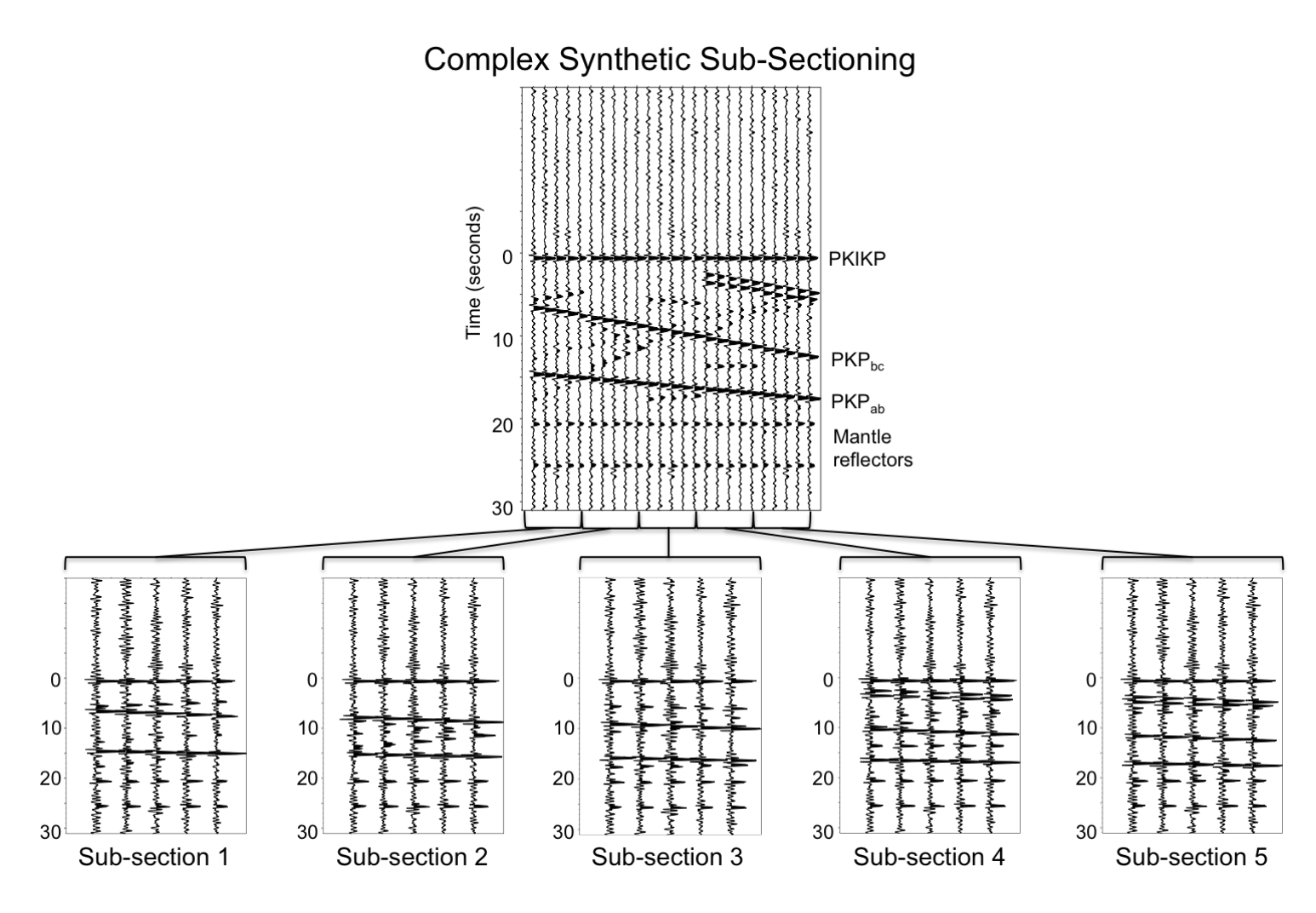


Fig. 2.7 Sub-sectioning of the full-line complex synthetic profile into five smaller sub-sectioned gathers. The unlabeled arrivals represent crustal reflectors of various apparent velocities and horizontal extents. The width of each subsection is chosen to span but not exceed the width of individual reflection branches. This ensures a maximum coherency measure when each subsection is slant stacked.

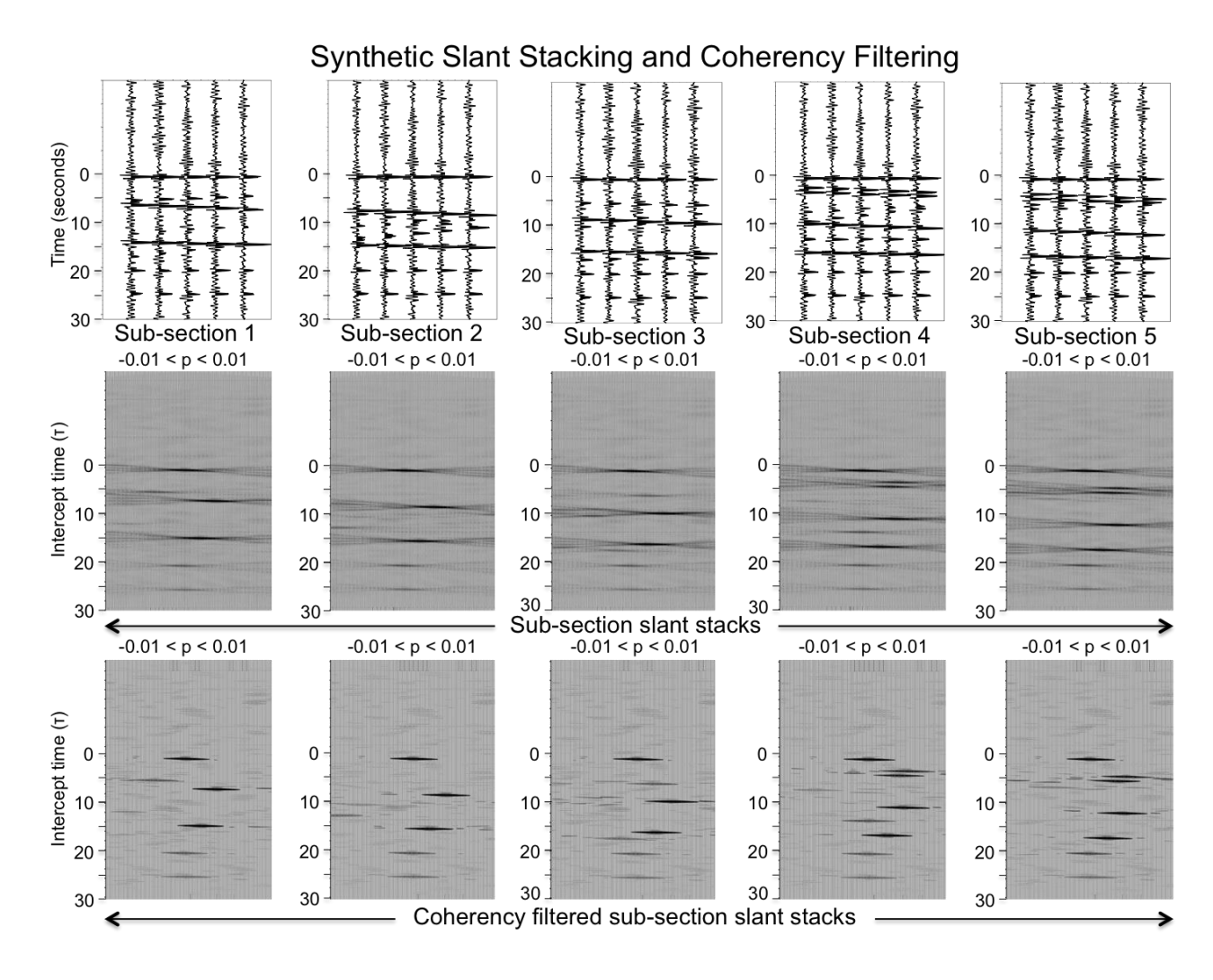


Fig. 2.8 Sub-sectioned gathers (top) slant stacked into the T-p domain (middle), where T is travel time referenced to the center of the gather and p is horizontal apparent slowness (inverse apparent velocity). Bottom: slant stacks after coherency filtering using semblance (lower cutoff: 0.7, for an original range of 0-1) as a measure of coherence. Note the transformation of arrivals from linear segments in the T-X domain to more localized regions in the T-p domain. In general, increasing the distance range of the input gather will decrease the width of the T-p peaks, yielding better resolution in p.

Removal of Interfering Arrivals through Apparent Velocity Filtering

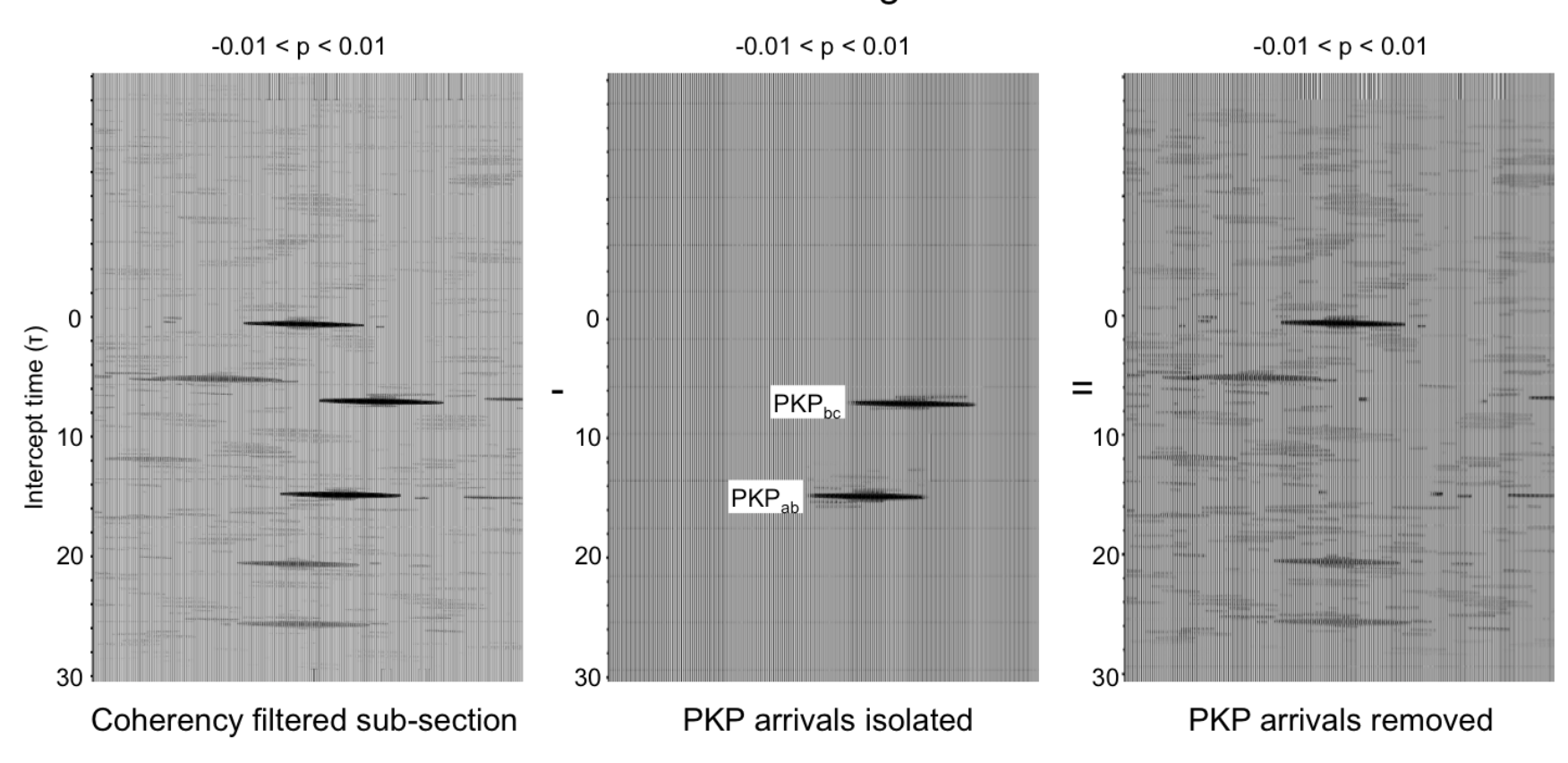


Fig. 2.9 Interfering PKP arrivals removed through apparent velocity filtering. Notice interfering arrivals are easily identified within coherency filtered slant stacks (left), isolated with no indication of sacrificed non-interfering signal (middle), and subtracted from the original slant stack (right). This, providing a clean base for inverse slant stacking back to the time domain, and for 2-D slant stack depth migration.

Apparent Velocity Filtering Sub-section 1 Sub-section 2 Sub-section 3 Sub-section 4 Sub-section 5 -0.01-0.01-0.01 < p < 0.01 -0.01-0.01Intercept time (T) 0 0 0 10-10 10-10 20 20-20 -20 -20-30 30 -30 30 30 Coherency filtered sub-section slant stacks -0.01-0.01-0.01-0.01-0.010 0 10-10 10 10-10-20-20 -20-20 20 30 30 30 30 30 Apparent velocity filtered sub-section slant stacks

Fig. 2.10 The results of apparent velocity filtering (bottom) each of the five coherency filtered sub-sectioned synthetic slant stacks (top). Note the clean removal of interfering PKP arrivals (appearing at approximately 10 and 16 seconds respectively), and that there appears to be no evidence to suggest non-interfering arrivals have been removed.

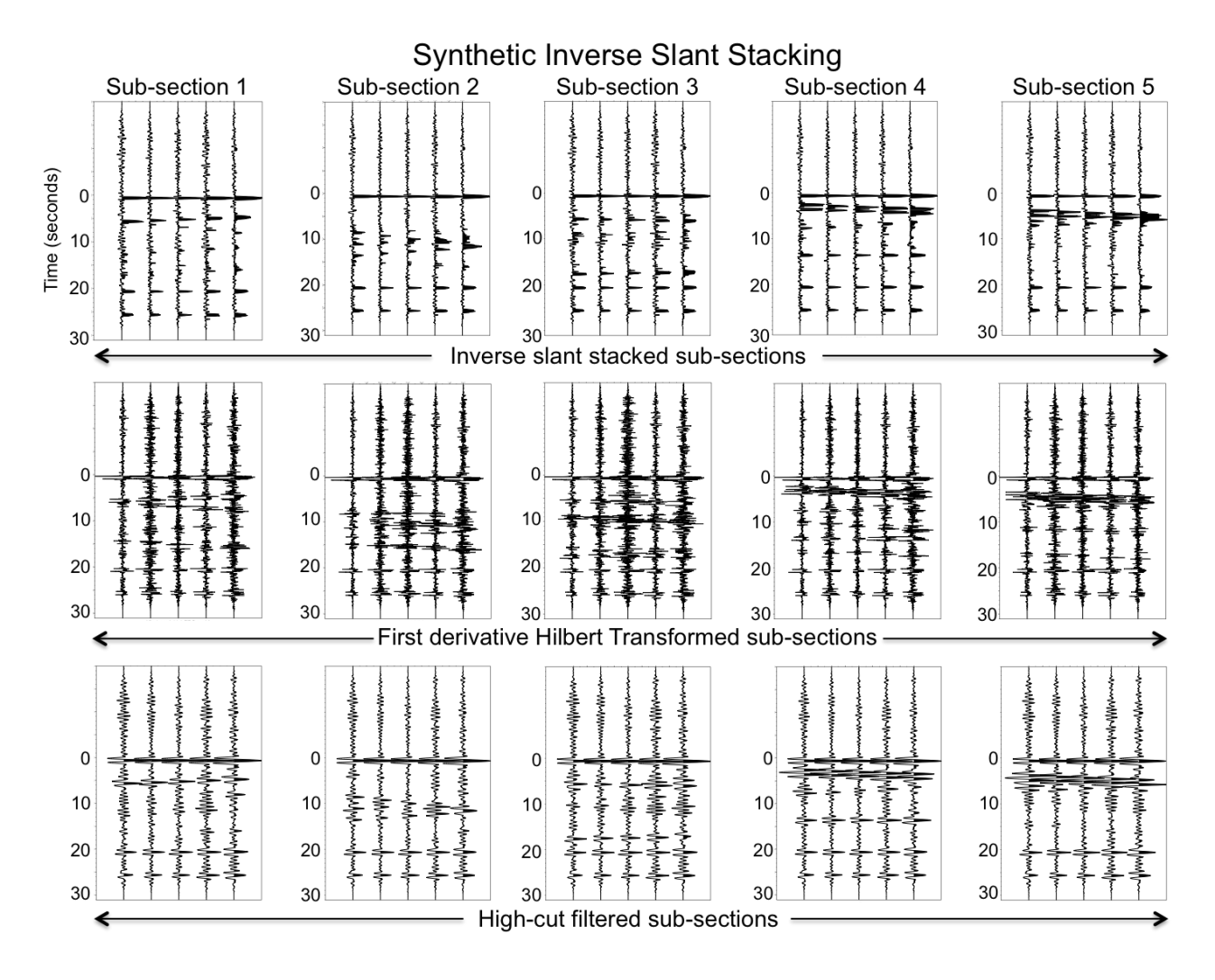


Fig. 2.11 Inverse slant stacking (top) of apparent velocity filtered synthetic slant stacks, and the results of applying the first derivative of the Hilbert transform (middle) and a mild high-cut filter (bottom). Notice the low frequency nature of the initial inverse slant stacked sections (top). This was compensated for with the first derivative of the Hilbert transform (middle). This also amplifies noise at higher frequencies outside the dominant signal bandwidth, thus necessitating the mild high-cut filter (bottom), and restoring the waveforms to an appropriate frequency range.

Full Complex Synthetic

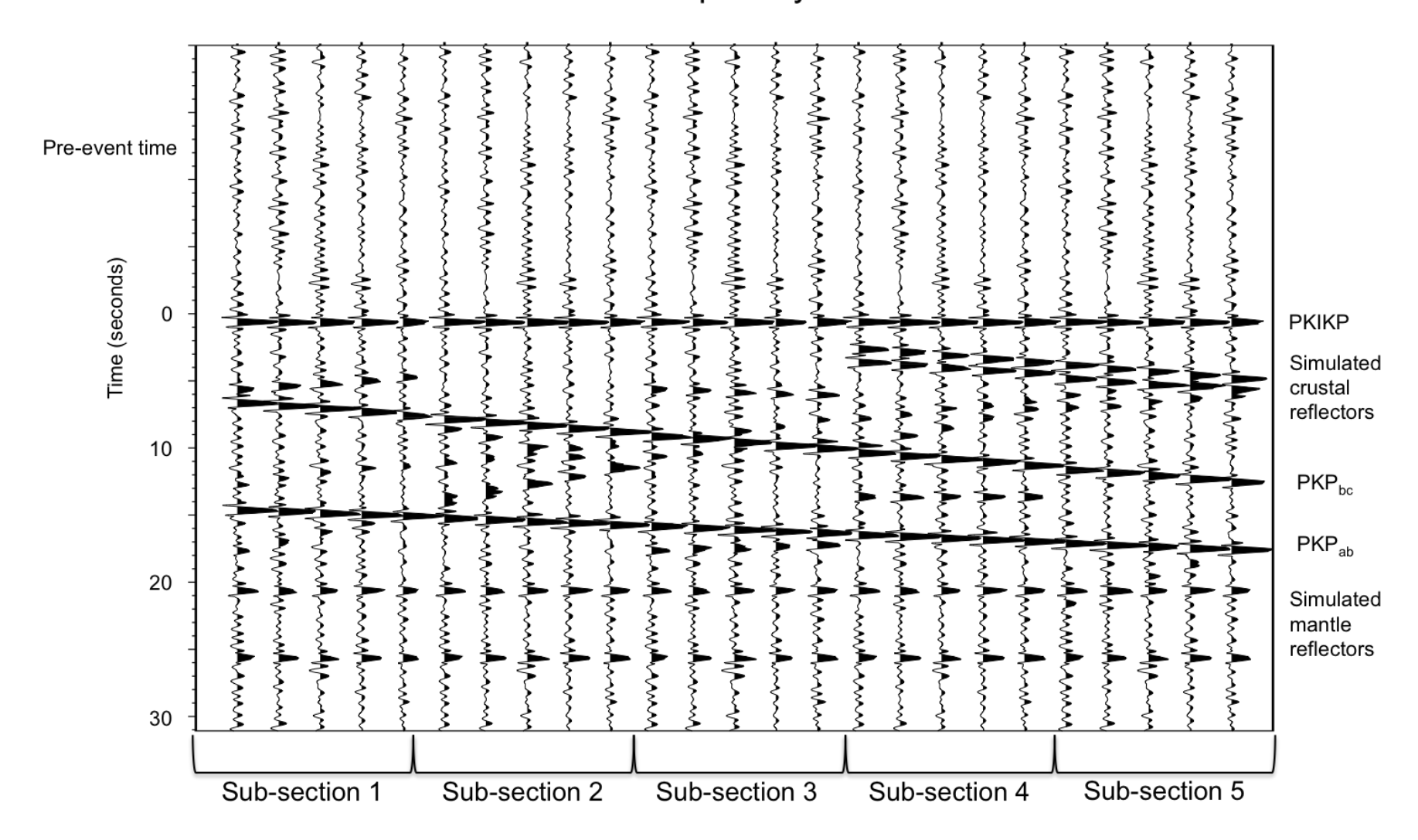


Fig. 2.12 a The full complex synthetic model before it has been apparent velocity and coherency filtered. Note the positions of simulated reflectors, and of the interfering PKP arrivals. This image is intended as a guide for interpreting fig. (2.12 b).

Full Recovered Complex Synthetic

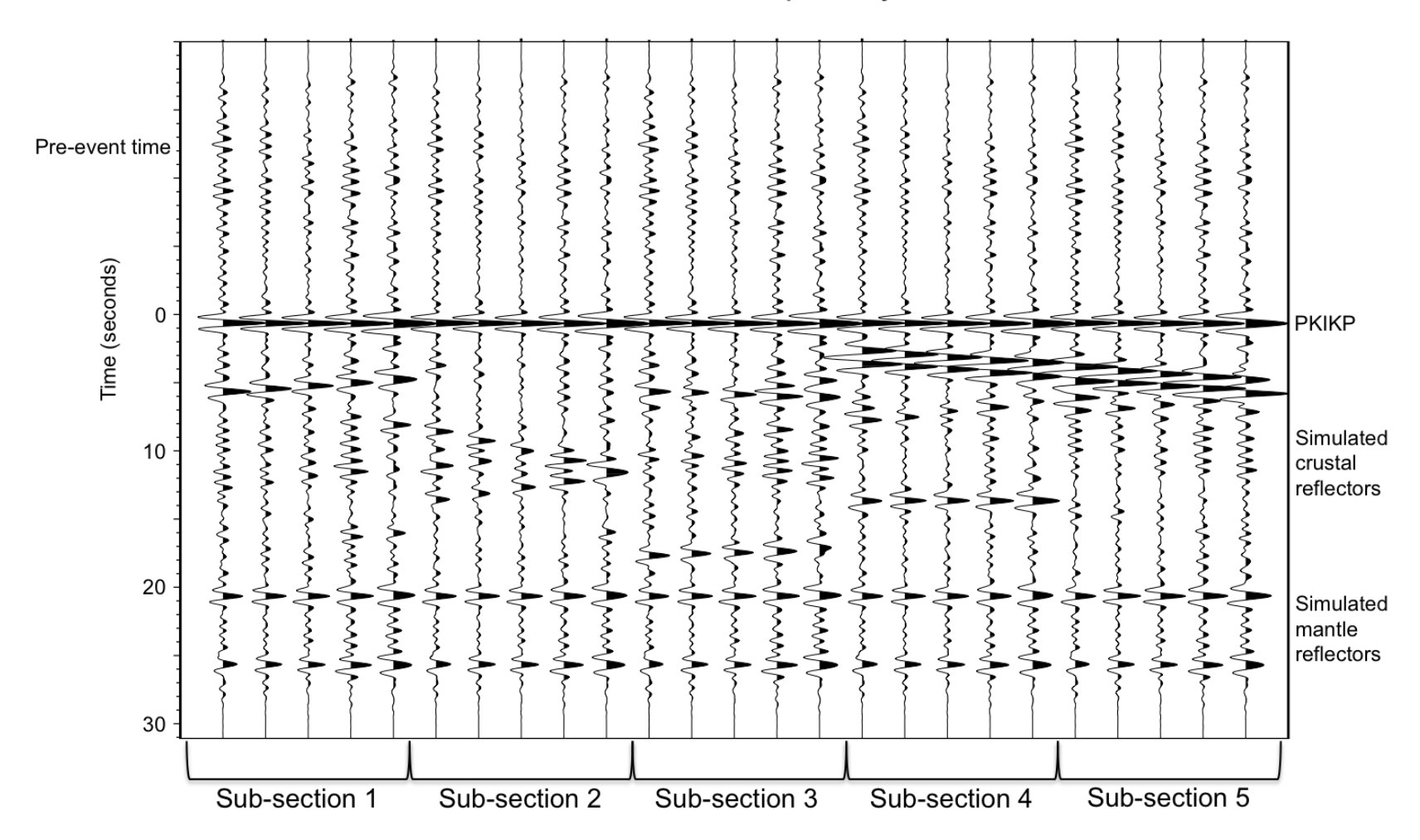


Fig. 2.12 b The result of combining the five recovered sub-sections to form a fully recovered synthetic section. Notice the high quality recovery of PKIKP, the simulated mantle reflectors, and the simulated crustal reflectors. Notice also, the complete removal of the interfering PKP arrivals, which formerly swept clear across the gather. Finally, note the great reduction in random noise as a result of the coherency filtering process.

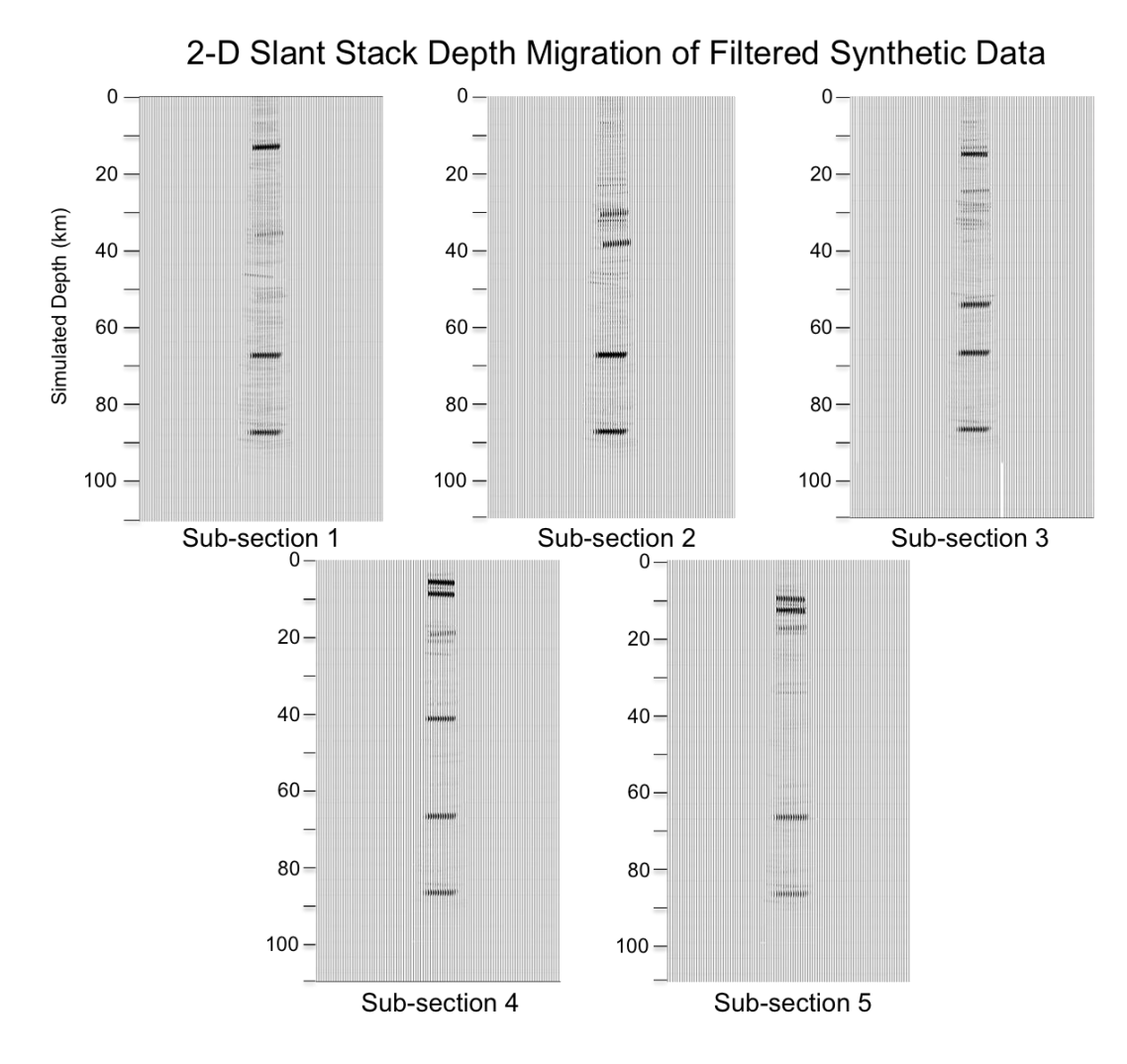


Fig. 2.13 The results of performing slant stack depth migration on filtered sub-section slant stacks. Note the addition of extra space on either side of each sub-sectioned gather, allowing for migration of data to positions outside the original horizontal extent of the gathers. Notice the formation of subtle artifacts on the edges of each migrated region; these disappear due to constructive interference when sections are subsequently added together. Finally, note that this migration was performed using a simple 2-layer velocity model, which assumed an average crustal velocity to 55 km depth, and an average mantle velocity down to 100 km depth.

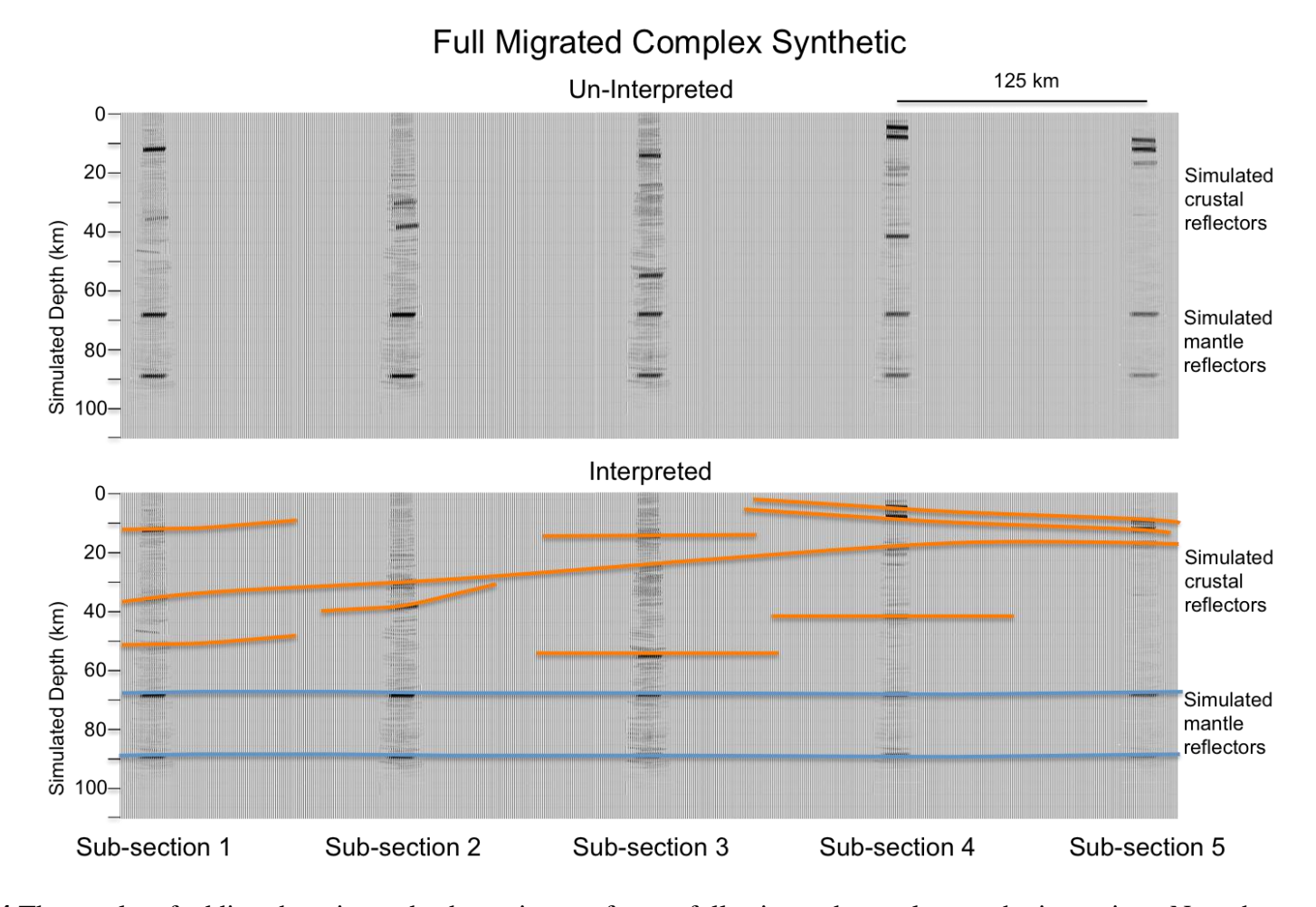


Fig. 2.14 The results of adding the migrated sub-sections to form a full-migrated complex synthetic section. Note the preservation of key crustal reflectors, as well as simulated mantle reflectors. Notice we only observe slight smearing of arrivals, relative to their dominant frequencies, and that most migration artifacts have been eliminated, as a result of summing the sub-sections to form a full-line image. Take notice of how well the full GloPSI workflow is able to preserve relatively small-simulated reflectors, and that even simulated reflectors with initially small relative amplitudes are preserved. Note we have taken a conservative approach to the width of drawn reflectors; this treatment becomes necessary when dealing with real data, helping to prevent un-realistic sub-surface interpretations.

Estimated Source Time Functions

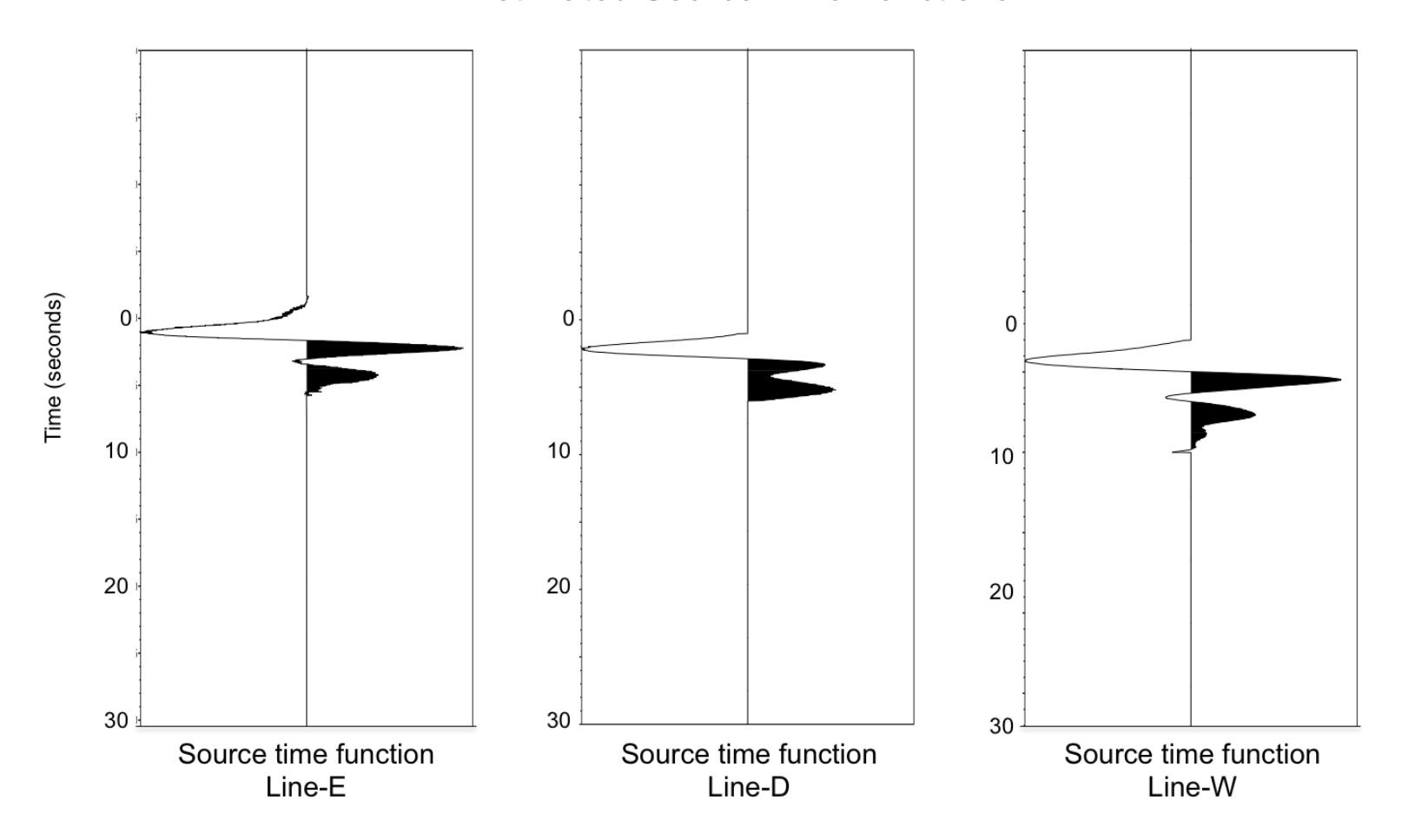


Fig. 2.15 Estimated source time functions for each of the three lines of the SESAME array. Note the length of each is restricted to the length in seconds of the magnitude of the source earthquake, in this case around 6 seconds. Notice also that each STF has been zeroed out beyond this time window.

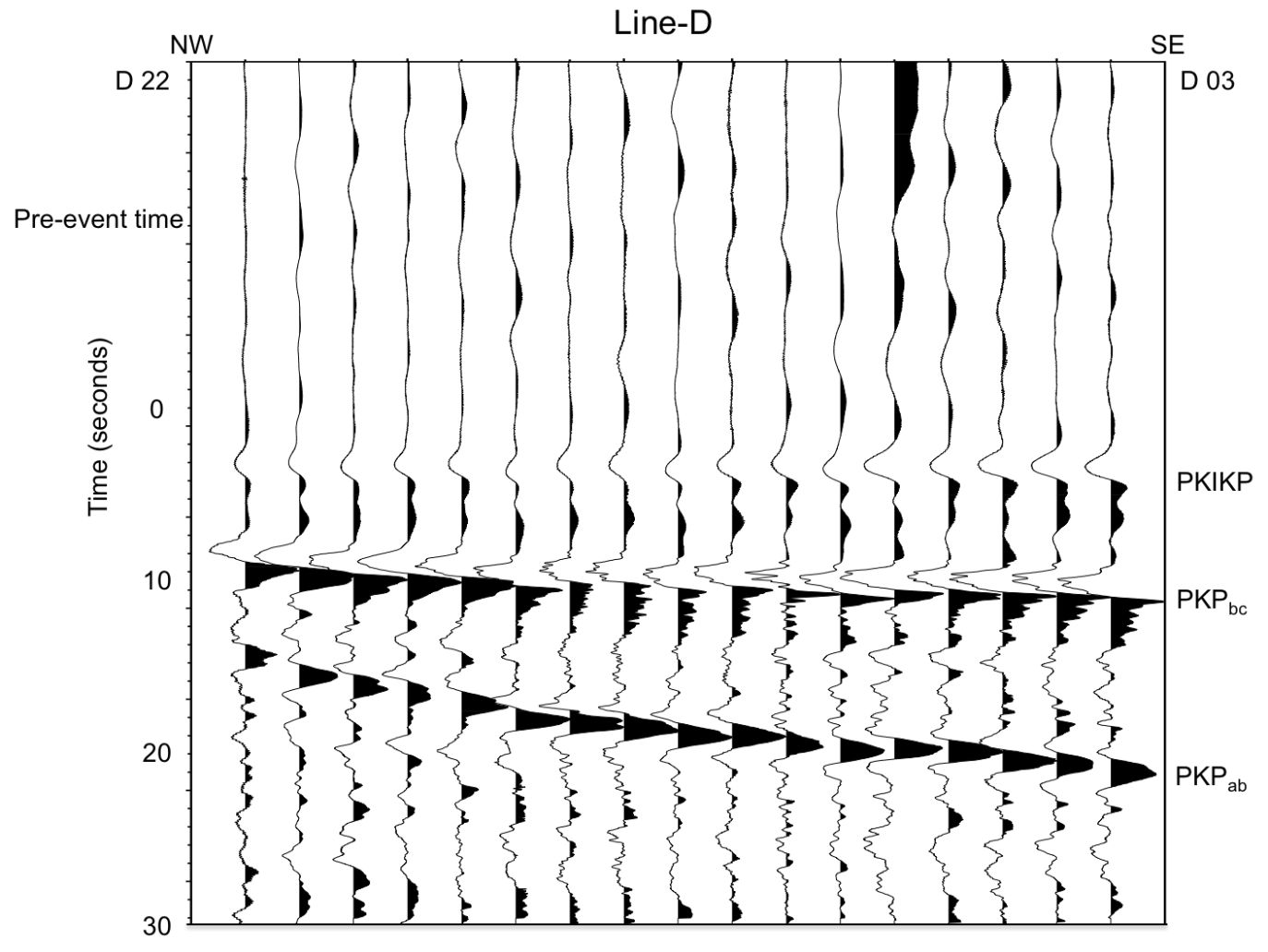


Fig. 2.16 a SESAME line-D prior to signal deconvolution, note the long (~ 6 second) duration of the apparent source time function. Notice also the clear difference in apparent velocities between PKIKP and the interfering PKP arrivals. Finally, note that stations (to this point) have been plotted with equal spacing's to make visual verification of cross-correlation statics easier.

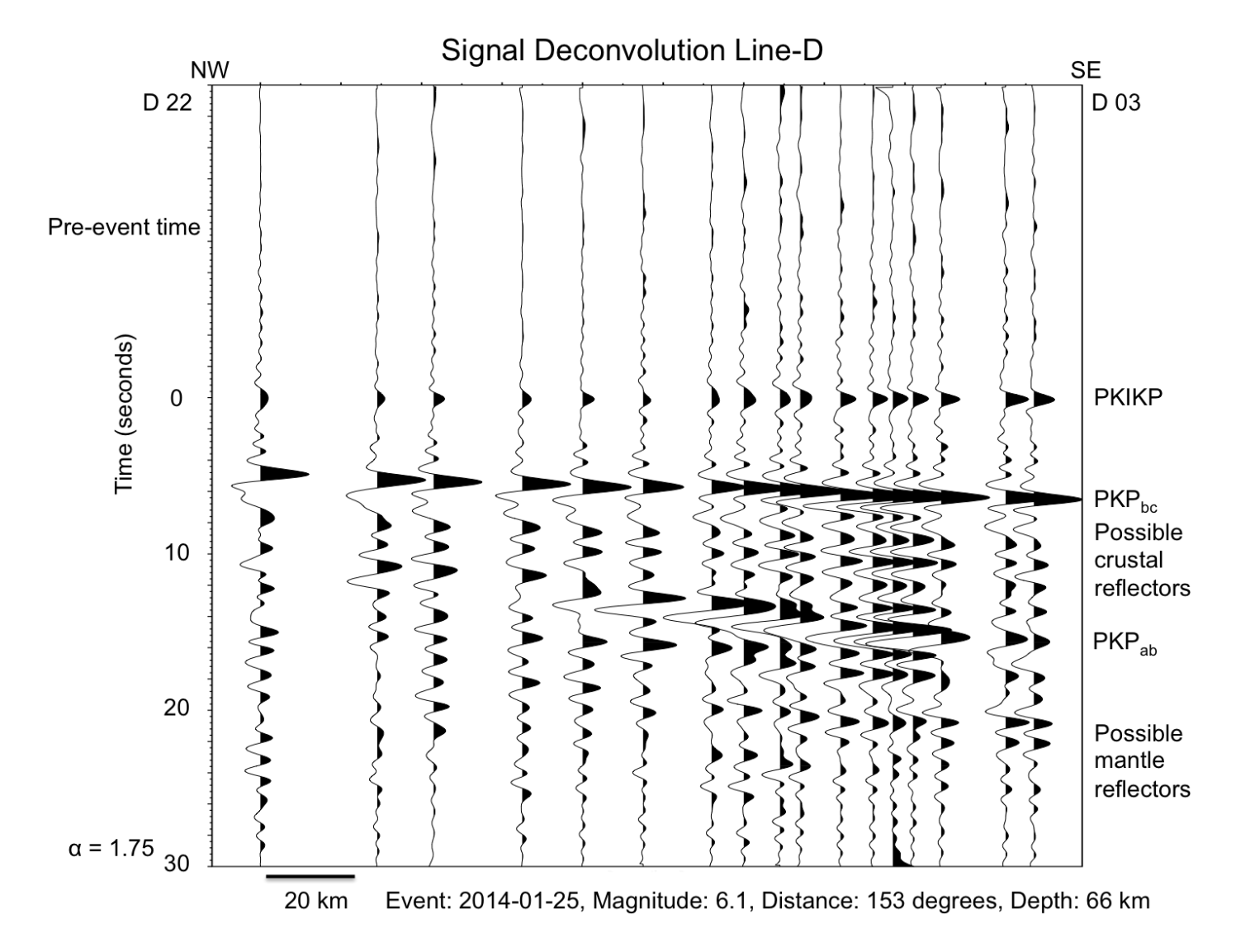


Fig. 2.16 b The results of signal deconvolution for the SESAME array line D. Notice the concentration of energy from formerly extended waveforms to relatively impulsive arrivals for PKIKP, PKP_{ab}, and PKP_{bc}. Also note the emergence of what may be real crustal structure, and possible mantle reflectors.

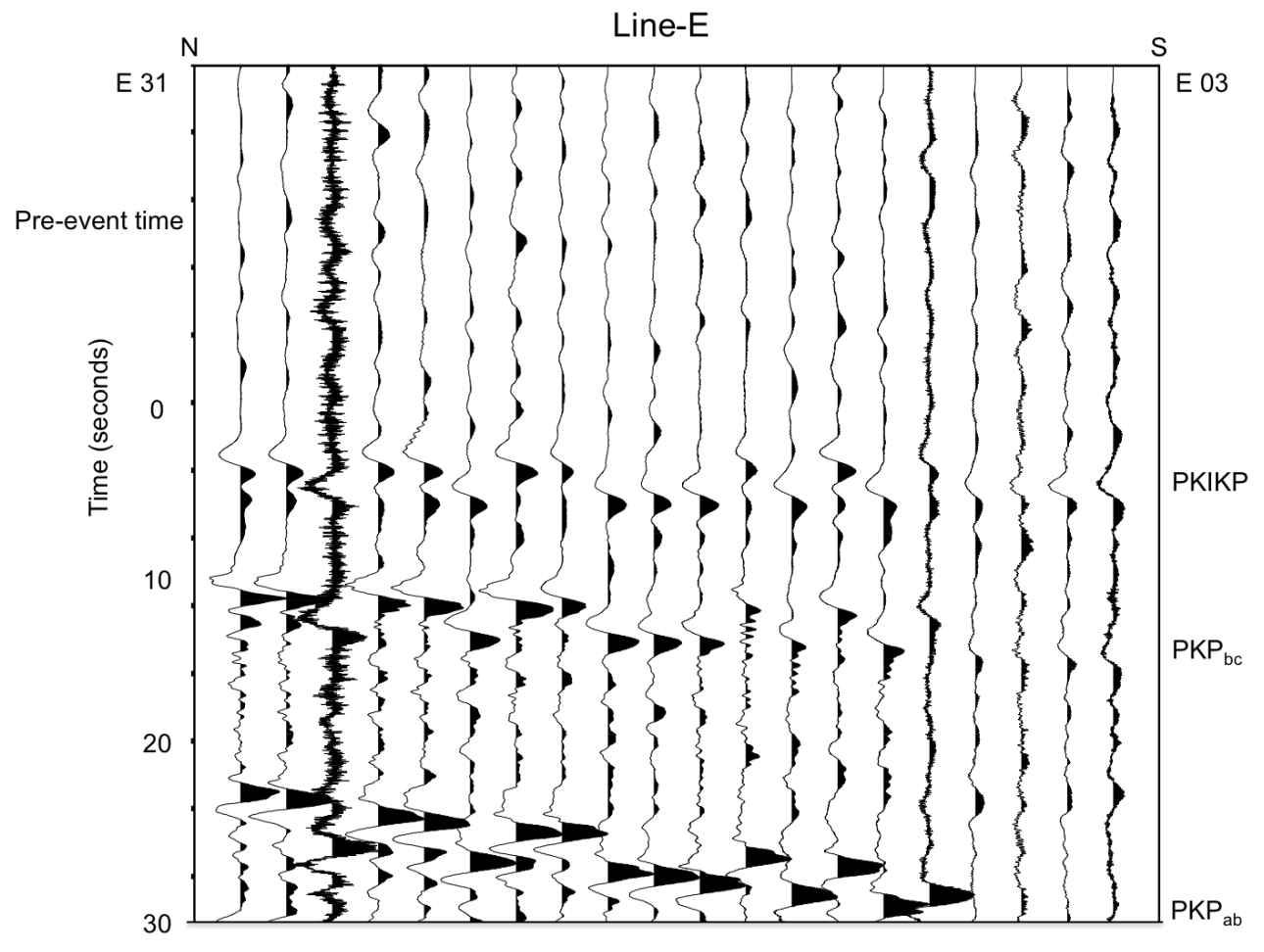


Fig. 2.16 c SESAME line-E prior to signal deconvolution, note the long (~ 6 second) duration of the apparent source time function. Notice also the clear difference in apparent velocities between PKIKP and the interfering PKP arrivals. Finally, note that stations (to this point) have been plotted with equal spacing's to make visual verification of cross-correlation statics easier, and that the use of cross-correlation statics were applied twice for this line, one time prior to deconvolution, and again after deconvolution. The second round of cross-correlation statics fixed the very apparent miss-alignment seen here.

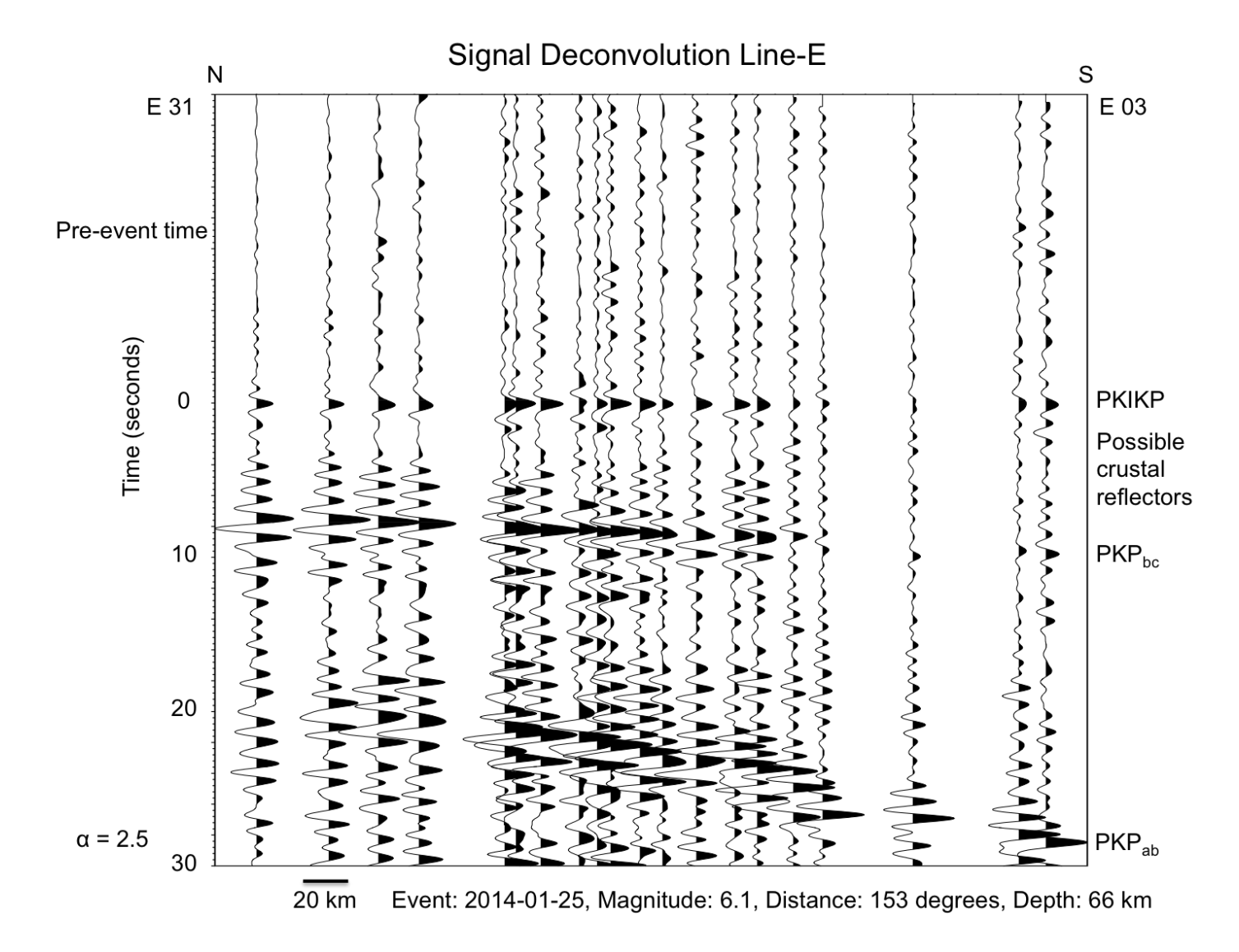


Fig. 2.16 d The results of signal deconvolution for the SESAME array line E. Notice the concentration of energy from formerly extended waveforms to relatively impulsive arrivals for PKIKP, PKP_{ab}, and PKP_{bc}. Also note the emergence of what may be real crustal structure.

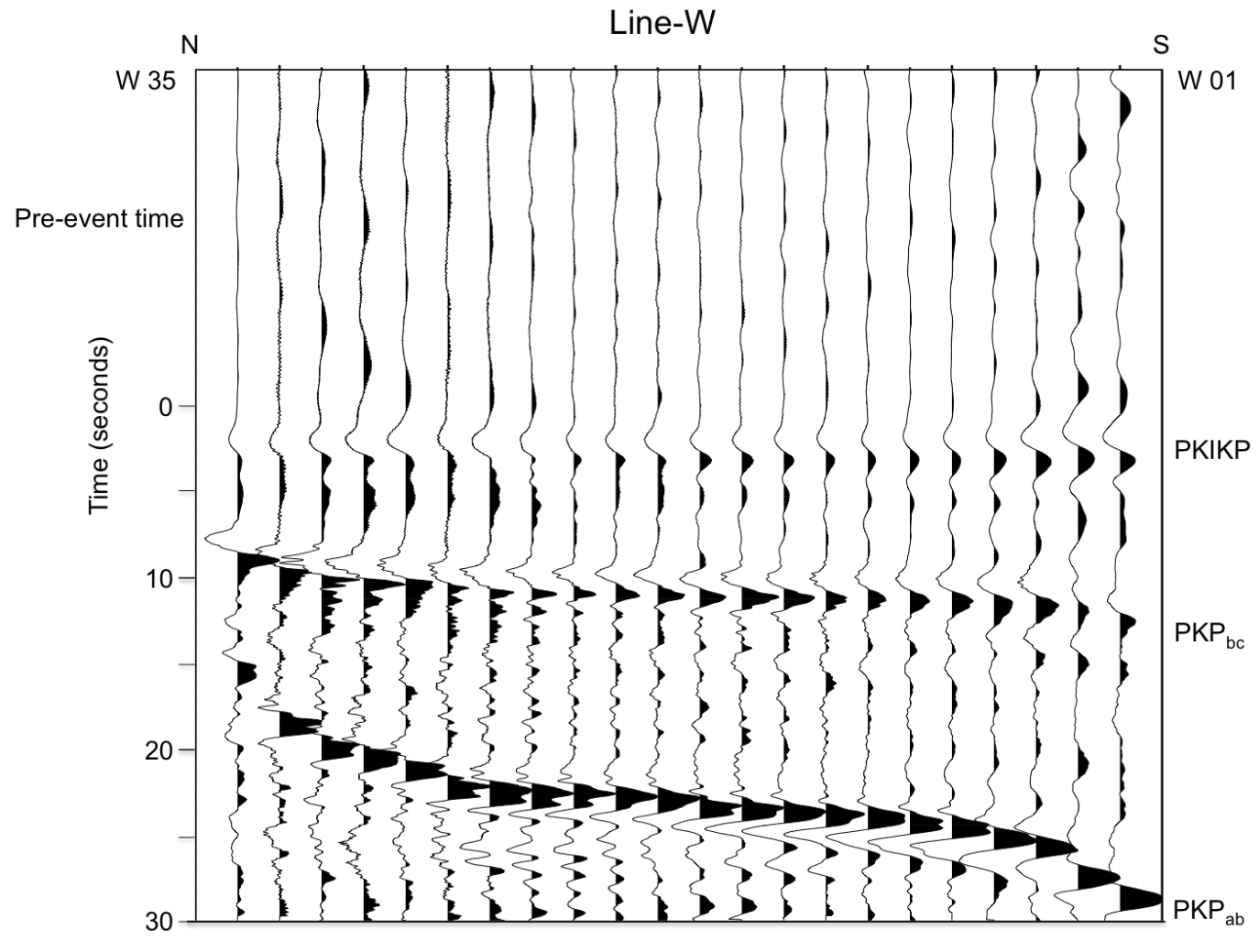


Fig. 2.16 e SESAME line-W prior to signal deconvolution, note the long (~ 6 second) duration of the apparent source time function. Notice also the clear difference in apparent velocities between PKIKP and the interfering PKP arrivals. Finally, note that stations (to this point) have been plotted with equal spacing's to make visual verification of cross-correlation statics easier.

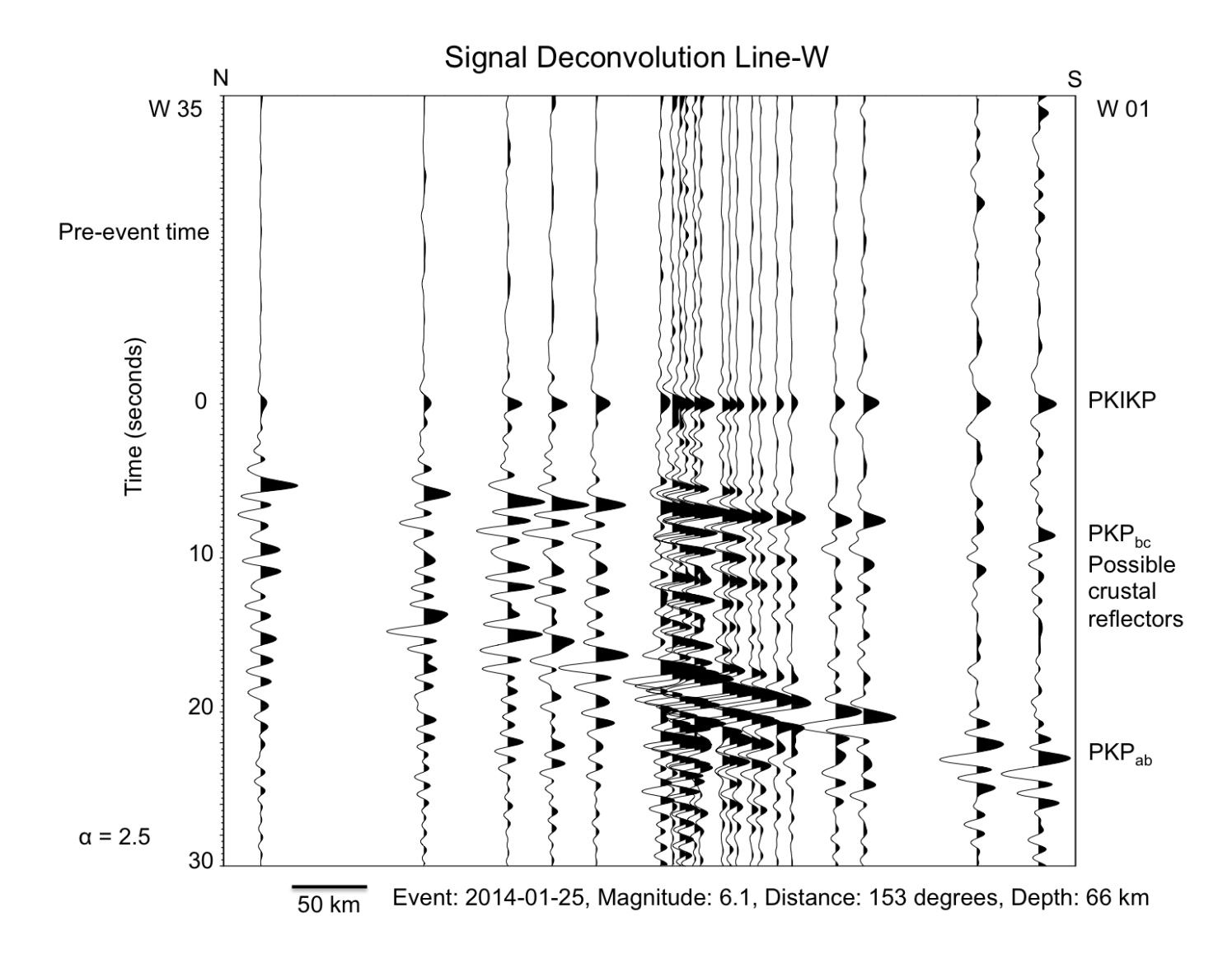


Fig. 2.16 f The results of signal deconvolution for the SESAME array line W. Notice the concentration of energy from formerly extended waveforms to relatively impulsive arrivals for PKIKP, PKP_{ab}, and PKP_{bc}. Also note the emergence of what may be real crustal structure.

Sub-Sectioning SESAME Line-W

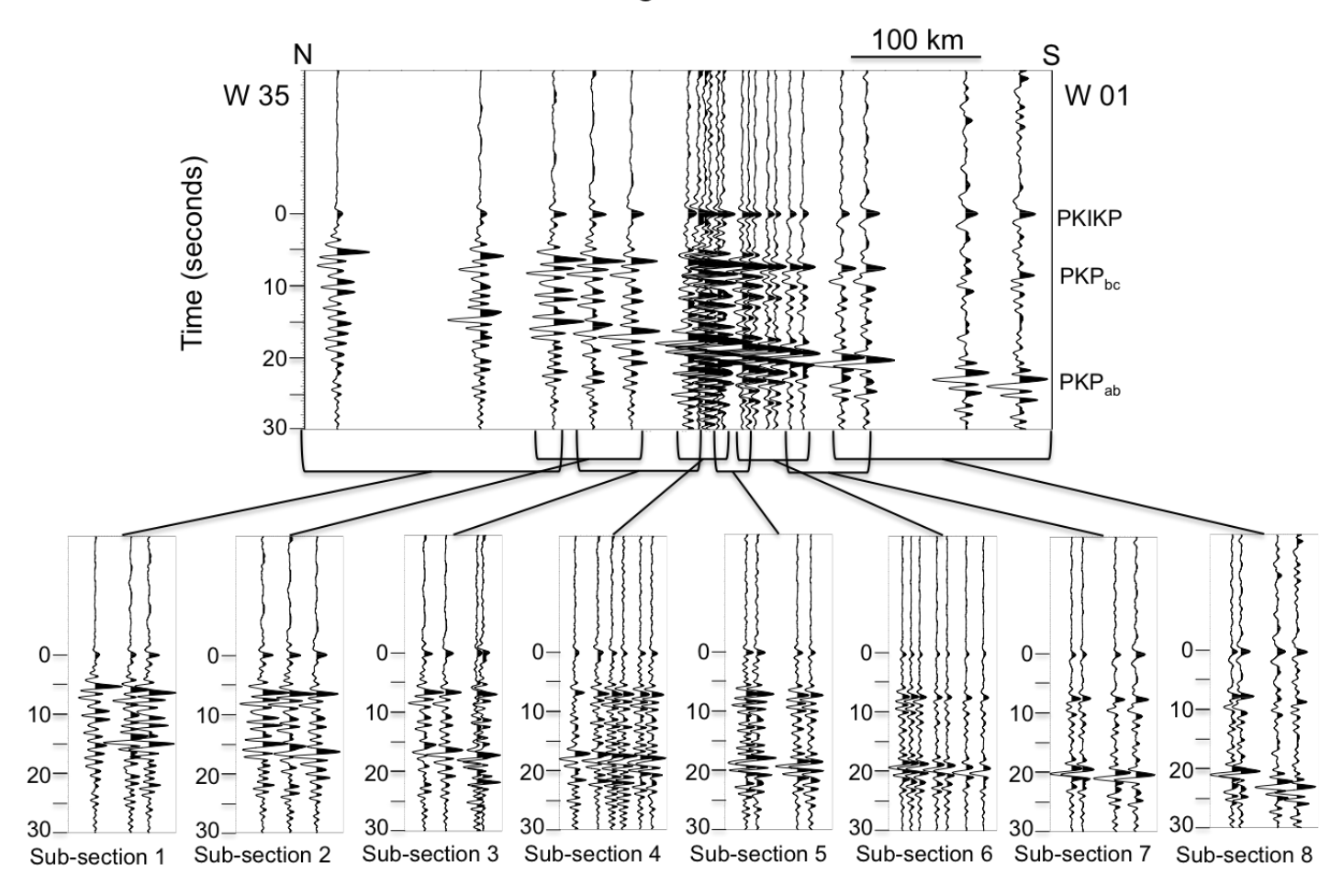


Fig. 2.17 a Sub-sectioning of SESAME line-W into five smaller sub-sectioned gathers. The unlabeled arrivals represent crustal reflectors of various apparent velocities and horizontal extents. The width of each subsection is chosen to span but not exceed the width of individual reflection branches. This ensures a maximum coherency measure when each subsection is slant stacked.

Sub-Sectioning SESAME Line-E

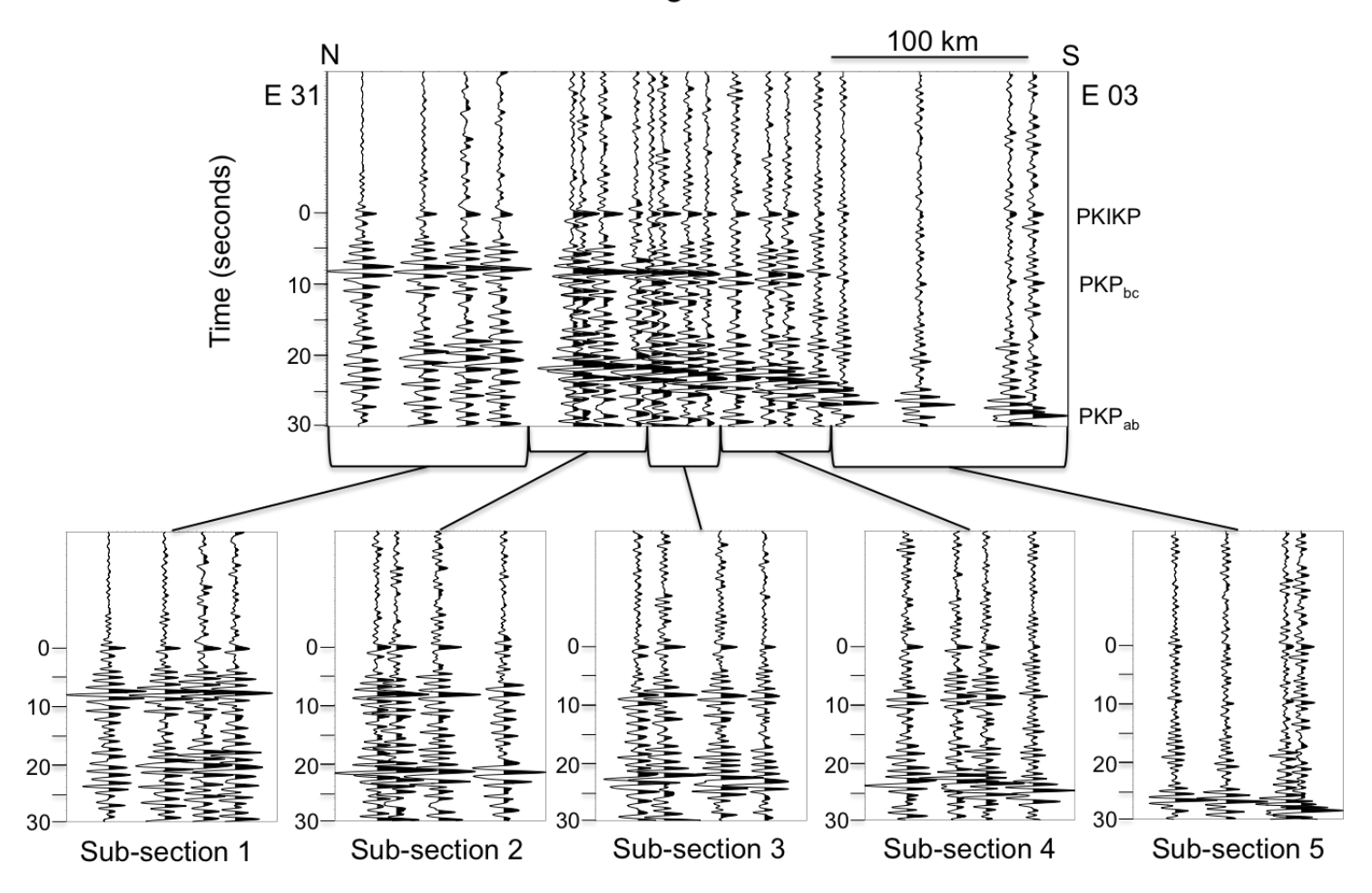


Fig. 2.17 b Sub-sectioning of SESAME line-E into five smaller sub-sectioned gathers. The unlabeled arrivals represent crustal reflectors of various apparent velocities and horizontal extents. The width of each subsection is chosen to span but not exceed the width of individual reflection branches. This ensures a maximum coherency measure when each subsection is slant stacked.

Selecting an Appropriate Slant Stacking Ray Parameter Range

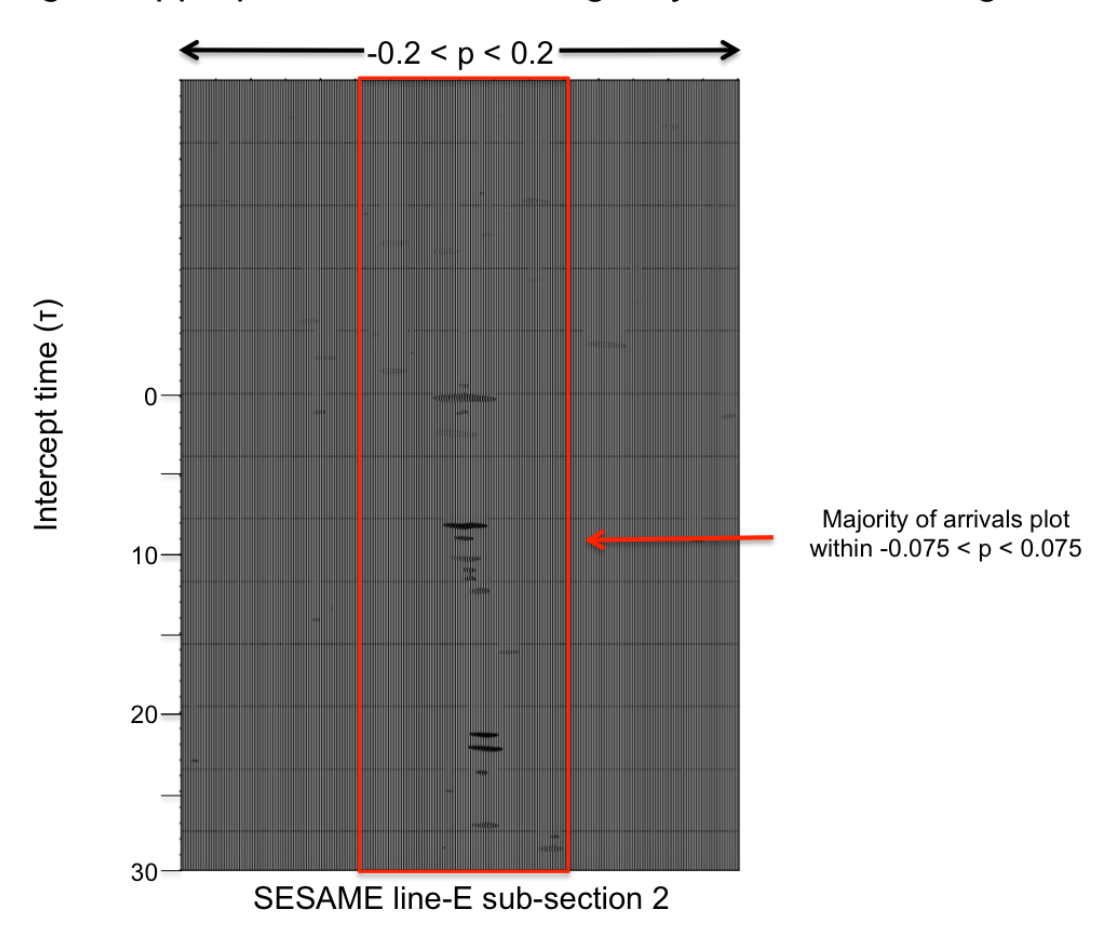


Fig. 2.18 a A visual representation of selecting an appropriate ray parameter range for slant stacking (using the SESAME line-E subsection 2 as a representative example). Note that the sub-section was originally slant stacked with a wide range of ray parameters (-0.2), allowing for identification of seismic arrivals. Notice that following coherency filtering all major seismic arrivals fall within a smaller window (<math>-0.075). The fact that the majority of seismic arrivals fall within this ray parameter range, allowed us to proceed using this smaller range in ray parameter for slant stacking. Finally, note that this image is representative of the SESAME array, which allows us to utilize this range on both the E and W lines.

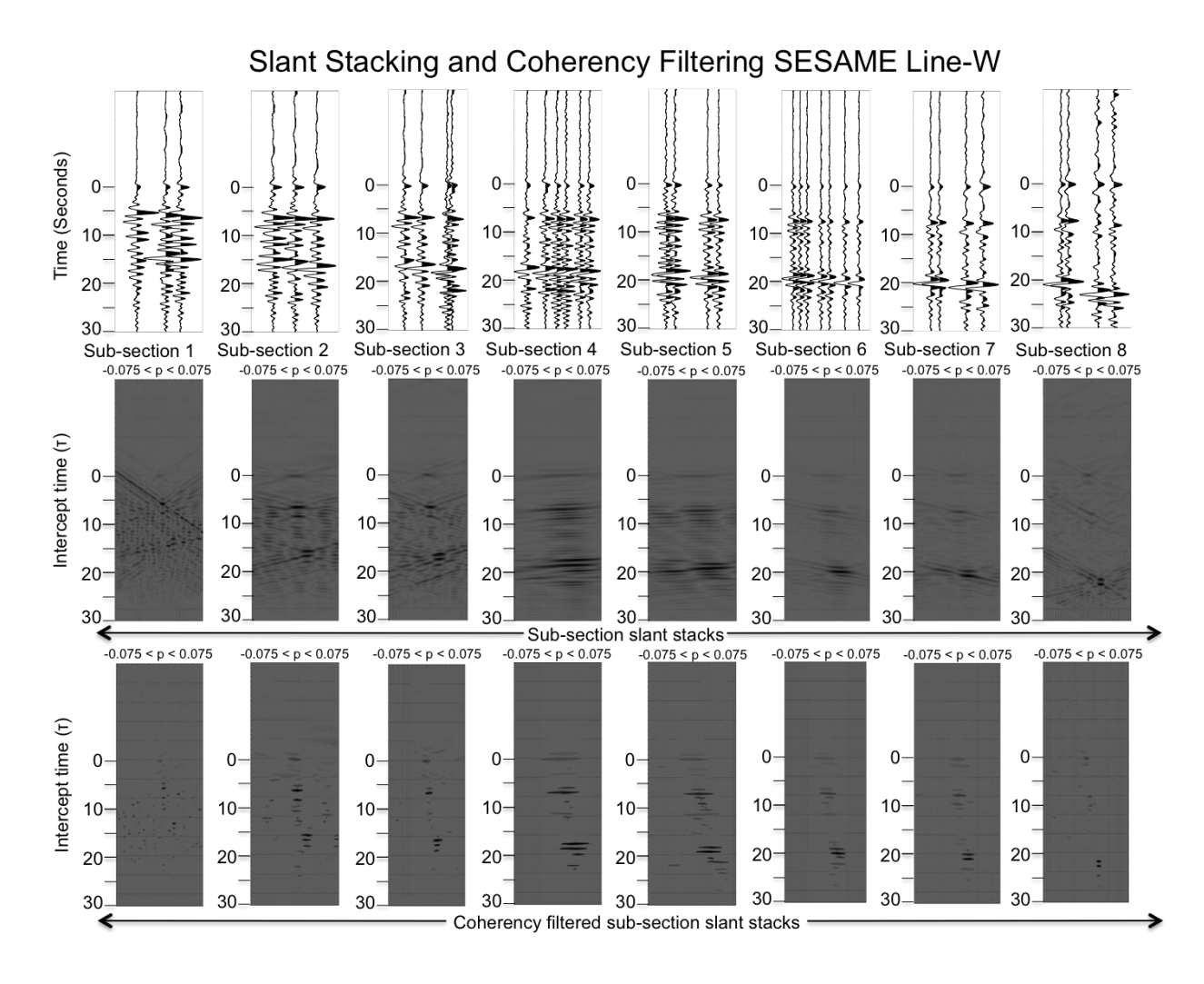


Fig. 2.18 b Sub-sectioned gathers (top) slant stacked into the T-p domain (middle), where T is travel time referenced to the center of the gather and p is horizontal apparent slowness (inverse apparent velocity). Bottom: slant stacks after coherency filtering using semblance (lower cutoff: 0.7, for an original range of 0-1) as a measure of coherence. Note the transformation of arrivals from linear segments in the T-X domain to more localized regions in the T-p domain. In general, increasing the distance range of the input gather will decrease the width of the T-p peaks, yielding better resolution in p.

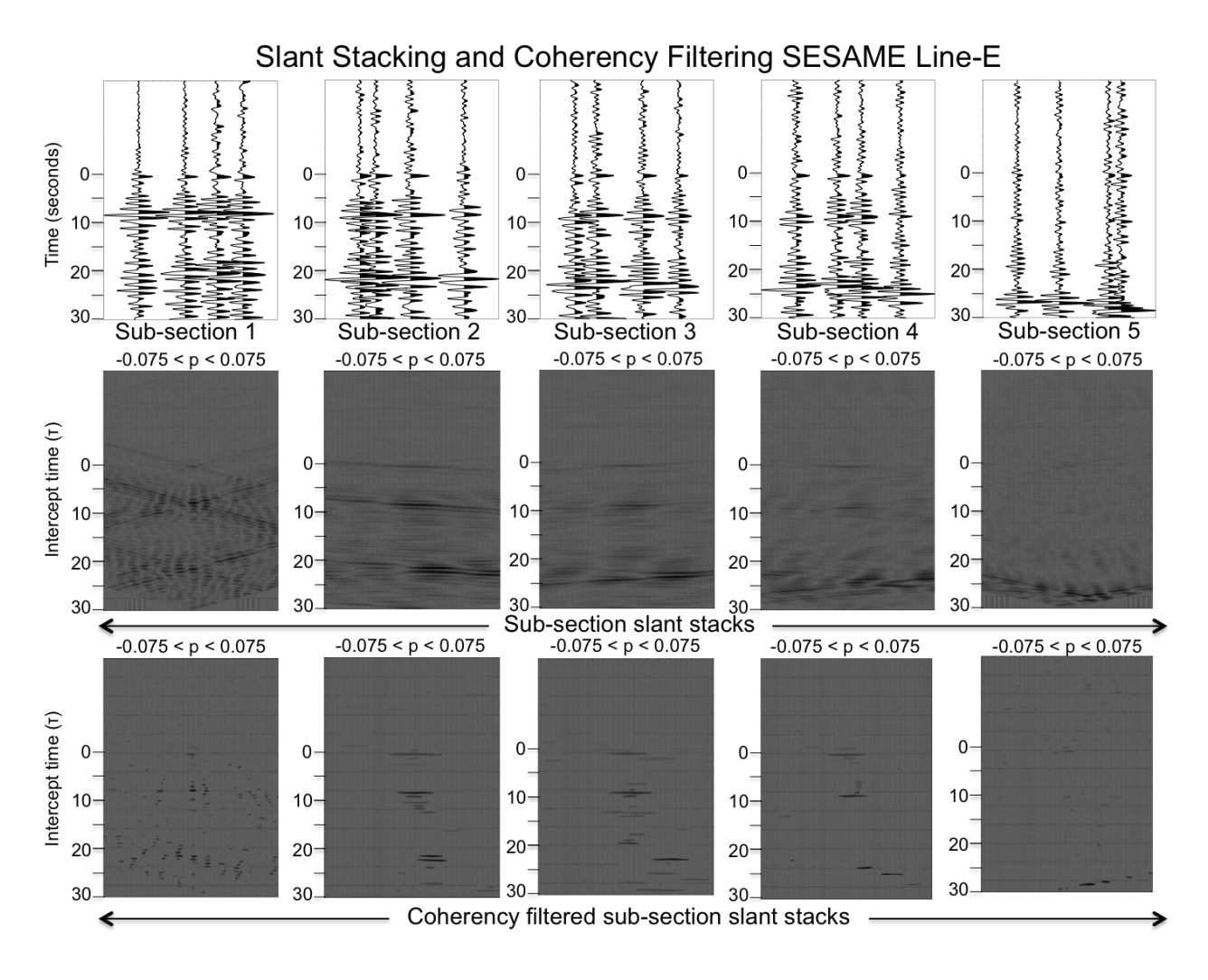


Fig. 2.18 c Sub-sectioned gathers (top) slant stacked into the T-p domain (middle), where T is travel time referenced to the center of the gather and p is horizontal apparent slowness (inverse apparent velocity). Bottom: slant stacks after coherency filtering using semblance (lower cutoff: 0.7, for an original range of 0-1) as a measure of coherence. Note the transformation of arrivals from linear segments in the T-X domain to more localized regions in the T-p domain. In general, increasing the distance range of the input gather will decrease the width of the T-p peaks, yielding better resolution in p.

Apparent Velocity Filtering SESAME Line-W

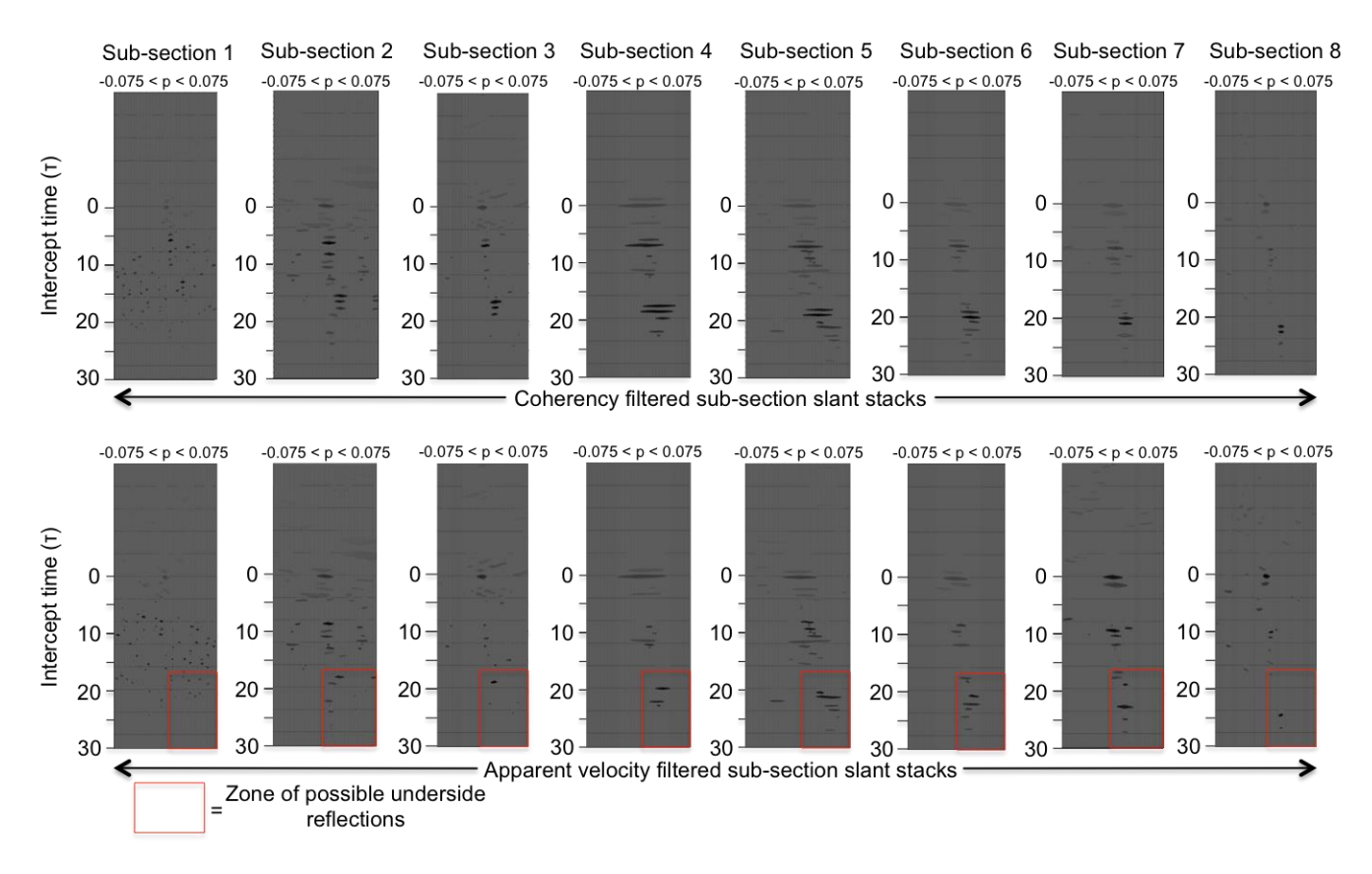


Fig. 2.19 a The results of apparent velocity filtering (bottom) each of the eight coherency filtered sub-sectioned slant stacks of SESAME line-W (top). Note the clean removal of interfering PKP arrivals (appearing at approximately 10 and 20-25 seconds respectively) and that there appears to be no evidence to suggest non-interfering arrivals have been removed. Take note of the zones of possible underside reflections (red boxes) delineated by the first predicted arrival of pPKIKP and including positive ray parameters only. Underside reflections appearing with negative ray parameters are not predicted, thus, energy with negative ray parameters appearing after pPKIKP most likely does not represent underside reflections. Notice the effect station spacing and array aperture have on the quality of the data, sub-sections four through seven show the highest quality slant stacked data, and have the closest station spacing.

Apparent Velocity Filtering SESAME Line-E

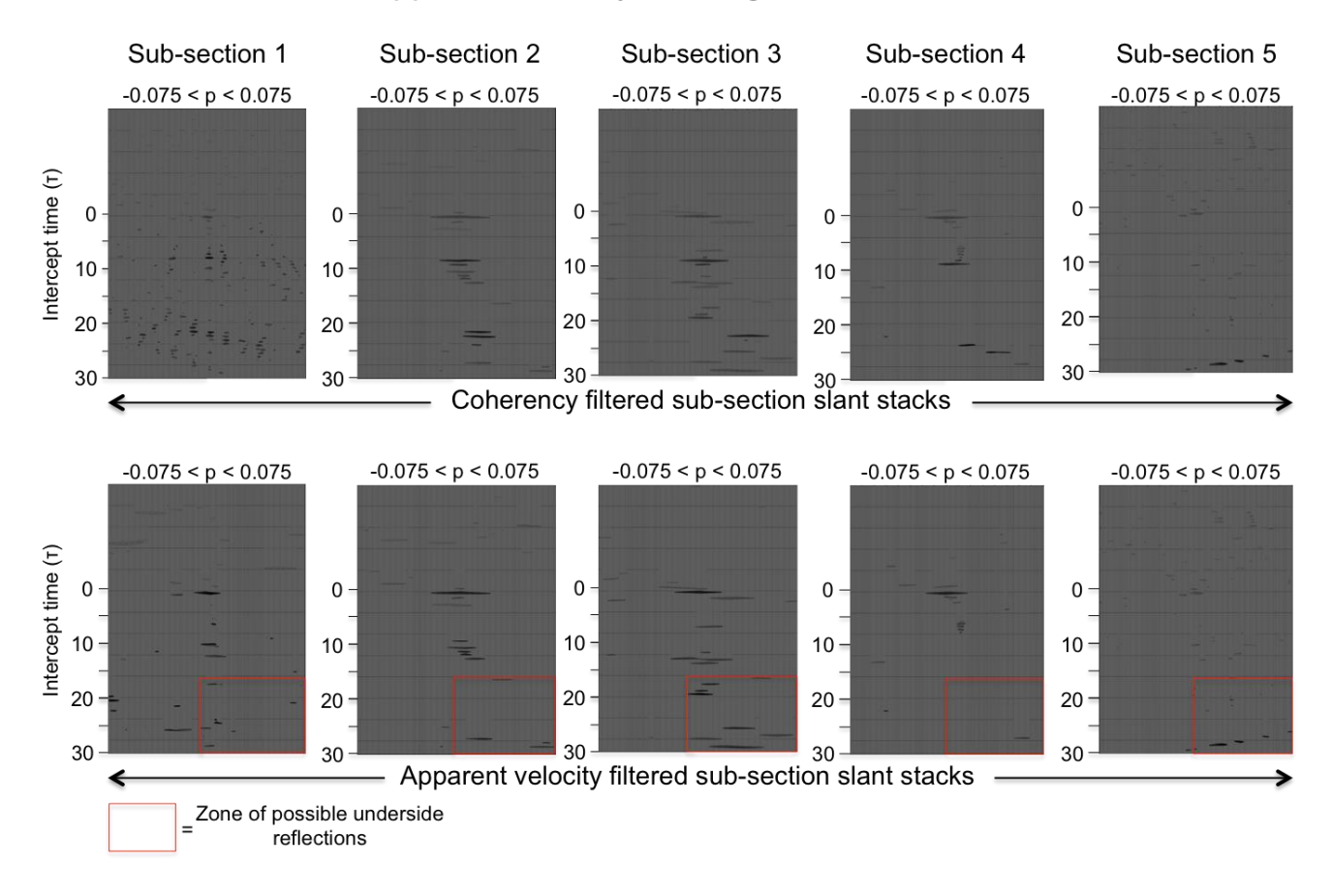


Fig. 2.19 b The results of apparent velocity filtering (bottom) each of the five coherency filtered sub-sectioned slant stacks of SESAME line-E (top). Note the clean removal of interfering PKP arrivals (appearing at approximately 10 and 20-25 seconds respectively), and that there appears to be no evidence to suggest non-interfering arrivals have been removed. Take note of the zones of possible underside reflections (red boxes) delineated by the first predicted arrival of pPKIKP and including positive ray parameters only. Underside reflections appearing with negative ray parameters are not predicted, thus, energy with negative ray parameters appearing after pPKIKP most likely does not represent underside reflections. Notice the effect station spacing and array aperture have on the quality of the data, sub-sections two and three show the highest quality slant stacked data, and have the closest station spacing.

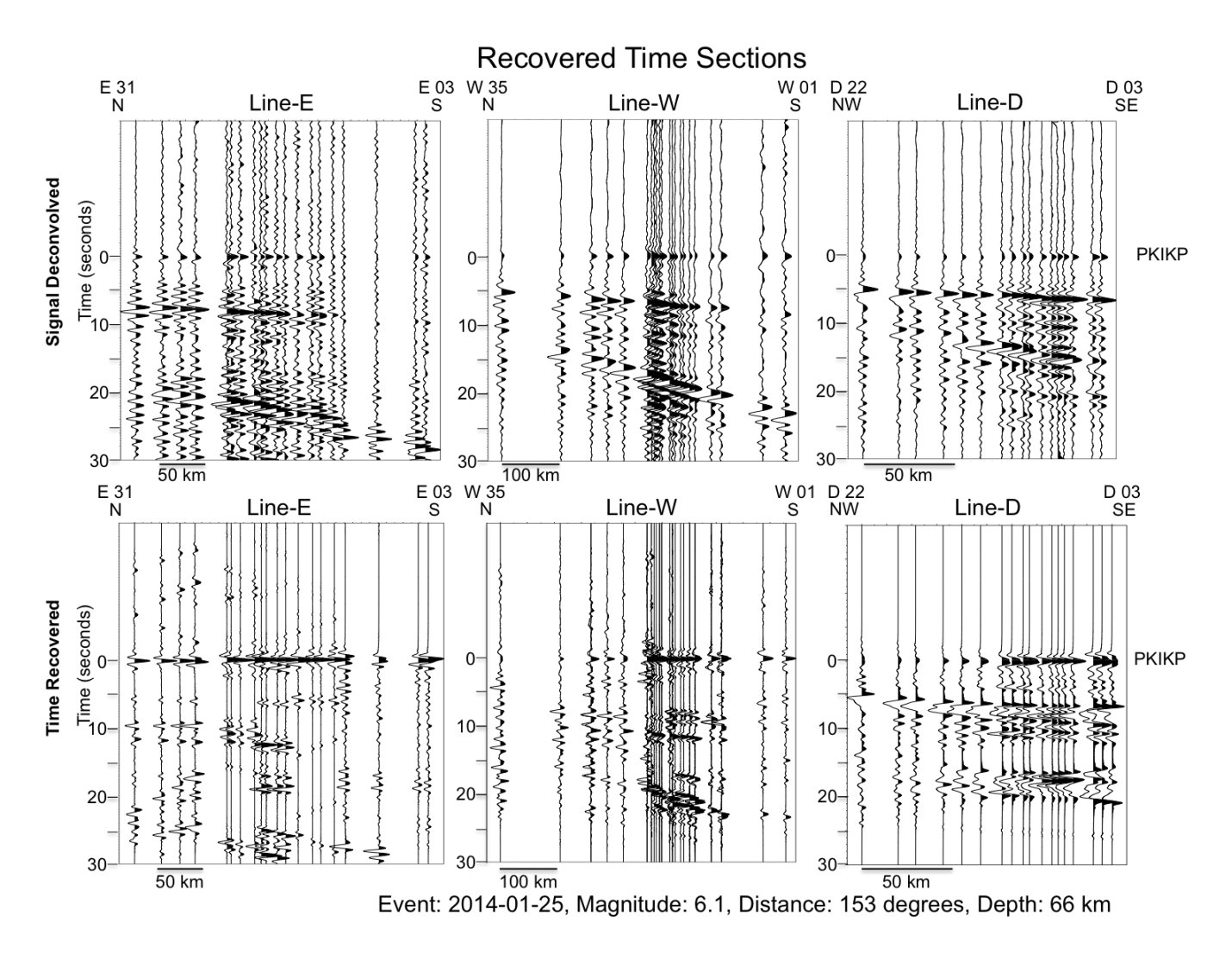


Fig. 2.20 The result of re-combining recovered sub-sections to form fully recovered sections. Notice the high quality recovery of PKiKP, and the many uninterpreted crustal reflectors. Notice also, the almost complete removal of the interfering PKP arrivals (with the exception of line-W), which formerly swept clear across the gathers. Finally, note the great reduction in random noise as a result of the coherency filtering process.

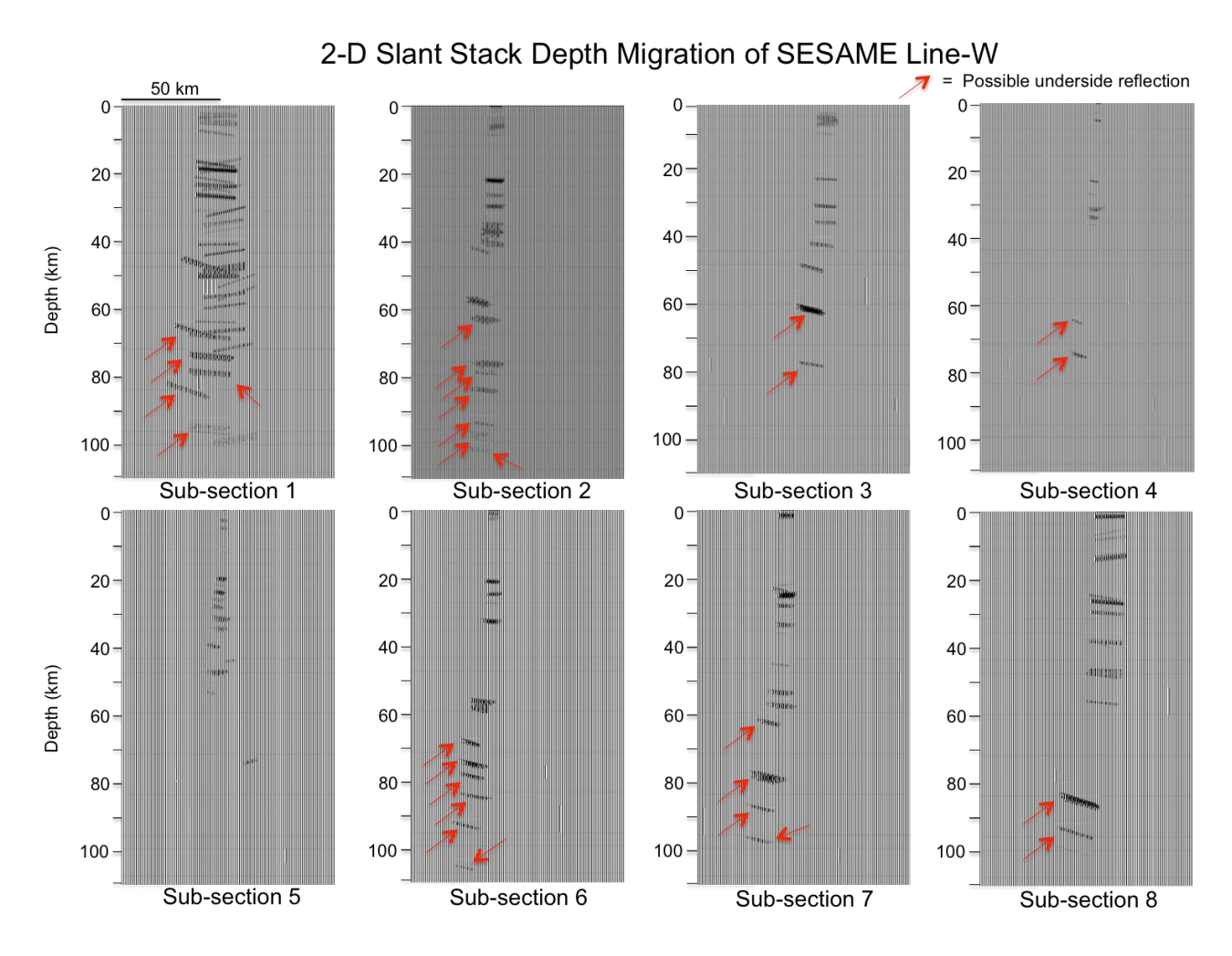


Fig. 2.21 a The results of migrating each of the eight SESAME line-W sub-sections, note that this migration was performed including ray parameters between -0.025 and 0.025, as this range encompassed all meaningful energy within the apparent velocity filtered slant stacks. Notice the existence of several likely remaining interfering arrivals (in particular observe this on sub-section 8 appearing at 80 km). Take note of possible underside reflections (red arrows). Finally, note the existence of what is likely a Moho reflector (illuminated well on sub-section 6 at roughly 30 km). These migration results urge caution when using data, which formerly contained interfering arrivals, as they may persist.

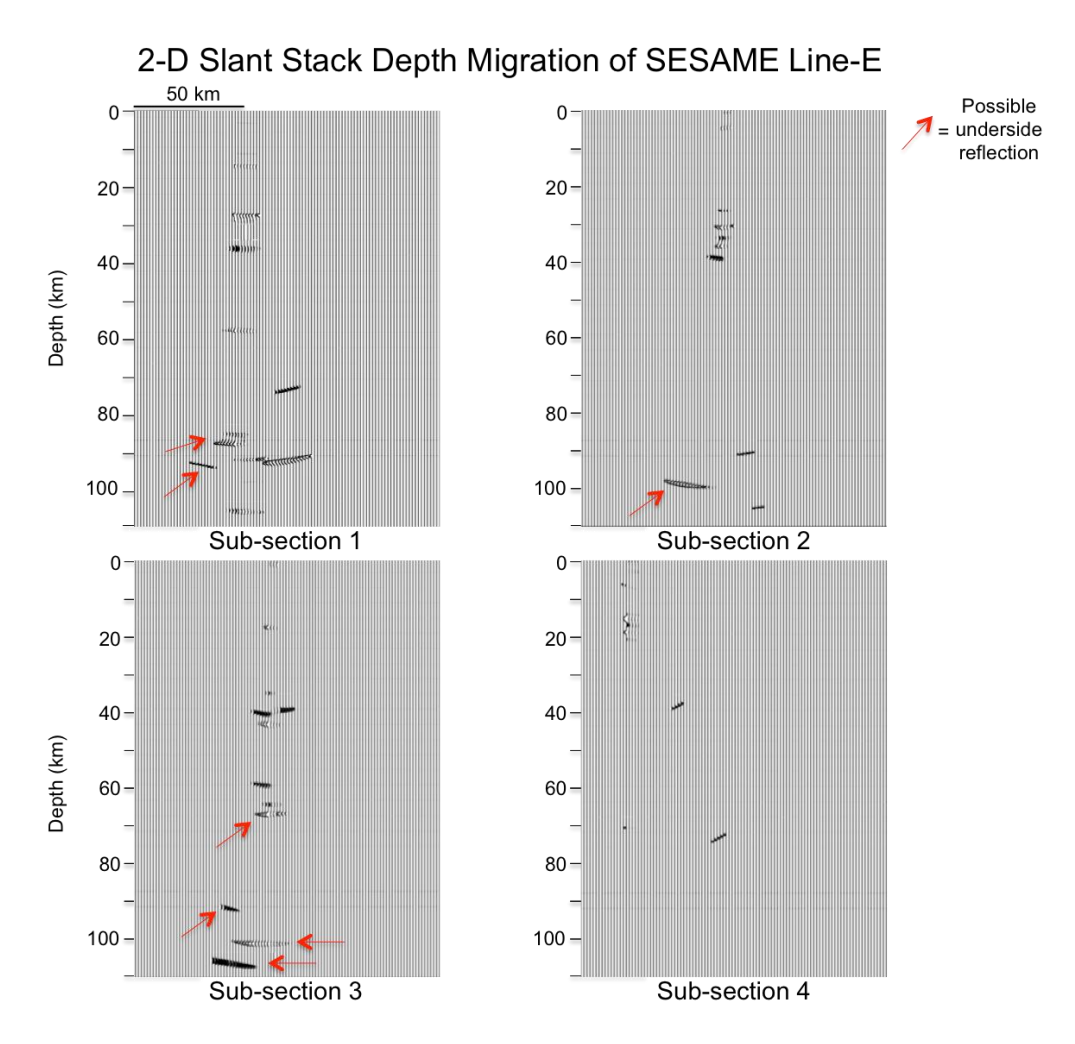


Fig. 2.21 b The results of migrating each of the four SESAME line-E sub-sections, note that this migration was performed including ray parameters between -0.025 and 0.025, as this range encompassed all meaningful energy within the apparent velocity filtered slant stacks. Note also that sub-section 5 was not migrated because of a lack of quality arrivals visible within the slant stack. Notice the existence of prominent Moho reflectors across all sub-sections (35 km), and the existence of what is potentially the lithosphere / asthenosphere boundary, seen well in sub-sections 1-3 (~ 90 km). Take note of possible underside reflections (red arrows). These migration results demonstrate the potential power of the GloPSI method, even while utilizing only a single earthquake source event.

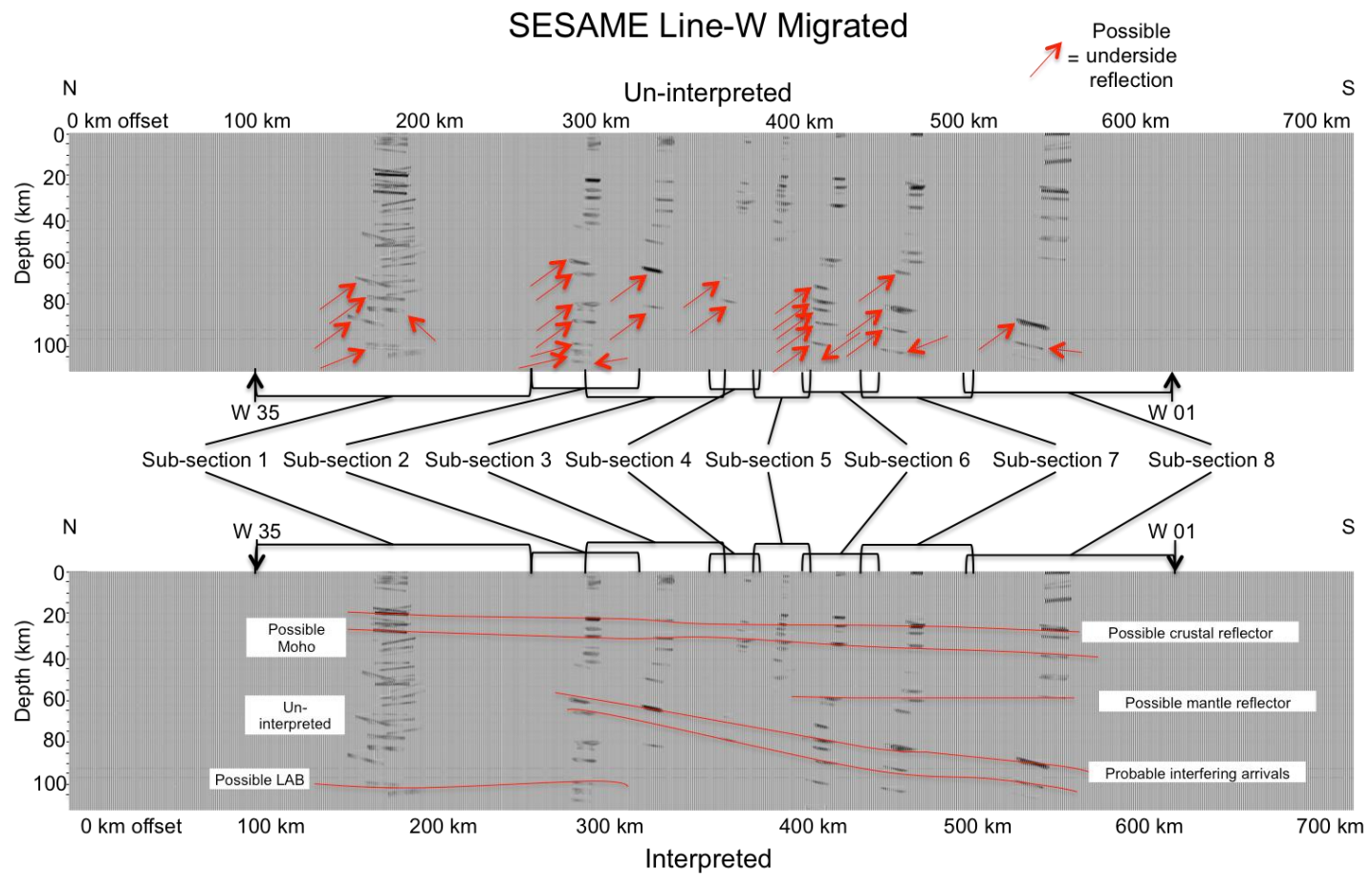


Fig. 2.21 c The results of adding the migrated sub-sections to form a full-migrated section. Note the preservation of key crustal reflectors, as well as possible mantle reflectors. Notice we only observe slight smearing of arrivals, relative to their dominant frequencies, and that most migration artifacts have been eliminated, as a result of summing the sub-sections to form a full-line image, however note that sub-section 1 may be to noisy to trust its migration result. Take note of possible underside reflections (red arrows). Finally, take notice of how well the full GloPSI workflow is able to preserve relatively small reflectors, and that even simulated reflectors with initially small relative amplitudes are preserved, even using only a single event.

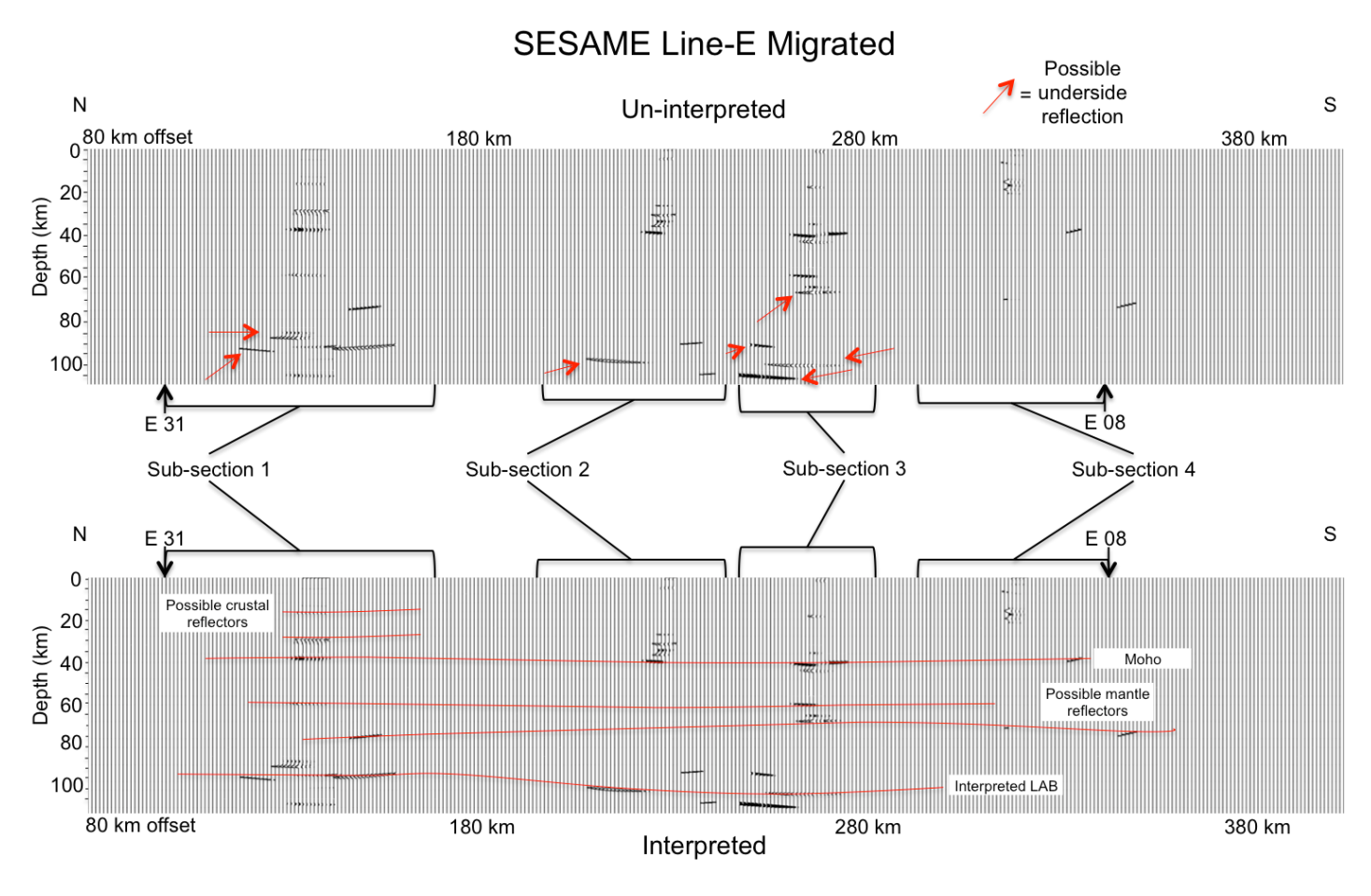


Fig. 2.21 d The results of adding the migrated sub-sections to form a full-migrated section. Note the preservation of key crustal reflectors, as well as possible mantle reflectors. Notice we only observe slight smearing of arrivals, relative to their dominant frequencies, and that most migration artifacts have been eliminated, as a result of summing the sub-sections to form a full-line image. Note that sub-section 5 was not migrated due to poor slant stack signal quality. Take note of possible underside reflections (red arrows). Finally, take notice of how well the full GloPSI workflow is able to preserve relatively small reflectors, and that even simulated reflectors with initially small relative amplitudes are preserved, even using only a single event.

CHAPTER 3

CONCLUSIONS

Through the development of an adapted GloPSI workflow, which intended to employ passive-source global phase broadband seismic recordings derived from natural earthquakes, to produce broadband reflection profiles of the southeastern United States, beneath the former location of the SESAME seismic array, we come to five major conclusions.

First, the adapted GloPSI workflow presented within this text offers a set of reliable and robust seismic methods which allow for reflection imaging of the earth using broadband earthquake derived seismic waves. Particularly, this method generates meaningful reflection images even using a single natural earthquake event, meaning with the addition of many more earthquake events, this method will likely allow for the generation of images which permit very high quality interpretations of sub-surface structure, even making many types of digital modeling possible, including rock physics modeling.

Second, signal deconvolution as it is employed within this study is a viable method for removing the effects of seismic sources from broadband reflection profiles. Previous studies employing the general GloPSI method, have utilized the method of auto-correlation to accomplish this processing task. Signal deconvolution offers an alternative to the auto-correlation method that provides better resolution of structure within the upper crust.

Third, the slant stacking processes employed within this study, along with the processes for removing interfering seismic arrivals, offer huge advantages in terms of the number of usable earthquake source events for GloPSI processing. Previous work suggested that distance ranges

from seismic source to receiver between 135 degrees and 150 degrees were unusable, because interfering seismic arrivals hampered the identification of PKIKP and associated reflections (Ruigrok and Wapenaar, 2012). However, slant stacking and the removal of interfering arrivals deals with both issues, greatly increasing the number of usable earthquake source events.

Fourth, 2-D slant stack depth migration offers a meaningful and reliable method for migrating data within the T-p domain into the seismic depth domain. Previously, GloPSI was almost exclusively performed only in the time-domain. This improvement, along with future work, will allow for far more detailed analysis and modeling of the sub-surface of the southeastern United States, and will permit more direct comparisons of future results with previous work, including the results of the COCORP experiments (Cook and Vasudivan, 1979).

Fifth and finally, the adapted GloPSI method presented here offers further interpreted constraints on the depth of the continental Moho and is the first reflection profiling technique to image what is interpreted to be structure within the sub-crustal lithosphere of the southeastern United States. We image the continental Moho beneath the Atlantic Coastal Plain at depths of roughly 35-40 km, and we place deeper lithospheric structure at depths between 90 km and 110 km, a similar depth to what was interpreted (using Sp receiver functions) by Abt et al. (2010) as the base of the lithosphere (LAB). Future studies, which will employ many natural earthquake events, will be able to further constrain these depths, and better interpret the sub-surface geometries of these features, as well as many other geologic features, which will likely be revealed with brute stacking of reflection profiles.

REFERENCES

- Abt, D. L., K. M. Fischer, S. W. French, H. A. Ford, H. Y. Yuan, and B. Romanowicz (2010), North American lithospheric discontinuity structure imaged by Ps and Sp receiver functions, *JOURNAL OF GEOPHYSICAL RESEARCH-SOLID EARTH*, 115.
- Alberts, E. C., D. N. Verellen, E. H. Parker, R. B. Hawman, K. M. Fischer, and L. S. Wagner (2016), Imaging the Moho beneath the Southern Appalachians using global seismic phases recorded by the sesame broadband array, *Abstracts with Programs Geological Society of America*, 48(3), @Abstractno.6-5.
- Baker, M. S., and R. B. Hawman (2011), Crustal structure in the Southern Appalachians; a comparison of results obtained from broadband data and three-component, wide-angle P and S reflection data, *Bulletin of the Seismological Society of America*, 101(6), 2796-2809.
- Cohen, J. K. and Stockwell, Jr. J. W., (2016), CWP/SU: Seismic Unix Release No. 44R4: an open source software package for seismic research and processing, Center for Wave Phenomena, Colorado School of Mines.
- Cook, F. A., and K. Vasudevan (2006), Reprocessing and enhanced interpretation of the initial COCORP Southern Appalachians traverse, *Tectonophysics*, 420(1/2), 161-174.
- Cook, F. A., L. D. Brown, S. Kaufman, J. E. Oliver, and T. A. Petersen (1981), COCORP seismic profiling of the Appalachian Orogen beneath the coastal plain of Georgia, *Geological Society of America Bulletin*, 92(10), 738-748.

- Cook, F. A., D. S. Albaugh, L. D. Brown, S. Kaufman, J. E. Oliver, and R. D. Hatcher, Jr. (1979), Thin-skinned tectonics in the crystalline southern Appalachians; COCORP seismic-reflection profiling of the Blue Ridge and Piedmont, *Geology [Boulder]*, 7(12), 563-567.
- Coruh, C., J. K. Costain, R. D. Hatcher, Jr., T. L. Pratt, R. T. Williams, and R. A. Phinney (1987), Results from regional Vibroseis profiling; Appalachian Ultra-Deep Core Hole site study, *Geophysical Journal of the Royal Astronomical Society*, 89(1), 147-156.
- Deschamps, F., S. Lebedev, T. Meier, and J. Trampert (2008), Stratified seismic anisotropy reveals past and present deformation beneath East-central United States, *Earth and Planetary Science Letters*, 274, 489-498.
- Dziewonski, A. M., and D. L. Anderson (1981), Preliminary reference Earth model, *Physics of the Earth and Planetary Interiors*, 25(4), 297-356.
- Fischer, K. M., H. A. Ford, D. L. Abt, and C. A. Rychert (2010a), The Lithosphere-asthenosphere boundary, *Ann. Rev. Earth Planet. Sci.*, 38, 551-575.
- Goldstein, P., A. Snoke, (2005), "SAC Availability for the IRIS Community", Incorporated Institutions for Seismology Data Management Center Electronic Newsletter.

 http://ds.iris.edu/ds/newsletter/vol7/no1/sac-availability-for-the-iris-community/
- Gung, Y. C., M. Panning, and B. Romanowicz (2003), Global anisotropy and the thickness of continents, *Nature*, **422**, 707–711.
- Hawman, R. B. (2008), Crustal thickness variations across the Blue Ridge Mountains, Southern Appalachians; an alternative procedure for migrating wide-angle reflection data, *Bulletin of the Seismological Society of America*, 98(1), 469-475.

- Hawman, R. B., M. O. Khalifa, and M. S. Baker (2012), Isostatic compensation for a portion of the southern Appalachians: Evidence from a reconnaissance study using wide-angle, three-component seismic soundings, *Geol. Soc. Am. Bull.*, 124, 291–317.
- Kennett, B. L. N., and E. R. Engdahl (1991), Traveltimes for global earthquake location and phase identification, *Geophysical Journal International*, *105*(2), 429-465.
- Neidell, N. S., and M. T. Taner (1971), SEMBLANCE AND OTHER COHERENCY

 MEASURES FOR MULTICHANNEL DATA, *GEOPHYSICS*, *36*(3), 482-497.
- Parker, E. H., Jr., R. B. Hawman, K. M. Fischer, and L. S. Wagner (2013), Crustal evolution across the Southern Appalachians; initial results from the SESAME broadband array, *Geophysical Research Letters*, 40(15), 3853-3857.
- Parker, E. H., Jr., R. B. Hawman, K. M. Fischer, and L. S. Wagner (2015), Constraining lithologic variability along the Alleghanian detachment in the Southern Appalachians using passive-source seismology, *Geology*, 43 431-434.
- Parker, H. E., Jr., R. B. Hawman, K. M. Fischer, and L. S. Wagner (2016), Estimating crustal thickness using SsPmp in regions covered by low-velocity sediments; imaging the Moho beneath the Southeastern Suture of the Appalachian Margin Experiment (SESAME) array, SE Atlantic Coastal Plain, *Geophysical Research Letters*, 43(18), 9627-9635.
- Phinney, R. A., and D. M. Jurdy (1979), Seismic imaging of deep crust, *GEOPHYSICS*, 44(10), 1637-1660.
- Phinney, R. A., K. R. Chowdhury, and L. N. Frazer (1981), Transformation and analysis of record sections, *Journal of Geophysical Research*. *Solid Earth*, 86(B1), 359.
- Priestley, K., and D. McKenzie (2006), The thermal structure of the lithosphere from shear wave velocities, *Earth Planet. Sci. Lett.*, 244, 285–301.

- Robinson, E. A. (1983), *Migration of geophysical data*, Boston: International Human Resources Development Corp., c1983.
- Robinson, E. A., T. S. Durrani, and L. G. Peardon (1986), *Geophysical signal processing*, Englewood Cliffs, N.J.: Prentice-Hall, c1986.
- Ruigrok, E., and K. Wapenaar (2012), Global-phase seismic interferometry unveils P-wave reflectivity below the Himalayas and Tibet, *GEOPHYSICAL RESEARCH LETTERS*, 39.
- Shearer, P. M. (2009), *Introduction to seismology*, Cambridge: Cambridge University Press, c2009. 2nd ed.
- Stoffa, P. L., P. Buhl, J. B. Diebold, and F. Wenzel (1981), Direct mapping of seismic data to the domain of intercept time and ray parameter—A plane- wave decomposition, *GEOPHYSICS*, 46(3), 255-267.
- Verellen, D. N., E. C. Alberts, E. H. Parker, R. B. Hawman, K. M. Fischer, and L. S. Wagner (2016), Investigation of p-wave reflectivity beneath the Southern Appalachians using the SESAME broadband array, *Abstracts with Programs Geological Society of America*, 48(7), @Abstractno.130-139.
- Yang, Z. H., A. F. Sheehan, W. L. Yeck, K. C. Miller, E. A. Erslev, L. L. Worthington, and S.
 H. Harder (2012), Imaging basin structure with teleseismic virtual source reflection
 profiles, GEOPHYSICAL RESEARCH LETTERS, 39.
- Yuan, H. and V. Levin (2014), Stratified seismic anisotropy and the lithosphere-asthenosphere boundary beneath eastern North America, *J. Geophys. Res.*, *Solid Earth*, 119, 3096-3114.

APPENDIX A

IN-HOUSE SOFTWARE

crosscorrstatquake

Purpose: Calculates and applies static corrections based on cross-correlation of seismic waveforms.

Inputs:

in = seismic trace gather

ntr = number of traces

nt = number of time samples

dt = sampling interval

npilot = trace to base cross-correlation off of

t1 = first time sample to consider in cross-correlation (in seconds)

t2 = last time sample to consider in cross-correlation (in seconds)

secmax = max time shift (in seconds)

Outputs:

out = statically corrected seismic trace gather

outc = number of time samples each trace is shifted

corr = cross-correlation values

Usage:

Note, for presentation purposes spaces are added before and after equal signs (in practice these are not utilized).

crosscorrstatquake in = infile out = outfile outc = outfile.c corr = outfile.corr ntr = 18 nt = 10001 dt = 0.02 npilot = 8 t1 = 18 t2 = 24 secmax = 3

envelopehilbderivmac

Purpose: Applies the first derivative of the Hilbert transform to a seismic trace gather.

Inputs:

in = seismic trace gather

nt = number of time samples

ntr = number of traces

hbt = which Hilbert derivative to apply

mode = which mode of application

Outputs:

out = first derivative Hilbert transformed seismic trace gather

Usage:

envelopehilbderivmac in = infile out = outfile nt = 2501 ntr = 4 hbt = 1 mode = 3

freqdeconsourcemac

Purpose: Performs frequency deconvolution of seismic trace gathers.

Inputs:

numer = seismic trace gather

denom = source-time function (as a single seismic trace)

ntr = number of traces

nt = number of time samples

```
dt = sampling interval
```

alpha = Gaussian filtering parameter

wh = "whitening" parameter

pre = time sample to assign as "time zero" (in seconds)

taper = length in seconds of trace taper

Outputs:

out = signal deconvolved seismic trace gather

Usage:

freqdeconsourcemac numer = infile1 denom = infile2 out = outfile ntr = 17 nt = 2501 dt = 0.02

alpha = 1.75 wh = 0.0001 pre = 20 taper = 1

maxglobalnorm

Purpose: Globally normalizes seismic trace gathers.

Inputs:

in = seismic trace gather

ntr = number of traces

nt = number of time samples

Outputs:

out = globally normalized seismic trace gather

out2 = max value in file

Usage:

maxglobalnorm in = infile1 out = outfile1 out2 = junk ntr = 800 nt = 5501

migslantzeroffset

Purpose: Performs 2 D slant stack depth migration of sparse seismic data.

Inputs:

```
stack = seismic slant stack
nlayer = number of layers in the velocity model
model = file containing the velocity model
para = file containing station offsets
filt = coherency filtering matrix
dt = sampling interval
nxorig = number of traces in the original seismic trace gather
dporig = ray parameter interval within the slant stack
pminorig = lowest ray parameter value in the slant stack
nporig = number of ray parameters in the slant stack
taumin = lowest tau value in the slant stack
ntau = number of tau samples
arrayelev = set to 1
arrayvel = set to 1
datum = set to 1
dx = offset sampling interval
dz = depth sampling interval
nx = number of offset samples
nz = number of depth samples
tmin = first time sample to migrate (in seconds)
```

tmax = last time sample to migrate (in seconds)

pmin = first ray parameter sample to migrate

pmax = last ray parameter sample to migrate

maxgap = max distance to allow interpolation across

fmult = width to draw the migrated reflector (compared to a relative value of 1)

fresnelyesno = apply Fresnel zone correction when drawing migrated reflectors

vavg = velocity to use in Fresnel zone calculation

freq = frequency to use in the Fresnel zone calculation

Outputs:

out = depth migrated seismic section

Usage:

migslantzeroffset stack = infile nlayer = $12 \text{ model} = \text{vel.txt para} = \text{station_offsets_1.txt filt} =$ infile.semb out = outfile dt = 0.02 nxorig = 4 dporig = 0.000375 pminorig = -0.075 nporig = 400taumin = -20 ntau = 2501 arrayelev = 1 arrayvel = 1 datum = 1 dx = 1 dz = 0.02 nx = 800 nz = 5501 tmin = 0 tmax = 30 pmin = -0.025 pmax = 0.025 maxgap = 10 fmult = 0.1 fresnelyesno = 1 vavg = 7.4 freq = 2

sacheaderstrip

Purpose: Strips the SAC header from files.

Inputs:

infile = SAC file

ntr = number of traces

nt = number of time samples

Outputs:

out = file with no header attached

hdr = file header stored as backup

Usage:

sacheaderstrip in = infile out = outfile hdr = outfile.hdr ntr = 18 nt = 10001

sampshiftarb

Purpose: Shifts individual traces within a seismic trace gather based on the shifts output of crosscorrstatquake.

Inputs:

in = seismic trace gather

ntr = number of traces

nt = number of time samples

mode = mode of application

para = file containing shift information (output of crosscorrstatquake)

Outputs:

out = shifted seismic trace gather

Usage:

sampshiftarb in = infile out = outfile ntr = 17 nt = 2501 mode = 2 para = outfile.c

seispickalt_2015

Purpose: Performs spatial and time windowing on seismic trace gathers.

Inputs:

```
in = seismic trace gather
```

nx = number of traces

nt = number of time samples

nt1 = first included time sample

nt2 = last included time sample

nx1 = first included trace

nx2 = last included trace

Outputs:

out = windowed seismic trace gather

Usage:

```
seispickalt_2015 in = infile out = outfile nx = 17 nt = 10001 nt1 = 1 nt2 = 2501 nx1 = 1 nx2 = 15
```

sembmutebelowmac

Purpose: Generates binary pass / fail matrix based on coherency (semblance based) of seismic slant stack data.

Inputs:

in = seismic slant stack data

ntr = number of traces

nt = number of time samples

maxorig = 1

thresh = cutoff percentage relative to the max semblance of 1 (above this value pass, below this value fail)

Outputs:

out = binary coherency filtering matrix

Usage:

sembmutebelowmac in = infile.semb out = outfile ntr = 400 nt = 2501 maxorig = 1 thresh = 0.65

slantstackforward

Purpose: Performs forward slant stacking of seismic trace gathers into the T-p domain.

Inputs:

```
in = seismic trace gathers
mode = mode of application
nx = number of traces
dt = time interval
nt = number of time samples
t0 = first time sample
taumin = first time sample to be stacked (in seconds)
ntau = number of stacked time samples
dp = ray parameter interval
pmin = the first ray parameter
np = the number of ray parameters
para = station offsets
Outputs:
```

outstack = slant stacked seismic trace gathers outsemb = slant stack semblance spectra

Usage:

```
slantstackforward in = infile outstack = outfile outsemb = outfile.semb mode = 2 \text{ nx} = 4 \text{ dt} = 0.02 \text{ nt} = 2501 \text{ t0} = 0.0 \text{ taumin} = 0 \text{ ntau} = 2501 \text{ dp} = 0.000375 \text{ pmin} = -0.075 \text{ np} = 400 \text{ para} = 0.000375 \text{ pmin} = -0.075 \text{ np} = 400 \text{ para} = 0.000375 \text{ pmin} = -0.000375 \text{ pmin} = -0.000
```

slantstackinverse

Purpose: Performs inverse slant stacking of slant stack data into the T-x domain.

Inputs:

```
in = seismic slant stack data

para = file containing station offsets
ireduce = 0

mode = mode of application

pmin = first ray parameter

np = number of ray parameters

dp = ray parameter interval

tau0 = first tau sample (in seconds)

ntau = number of input traces

dt = time interval
```

Outputs:

nx = number of traces

out = inverse slant stacked seismic trace gather

nt = number of time samples in input trace

tmin = first time sample (in seconds) for output trace

Usage:

slantstackinverse in = infile out = outfile para = offsets_1.txt ireduce = 0 mode = 2 pmin = -0.075 np = 400 dp = 0.000375 tau = 0 ntau = 2501 dt = 0.02 nx = 4 tmin = 0.0 nt = 2501

synsecmac

Purpose: Generates a series of spikes used for the construction of synthetic seismic trace gathers.

Inputs:

nx = number of traces

nt = number of time samples

dt = sampling interval

t0 = first time sample (in seconds)

np = number of synthetic events

events = file containing event information

offsets = file containing synthetic station offsets

Outputs:

out = synthetic seismic trace gather (spikes only)

Usage:

 $synsecmac \ out = outfile \ nx = 5 \ nt = 2501 \ dt = 0.02 \ t0 = 0 \ np = 8 \ events = synthetic_events_1.txt$ $offsets = station_offsets_1.txt$

tracemultmac

Purpose: Multiplies two equally sized seismic trace gathers by one another.

Inputs:

```
in1 = first seismic trace gather
```

in2 = second seismic trace gather

ntr = number of traces

nt = number of time samples

Outputs:

out = product seismic trace gather

Usage:

tracemultmac in 1 = infile 1 in 2 = infile 2 out = outfile ntr = 400 nt = 2501

tracescaleaddmac

Purpose: Sums and scales two equally sized seismic trace gathers.

Inputs:

in1 = first seismic trace gather

in2 = second seismic trace gather

ntr = number of traces

nt = number of time samples

ratio 12 = scaling factor

Outputs:

out = summed and scaled seismic trace gather

Usage:

tracescaleaddmac in1 = infile1 in2 = infile2 out = outfile ntr = 800 nt = 5501 ratio12 = 1

vertstack

Purpose: Vertically stacks traces within a seismic trace gather.

Input:

```
in = seismic trace gather
```

nt = number of time samples

ntr = number of traces

Output:

out = vertically stacked seismic trace

Usage:

vertstack in = infile out = outfile nt=2501 ntr=17

windowstacktaper

Purpose: Creates a tapered (time and spatial) window within a seismic trace gather, maintaining the trace gathers original size, however, muting all data outside the tapered window.

Inputs:

in = seismic trace gather

nx = number of traces

nt = number of time samples

nx1 = first trace in the window

nx2 = last trace in the window

t0 = first time sample (in seconds)

t1 =first time sample in the window (in seconds)

t2 = last time sample in the window (in seconds)

dt = sampling interval

nxtap = number of traces to include in the taper

nttap = number of time samples to include in the taper

Outputs:

out = seismic trace gather containing only the tapered window

Usage:

windowstacktaper in = infile1 out = outfile nx = 400 nt = 2501 nx1 = 225 nx2 = 300 t0 = 0 t1 = 2501 nx1 = 25

$$39 t2 = 42 dt = 0.02 nxtap = 0 nttap = 0$$

APPENDIX B

EXAMPLE UNIX SHELL SCRIPTS

Construction of the Complex Synthetic Section / Sub-Sections

The following is a set of example shell scripts which may be used to generate a full complex synthetic seismic section and its sub-sections. Note that along with a script for combining synthetic sub-sections we have included scripts for the generation of synthetic sub-section 1 only. We have excluded scripts for sub-sections 2-5 because demonstrating them would be redundant.

Sub-Section 1

Shell Name: synthetic_construction_sub_section_1.txt

Shell:

Generate spikes.

synsecmac out = outfile nx = 5 nt = 2501 dt = 0.02 t0 = 0 np = 8 events = synthetic_events_1.txt offsets = station_offsets_1.txt

Add header information.

suaddhead < infile ns=2501 | \

sushw key = dt $a = 20000 > \$

outfile.su

Convolve spikes with synthetic waveform.

```
suconv < infile.su > outfile.su filter = 0.05, 0.1, 0.15, 0.175, 0.2, 0.2, 0.175, 0.15, 0.1, 0.05, 0, -
0.1, -0.2, -0.3, -0.3, -0.2, 0.1, 0, 0.1, 0.2, 0.3, 0.4, 0.5, 0.6, 0.7, 0.8, 0.9, 0.92, 0.93, 0.94, 0.95,
0.95, 0.95, 0.94, 0.93, 0.92, 0.91, 0.9, 0.8, 0.7, 0.6, 0.5, 0.4, 0.3, 0.2, 0.1, 0, -0.1, -0.2, -0.3, -0.3, -0.3
-0.3, -0.2, -0.1, 0
## Add random noise.
suaddnoise < infile.su > outfile.su sn = 10 noise = gauss seed = from_clock f=0.25, 0.5, 0.75, 1,
1.25, 1.5, 1.75, 2, 2.25, 2.5 \text{ amps} = 0, 0.25, 0.5, 1, 1, 1, 1, 0.5, 0.25, 0
## Plot.
suop < infile.su op = norm | \
supswigp xcur = 1.0 \text{ wbox} = 6 \text{ hbox} = 8.5 \text{ style} = \text{seismic} \setminus
nbpi = 300 linewidth = 0 \setminus
title = "synthetic_group_1" \
label1 = "Time (s)" labelsize = 9 \text{ n2tic} = 2 \text{ xbeg} = -0.2 \setminus
xend = 1 interp = 1 n1tic = 5 titlesize = 8 key = offset > \
outfile.su.ps
suop < infile.su op = norm | \
supswigp xcur = 1.0 \text{ wbox} = 6 \text{ hbox} = 8.5 \text{ style} = \text{seismic} \setminus
nbpi = 300 linewidth = 0 \setminus
title="synthetic convolved group 1" \
```

label1="Time (s)" labelsize = $9 \text{ n2tic} = 2 \text{ xbeg} = -0.2 \setminus$

```
xend = 1 interp = 1 n1tic = 5 titlesize = 8 key = offset > \
outfile.su.ps
suop < infile.su op = norm | \</pre>
supswigp xcur = 1.0 \text{ wbox} = 6 \text{ hbox} = 8.5 \text{ style} = seismic \setminus
nbpi = 300 linewidth = 0 \setminus
title="synthetic convolved noised group 1" \
label1 = "Time (s)" labelsize = 9 \text{ n2tic} = 2 \text{ xbeg} = -0.2 \setminus
xend = 1 interp = 1 n1tic = 5 titlesize = 8 key = offset > \
outfile.su.ps
Shell Name: station_offsets_1.txt
Shell:
## Assign station offsets (delta degrees).
0.5
1
1.5
2
2.5
Shell Name: synthetic_events_1.txt
Shell:
```

Specify synthetic events. First column apparent velocity, second column left trace intercept time, third column relative amplitude.

0 20 1

2.15 26 1

4.233 34 1

0.400.5

0 45 0.5

-2.2 25 0.5

-1.5 32 0.25

-0.75 37 0.3

Sum Sub-Sections

Shell Name: add_synthetic_sub_sections.txt

Shell:

Construct the spiked gather.

cp infile1 outfile

dd if= infile2 >> outfile

dd if= infile3 >> outfile

dd if= infile4 >> outfile

dd if= infile5 >> outfile

Add header and plot.

suaddhead < infile ns = 2501 | \

```
sushw key = dt a = 20000 > \
outfile.su
suop < infile.su op = norm | \</pre>
supswigp xcur = 1.0 \text{ wbox} = 6 \text{ hbox} = 8.5 \text{ style} = \text{seismic} \setminus
nbpi = 300 linewidth = 0 \setminus
title = "full synthetic" \
label1= "Time (s)" labelsize = 9 \text{ n2tic} = 2 \text{ xbeg} = -0.2 \setminus
xend = 1 interp = 1 n1tic = 5 titlesize = 8 key = offset > 
outfile.su.ps
## Strip the SU headers from the convolved sub-sections (before noise added).
sustrip < infile1.su > outfile1
sustrip < infile2.su > outfile2
sustrip < infile3.su > outfile3
sustrip < infile4.su > outfile4
sustrip < infile5.su > outfile5
## Construct the convolved gather (before added noise).
cp infile1 outfile
dd if = infile2 >> outfile
dd if = infile3 >> outfile
dd if = infile4 >> outfile
```

```
## Add header and plot.
suaddhead < infile ns = 2555 \mid \ 
sushw key = dt a = 20000 > \
outfile.su
suop < infile.su op = norm | \</pre>
supswigp xcur = 1.0 \text{ wbox} = 6 \text{ hbox} = 8.5 \text{ style} = \text{seismic} \setminus
nbpi = 300 linewidth = 0 \setminus
title = "full synthetic convolved" \
label1 = "Time (s)" labelsize = 9 \text{ n2tic} = 2 \text{ xbeg} = -0.2 \setminus
xend = 1 interp = 1 n1tic = 5 titlesize = 8 key = offset > 
outfile.su.ps
## Strip the SU headers from the convolved sub-sections (with noise added).
sustrip < infile1.su > outfile1
sustrip < infile2.su > outfile2
sustrip < infile3.su > outfile3
sustrip < infile4.su > outfile4
sustrip < infile5.su > outfile5
```

dd if = infile5 >> outfile

Construct the final gather.

```
cp infile1 outfile
dd if = infile2 >> outfile
dd if = infile3 >> outfile
dd if = infile4 >> outfile
dd if = infile5 >> outfile
## Add header and plot.
suaddhead < infile ns = 2555 | \
sushw key = dt a = 20000 > \
outfile.su
suop < infile.su op = norm | \
supswigp xcur = 1.0 \text{ wbox} = 6 \text{ hbox} = 8.5 \text{ style} = \text{seismic} \setminus
nbpi = 300 linewidth = 0 \setminus
title = "full synthetic convolved added noise" \
label1 = "Time (s)" labelsize = 9 \text{ n2tic} = 2 \text{ xbeg} = -0.2 \setminus
xend = 1 interp = 1 n1tic = 5 titlesize = 8 key = offset > \
outfile.su.ps
```

Adapted Global Phase Seismic Interferometry (GloPSI)

The following, uses SESAME line-D (event 2014_01_25_m6.1) as an example for presentation of the initial pre-processing SAC macro, however, in subsequent examples specific infile / outfile names are exchanged for generalized names (e.g. infile / outfile) to allow users to

select their own naming systems and to simplify the presentation of example Unix shell scripts. In addition, later examples are not necessarily keyed to a specific SESAME line and the values within individual processing steps are not necessarily relevant.

Steps 1-3

Obtaining Data, Time Windowing, and the Removal of Linear Trends and the Trace Mean

```
Shell Name: pre_proc.macro
Shell:
## D03
## Read to memory.
r Z9.D03..BHZ.M__at__2014-01-25T05.28.58.000Z.SAC
## Apply first cut.
## Pick the arrival of PKIKP.
ppk
## next: 1) position cursor at onset of the direct P wave
## then: 2) press "t" and "0" (for "timezero, t0")
## then: 3) type "quit" ("q")
setbb t0 &1, t0
evaluate to cutmin %t0 - 25
evaluate to cutmax \%t0 + 200
ch t0 %t0
w ph.2014.01.25.m6.1.d03.cut1.BHZ
cut %cutmin %cutmax
```

```
## Read to memory.
r ph.2014.01.25.m6.1.d03.cut1.BHZ
## Perform second cut.
## Pick the arrival of PKIKP.
ppk
setbb t0 &1, t0
evaluate to cutmin %t0 - 20
evaluate to cutmax \%t0 + 180
ch t0 %t0
w ph.2014.01.25.m6.1.d03.cut2.BHZ
cut %cutmin %cutmax
## Read to memory.
r ph.2014.01.25.m6.1.d03.cut2.BHZ
cut off
## Remove the trace mean, remove linear trends, and apply a taper.
rmean
rtr
taper w 0.01
```

w ph.2014.01.25.m6.1.d03.cut2.swin.BHZ

#D04

r Z9.D04..BHZ.M__at__2014-01-25T05.28.58.000Z.SAC

ppk

setbb t0 &1,t0

evaluate to cutmin %t0 - 25

evaluate to cutmax %t0 + 200

ch t0 %t0

w ph.2014.01.25.m6.1.d04.cut1.BHZ

cut %cutmin %cutmax

r ph.2014.01.25.m6.1.d04.cut1.BHZ

ppk

setbb t0 &1,t0

evaluate to cutmin %t0 - 20

evaluate to cutmax %t0 + 180

ch t0 %t0

w ph.2014.01.25.m6.1.d04.cut2.BHZ

cut %cutmin %cutmax

r ph.2014.01.25.m6.1.d04.cut2.BHZ

```
cut off
rmean
rtr
taper w 0.01
w ph.2014.01.25.m6.1.d04.cut2.swin.BHZ
#D05
r Z9.D05..BHZ.M_at_2014-01-25T05.28.58.000Z.SAC
ppk
setbb t0 &1,t0
evaluate to cutmin %t0 - 25
evaluate to cutmax \%t0 + 200
ch t0 %t0
w ph.2014.01.25.m6.1.d05.cut1.BHZ
cut %cutmin %cutmax
r ph.2014.01.25.m6.1.d05.cut1.BHZ
ppk
setbb t0 &1,t0
```

evaluate to cutmin %t0 - 20

evaluate to cutmax %t0 + 180ch t0 %t0 w ph.2014.01.25.m6.1.d05.cut2.BHZ cut %cutmin %cutmax r ph.2014.01.25.m6.1.d05.cut2.BHZ cut off rmean rtr taper w 0.01 w ph.2014.01.25.m6.1.d05.cut2.swin.BHZ #D07 r Z9.D07..BHZ.M_at_2014-01-25T05.28.58.000Z.SAC ppk setbb t0 &1,t0 evaluate to cutmin %t0 - 25 evaluate to cutmax %t0 + 200ch t0 %t0 w ph.2014.01.25.m6.1.d07.cut1.BHZ

cut %cutmin %cutmax

r ph.2014.01.25.m6.1.d07.cut1.BHZ

ppk

setbb t0 &1,t0

evaluate to cutmin %t0 - 20

evaluate to cutmax %t0 + 180

ch t0 %t0

w ph.2014.01.25.m6.1.d07.cut2.BHZ

cut %cutmin %cutmax

r ph.2014.01.25.m6.1.d07.cut2.BHZ

cut off

rmean

rtr

taper w 0.01

 $w\ ph.2014.01.25.m6.1.d07.cut2.swin.BHZ$

#D08

r Z9.D08..BHZ.M__at__2014-01-25T05.28.57.000Z.SAC

```
ppk
```

setbb t0 &1,t0

evaluate to cutmin %t0 - 25

evaluate to cutmax %t0 + 200

ch t0 %t0

w ph.2014.01.25.m6.1.d08.cut1.BHZ

cut %cutmin %cutmax

r ph.2014.01.25.m6.1.d08.cut1.BHZ

ppk

setbb t0 &1,t0

evaluate to cutmin %t0 - 20

evaluate to cutmax %t0 + 180

ch t0 %t0

w ph.2014.01.25.m6.1.d08.cut2.BHZ

cut %cutmin %cutmax

r ph.2014.01.25.m6.1.d08.cut2.BHZ

cut off

rmean

rtr

```
taper w 0.01
```

w ph.2014.01.25.m6.1.d08.cut2.swin.BHZ

#D09

r Z9.D09..BHZ.M_at_2014-01-25T05.28.57.000Z.SAC

ppk

setbb t0 &1,t0

evaluate to cutmin %t0 - 25

evaluate to cutmax %t0 + 200

ch t0 %t0

w ph.2014.01.25.m6.1.d09.cut1.BHZ

cut %cutmin %cutmax

r ph.2014.01.25.m6.1.d09.cut1.BHZ

ppk

setbb t0 &1,t0

evaluate to cutmin %t0 - 20

evaluate to cutmax %t0 + 180

ch t0 %t0

w ph.2014.01.25.m6.1.d09.cut2.BHZ

cut %cutmin %cutmax

r ph.2014.01.25.m6.1.d09.cut2.BHZ cut off rmean rtr taper w 0.01 w ph.2014.01.25.m6.1.d09.cut2.swin.BHZ #D10 r Z9.D10..BHZ.M_at_2014-01-25T05.28.57.000Z.SAC ppk setbb t0 &1,t0 evaluate to cutmin %t0 - 25 evaluate to cutmax %t0 + 200ch t0 %t0 w ph.2014.01.25.m6.1.d10.cut1.BHZ cut %cutmin %cutmax r ph.2014.01.25.m6.1.d10.cut1.BHZ

ppk

setbb t0 &1,t0 evaluate to cutmin %t0 - 20 evaluate to cutmax %t0 + 180ch t0 %t0 w ph.2014.01.25.m6.1.d10.cut2.BHZ cut %cutmin %cutmax r ph.2014.01.25.m6.1.d10.cut2.BHZ cut off rmean rtr taper w 0.01 $w\ ph.2014.01.25.m6.1.d10.cut2.swin.BHZ$ # D11 r Z9.D11..BHZ.M_at_2014-01-25T05.28.57.000Z.SAC ppk setbb t0 &1,t0 evaluate to cutmin %t0 - 25

evaluate to cutmax %t0 + 200

ch t0 %t0

w ph.2014.01.25.m6.1.d11.cut1.BHZ cut %cutmin %cutmax r ph.2014.01.25.m6.1.d11.cut1.BHZ ppk setbb t0 &1,t0 evaluate to cutmin %t0 - 20 evaluate to cutmax %t0 + 180ch t0 %t0 w ph.2014.01.25.m6.1.d11.cut2.BHZ cut %cutmin %cutmax r ph.2014.01.25.m6.1.d11.cut2.BHZ cut off rmean rtr taper w 0.01 w ph.2014.01.25.m6.1.d11.cut2.swin.BHZ

#D12

r Z9.D12..BHZ.M__at__2014-01-25T05.28.57.000Z.SAC

ppk

setbb t0 &1,t0

evaluate to cutmin %t0 - 25

evaluate to cutmax %t0 + 200

ch t0 %t0

w ph.2014.01.25.m6.1.d12.cut1.BHZ

cut %cutmin %cutmax

r ph.2014.01.25.m6.1.d12.cut1.BHZ

ppk

setbb t0 &1,t0

evaluate to cutmin %t0 - 20

evaluate to cutmax %t0 + 180

ch t0 %t0

w ph.2014.01.25.m6.1.d12.cut2.BHZ

cut %cutmin %cutmax

r ph.2014.01.25.m6.1.d12.cut2.BHZ

cut off

rmean

```
rtr
```

taper w 0.01

w ph.2014.01.25.m6.1.d12.cut2.swin.BHZ

#D13

r Z9.D13..BHZ.M_at_2014-01-25T05.28.57.000Z.SAC

ppk

setbb t0 &1,t0

evaluate to cutmin %t0 - 25

evaluate to cutmax %t0 + 200

ch t0 %t0

w ph.2014.01.25.m6.1.d13.cut1.BHZ

cut %cutmin %cutmax

r ph.2014.01.25.m6.1.d13.cut1.BHZ

ppk

setbb t0 &1,t0

evaluate to cutmin %t0 - 20

evaluate to cutmax %t0 + 180

ch t0 %t0

w ph.2014.01.25.m6.1.d13.cut2.BHZ

cut %cutmin %cutmax

r ph.2014.01.25.m6.1.d13.cut2.BHZ

cut off

rmean

rtr

taper w 0.01

 $w\ ph.2014.01.25.m6.1.d13.cut2.swin.BHZ$

#D14

r Z9.D14..BHZ.M_at_2014-01-25T05.28.57.000Z.SAC

ppk

setbb t0 &1,t0

evaluate to cutmin %t0 - 25

evaluate to cutmax %t0 + 200

ch t0 %t0

w ph.2014.01.25.m6.1.d14.cut1.BHZ

cut %cutmin %cutmax

r ph.2014.01.25.m6.1.d14.cut1.BHZ

ppk setbb t0 &1,t0 evaluate to cutmin %t0 - 20 evaluate to cutmax %t0 + 180ch t0 %t0 w ph.2014.01.25.m6.1.d14.cut2.BHZ cut %cutmin %cutmax r ph.2014.01.25.m6.1.d14.cut2.BHZ cut off rmean rtr taper w 0.01 w ph.2014.01.25.m6.1.d14.cut2.swin.BHZ #D15 r Z9.D15..BHZ.M_at_2014-01-25T05.28.57.000Z.SAC ppk

setbb t0 &1,t0

evaluate to cutmin %t0 - 25

evaluate to cutmax %t0 + 200ch t0 %t0 w ph.2014.01.25.m6.1.d15.cut1.BHZ cut %cutmin %cutmax r ph.2014.01.25.m6.1.d15.cut1.BHZ ppk setbb t0 &1,t0 evaluate to cutmin %t0 - 20 evaluate to cutmax %t0 + 180ch t0 %t0 w ph.2014.01.25.m6.1.d15.cut2.BHZ cut %cutmin %cutmax r ph.2014.01.25.m6.1.d15.cut2.BHZ cut off

rmean

rtr

taper w 0.01

w ph.2014.01.25.m6.1.d15.cut2.swin.BHZ

```
#D17
```

r Z9.D17..BHZ.M_at_2014-01-25T05.28.56.000Z.SAC

ppk

setbb t0 &1,t0

evaluate to cutmin %t0 - 25

evaluate to cutmax %t0 + 200

ch t0 %t0

w ph.2014.01.25.m6.1.d17.cut1.BHZ

cut %cutmin %cutmax

r ph.2014.01.25.m6.1.d17.cut1.BHZ

ppk

setbb t0 &1,t0

evaluate to cutmin %t0 - 20

evaluate to cutmax %t0 + 180

ch t0 %t0

w ph.2014.01.25.m6.1.d17.cut2.BHZ

cut %cutmin %cutmax

r ph.2014.01.25.m6.1.d17.cut2.BHZ

cut off

rmean rtr taper w 0.01 w ph.2014.01.25.m6.1.d17.cut2.swin.BHZ #D18 r Z9.D18..BHZ.M_at_2014-01-25T05.28.56.000Z.SAC ppk setbb t0 &1,t0 evaluate to cutmin %t0 - 25 evaluate to cutmax %t0 + 200ch t0 %t0 w ph.2014.01.25.m6.1.d18.cut1.BHZ cut %cutmin %cutmax r ph.2014.01.25.m6.1.d18.cut1.BHZ ppk

setbb t0 &1,t0

evaluate to cutmin %t0 - 20

evaluate to cutmax %t0 + 180

ch t0 %t0 $w\ ph.2014.01.25.m6.1.d18.cut 2.BHZ$ cut %cutmin %cutmax r ph.2014.01.25.m6.1.d18.cut2.BHZ cut off rmean rtr taper w 0.01 w ph.2014.01.25.m6.1.d18.cut2.swin.BHZ # D19 r Z9.D19..BHZ.M_at_2014-01-25T05.28.56.000Z.SAC ppk setbb t0 &1,t0 evaluate to cutmin %t0 - 25 evaluate to cutmax %t0 + 200

ch t0 %t0

w ph.2014.01.25.m6.1.d19.cut1.BHZ

cut %cutmin %cutmax

r ph.2014.01.25.m6.1.d19.cut1.BHZ

ppk setbb t0 &1,t0 evaluate to cutmin %t0 - 20 evaluate to cutmax %t0 + 180ch t0 %t0 w ph.2014.01.25.m6.1.d19.cut2.BHZ cut %cutmin %cutmax r ph.2014.01.25.m6.1.d19.cut2.BHZ cut off rmean rtr taper w 0.01 w ph.2014.01.25.m6.1.d19.cut2.swin.BHZ #D20 r Z9.D20..BHZ.M__at__2014-01-25T05.28.55.000Z.SAC ppk setbb t0 &1,t0

evaluate to cutmin %t0 - 25

evaluate to cutmax %t0 + 200

ch t0 %t0

w ph.2014.01.25.m6.1.d20.cut1.BHZ

cut %cutmin %cutmax

r ph.2014.01.25.m6.1.d20.cut1.BHZ

ppk

setbb t0 &1,t0

evaluate to cutmin %t0 - 20

evaluate to cutmax %t0 + 180

ch t0 %t0

w ph.2014.01.25.m6.1.d20.cut2.BHZ

cut %cutmin %cutmax

r ph.2014.01.25.m6.1.d20.cut2.BHZ

cut off

rmean

rtr

taper w 0.01

w ph.2014.01.25.m6.1.d20.cut2.swin.BHZ

```
#D21
```

r Z9.D21..BHZ.M__at__2014-01-25T05.28.55.000Z.SAC

ppk

setbb t0 &1,t0

evaluate to cutmin %t0 - 25

evaluate to cutmax %t0 + 200

ch t0 %t0

w ph.2014.01.25.m6.1.d21.cut1.BHZ

cut %cutmin %cutmax

r ph.2014.01.25.m6.1.d21.cut1.BHZ

ppk

setbb t0 &1,t0

evaluate to cutmin %t0 - 20

evaluate to cutmax %t0 + 180

ch t0 %t0

w ph.2014.01.25.m6.1.d21.cut2.BHZ

cut %cutmin %cutmax

r ph.2014.01.25.m6.1.d21.cut2.BHZ

cut off rmean rtr taper w 0.01 w ph.2014.01.25.m6.1.d21.cut2.swin.BHZ #D22 r Z9.D22..BHZ.M__at__2014-01-25T05.28.55.000Z.SAC ppk setbb t0 &1,t0 evaluate to cutmin %t0 - 25 evaluate to cutmax %t0 + 200ch t0 %t0 w ph.2014.01.25.m6.1.d22.cut1.BHZ cut %cutmin %cutmax r ph.2014.01.25.m6.1.d22.cut1.BHZ ppk

setbb t0 &1,t0

evaluate to cutmin %t0 - 20

evaluate to cutmax %t0 + 180ch t0 %t0 w ph.2014.01.25.m6.1.d22.cut2.BHZ cut %cutmin %cutmax r ph.2014.01.25.m6.1.d22.cut2.BHZ cut off rmean rtr taper w 0.01 w ph.2014.01.25.m6.1.d22.cut2.swin.BHZ **Steps 4-6** Stripping the SAC headers, assembling Line Gathers, and Static Corrections **Shell Name:** first_line_gather_and_static_calculations.txt **Shell:** ## Construct the initial gather. cp infile1 outfile dd if = infile2 >> outfile dd if = infile3 >> outfile

dd if = infile4 >> outfile

dd if = infile5 >> outfile

dd if = infile6 >> outfile

dd if = infile7 >> outfile

dd if = infile8 >> outfile

dd if = infile9 >> outfile

dd if = infile10 >> outfile

dd if = infile11 >> outfile

dd if = infile12 >> outfile

dd if = infile13 >> outfile

dd if = infile14 >> outfile

dd if = infile14 >> outfile

dd if = infile16 >> outfile

dd if = infile17 >> outfile

dd if = infile18 >> outfile

Strip the SAC headers.

sacheaderstrip in = infile \setminus

out = outfile \

 $hdr = outfile.hdr ntr = 18 \setminus$

nt = 10001

Apply a first pass bandpass filter.

suaddhead < infile ns = 10001 | \

sushw key = dt $a = 20000 > \$

```
outfile.su
sufilter < infile.su f = 0,0.25, 0.5, 0.75, 1, 1.25, 1.5, 1.75, 2 amps = 0, 0, 0.75, 1, 1, 1, 0.75, 0, 0
> outfile.su
## Strip the file header.
sustrip < infile.su > outfile
## Calculate static corrections.
crosscorrstatquake in = infile out = outfile outc = outfile.c corr = outfile.corr ntr = 18 nt =
10001 dt = 0.02 \text{ npilot} = 8 t1 = 18 t2 = 24 \text{ secmax} = 3
## Window the gather.
seispickalt_2015 in = infile out = outfile nx = 18 nt = 10001 nt1 = 1 nt2 = 2501
## Plot.
suaddhead < infile ns = 10001 | \
sushw key = dt a = 20000 > \
outfile.su
suop < infile.su op = norm | \
supswigp xcur = 1.0 \text{ wbox} = 6 \text{ hbox} = 8.5 \text{ style} = seismic \setminus
```

 $nbpi = 300 linewidth = 0 \setminus$

title = "Gather_Line_D" \

```
label1 = "Time (s)" labelsize = 9 \text{ n2tic} = 2 \text{ xbeg} = -0.2 \setminus
xend = 1 interp = 1 n1tic = 5 titlesize = 8 key = offset > \
outfile.su.ps
suaddhead < infile ns = 10001 | \
sushw key = dt a = 20000 > \
outfile.su
suop < infile.su op = norm | \
supswigp xcur = 1.0 \text{ wbox} = 6 \text{ hbox} = 8.5 \text{ style} = \text{seismic} \setminus
nbpi = 300 linewidth = 0 \setminus
title="Gather Line D statout" \
label1 = "Time (s)" labelsize = 9 \text{ n2tic} = 2 \text{ xbeg} = -0.2 \setminus
xend = 1 interp = 1 n1tic = 5 titlesize = 8 key = offset > 
outfile.su.ps
suaddhead < infile ns = 10001 | \
sushw key = dt a = 20000 > \
outfile.su
supswigp xcur = 1.0 \text{ wbox} = 6 \text{ hbox} = 8.5 \text{ style} = seismic \setminus
nbpi = 300 linewidth = 0 \setminus
```

```
title = "Gather Line D statout windowed filtered" \
label1 = "Time (s)" labelsize = 9 \text{ n2tic} = 2 \text{ xbeg} = -0.2 \setminus
xend = 1 interp = 1 n1tic = 5 titlesize = 8 key = offset > 
outfile.su.ps
suaddhead < infile ns = 2501 \mid \ 
sushw key = dt a = 20000 > \
outfile.su
suop < infile.su op = norm | \
supswigp xcur = 1.0 \text{ wbox} = 6 \text{ hbox} = 8.5 \text{ style} = \text{seismic} \setminus
nbpi = 300 linewidth = 0 \setminus
title = "Gather_Line_D_statout_windowed_filtered" \
label1 = "Time (s)" labelsize = 9 \text{ n2tic} = 2 \text{ xbeg} = -0.2 \setminus
xend = 1 interp = 1 n1tic = 5 titlesize = 8 key = offset > \
outfile.su.ps
Shell Name: second_line_gather_and_static_corrections.txt
Shell:
## Reconstruct the line gather (with no filtering applied).
cp infile1 outfile
dd if = infile2 >> outfile
dd if = infile3 >> outfile
```

dd if = infile4 >> outfile

dd if = infile5 >> outfile

dd if = infile6 >> outfile

dd if = infile7 >> outfile

dd if = infile8 >> outfile

dd if = infile9 >> outfile

dd if = infile10 >> outfile

dd if = infile11 >> outfile

dd if = infile12 >> outfile

dd if = infile13 >> outfile

dd if = infile14 >> outfile

dd if = infile14 >> outfile

dd if = infile16 >> outfile

dd if = infile17 >> outfile

Strip the SAC headers.

sacheaderstrip in = infile \

out = outfile \

 $hdr = outfile.hdr ntr = 17 \setminus$

nt = 10001

Window the gather.

seispickalt_2015 in = infile out = outfile nx = 17 nt = 10001 nt1 = 1 nt2 = 2501

```
## Apply calculated static corrections.
sampshiftarb in = infile out = outfile ntr = 17 nt = 2501 mode = 2 para = outfile.c
## Plot.
suaddhead < infile ns = 10001 | \
sushw key = dt a = 20000 > \
outfile.su
suop < infile.su op = norm | \
supswigp xcur = 1.0 \text{ wbox} = 6 \text{ hbox} = 8.5 \text{ style} = \text{seismic} \setminus
nbpi = 300 linewidth = 0 \setminus
title = "Gather_Line_D" \
label1 = "Time (s)" labelsize = 9 \text{ n2tic} = 2 \text{ xbeg} = -0.2 \setminus
xend = 1 interp = 1 n1tic = 5 titlesize = 8 key = offset > 
outfile.su.ps
suaddhead < infile ns = 10001 | \
sushw key = dt a = 20000 > \
outfile.su
suop < infile.su op = norm \mid \ 
supswigp xcur = 1.0 \text{ wbox} = 6 \text{ hbox} = 8.5 \text{ style} = seismic \setminus
```

```
nbpi = 300 linewidth = 0 \setminus
title = "Gather Line D statout" \
label1 = "Time (s)" labelsize = 9 \text{ n2tic} = 2 \text{ xbeg} = -0.2 \setminus
xend = 1 interp = 1 n1tic = 5 titlesize = 8 key = offset > 
outfile.su.ps
suaddhead < infile ns = 10001 | \
sushw key = dt a=20000 > \
outfile.su
suop < infile.su op = norm | \
supswigp xcur = 1.0 \text{ wbox} = 6 \text{ hbox} = 8.5 \text{ style} = \text{seismic} \setminus
nbpi = 300 linewidth = 0 \setminus
title = "Gather_Line_D_statout_windowed_filtered" \
label1 = "Time (s)" labelsize = 9 \text{ n2tic} = 2 \text{ xbeg} = -0.2 \setminus
xend = 1 interp = 1 n1tic = 5 titlesize = 8 key = offset > \
outfile.su.ps
suaddhead < infile ns = 2501 \mid \ 
sushw key = dt a = 20000 > \
outfile.su
suop < infile.su op = norm \mid \
```

```
supswigp xcur = 1.0 \text{ wbox} = 6 \text{ hbox} = 8.5 \text{ style} = \text{seismic} \setminus
nbpi = 300 linewidth = 0 \setminus
title = "Gather_Line_D_statout_windowed" \
label1 = "Time (s)" labelsize = 9 \text{ n2tic} = 2 \text{ xbeg} = -0.2 \setminus
xend = 1 interp = 1 n1tic = 5 titlesize = 8 key = offset > 
outfile.su.ps
```

<u>Step 7</u>

Estimating the Source time Function

```
Shell Name: STF.txt
```

 $nbpi = 300 linewidth = 0 \setminus$

title = "STF" \

```
Shell:
## Stack the line gather.
vertstack in = infile out = outfile nt=2501 ntr=17
## Plot.
suaddhead < infile ns = 2501 | \
sushw key = dt a = 20000 > \
outfile.su
suop < infile.su op = norm | \
supswigp xcur = 1.0 \text{ wbox} = 6 \text{ hbox} = 8.5 \text{ style} = seismic \setminus
```

```
label1 = "Time (s)" labelsize = 9 \text{ n2tic} = 2 \text{ xbeg} = -0.2 \setminus
xend = 1 interp = 1 n1tic = 5 titlesize = 8 key = offset > \
outfile.su.ps
Shell Name: STF_zero.txt
Shell:
## Zero the end of the STF trace.
suzero < infile.su > outfile.su itmin = 1301 itmax = 2501
## Zero the start of the STF trace.
suzero < infile.su > outfile.su itmin = 0 itmax = 1051
## Plot.
suop < infile.su op = norm | \
supswigp xcur = 1.0 \text{ wbox} = 6 \text{ hbox} = 8.5 \text{ style} = seismic \setminus
nbpi = 300 linewidth = 0 \setminus
title = "STF" \
label1 = "Time (s)" labelsize = 9 \text{ n2tic} = 2 \text{ xbeg} = -0.2 \setminus
xend = 1 interp = 1 n1tic = 5 titlesize = 8 key = offset > 
outfil.su.ps
## Strip the file header.
```

sustrip < infile.su > outfile

Step 8

Signal Deconvolution

```
Shell Name: Decon.txt
Shell:
## Convert the station offset file to a binary.
a2b < offsets.txt n1=1 > \setminus
offsets.bin
## Deconvolve the line gather.
freqdeconsourcemac numer = infile1 denom = infile2 out = outfile ntr = 17 nt = 2501 dt = 0.02
alpha = 1.75 \text{ wh} = 0.0001 \text{ pre} = 20 \text{ taper} = 1
## Plot.
suaddhead < infile ns = 2501 \mid \ 
sushw key = dt a = 20000 > \
outfile.su
sushw < infile.su \setminus
infile = offsets.bin key = offset > \
outfile.su
suop < infile.su op = norm | \</pre>
```

```
supswigp xcur = 1 \text{ wbox} = 8 \text{ hbox} = 11 \text{ style} = seismic \setminus
nbpi = 300 linewidth = 0 \setminus
title = "Decon_line_D" \
label1 = "Time (s)" labelsize = 9 \text{ n2tic} = 2 \text{ xbeg} = -0.2 \setminus
xend = 1 interp = 1 n1tic = 5 titlesize = 8 key = offset > 
outfile.su.ps
Shell Name: offsets.txt
Shell:
## Establish the station offsets (km from furthest north station at offset = 100 km).
100
129.2011
143.1467
165.5455
180.8437
195.2430
212.3931
220.5242
229.6425
234.9781
244.9282
252.1161
257.3184
```

262.9755

269.2093

285.4147

292.2251

300.0669

Steps 9-12, 14

<u>Sub-Sectioning and Slant Stacking, Semblance Based Coherency Filtering, the Removal of interfering seismic arrivals, Inverse Slant Stacking, and 2 D Slant Stack Migration</u>

Shell Name: sub_sectioning.txt

Shell:

Sub section the gather.

seispickalt_2015 in = infile out = outfile1 nx = 20 nx1 = 1 nx2 = 4 nt = 2501 nt1 = 1 nt2 = 2501seispickalt_2015 in = infile out = outfile2 nx = 20 nx1 = 5 nx2 = 8 nt = 2501 nt1 = 1 nt2 = 2501seispickalt_2015 in = infile out = outfile3 nx = 20 nx1 = 9 nx2 = 12 nt = 2501 nt1 = 1 nt2 = 2501

seispickalt_2015 in = infile out = outfile4 nx = 20 nx1 = 13 nx2 = 16 nt = 2501 nt1 = 1 nt2 = 2501

seispickalt_2015 in = infile out = outfile5 nx = 20 nx1 = 17 nx2 = 20 nt = 2501 nt1 = 1 nt2 = 2501

Convert offsets to binary files.

 $a2b < offsets_1.txt \ n1=1 > \$

```
offsets_1.bin
a2b < offsets\_2.txt \ n1=1 > \setminus
offsets\_2.bin
a2b < offsets\_3.txt n1=1 > \setminus
offsets\_3.bin
a2b < offsets\_4.txt \ n1=1 > \setminus
offsets\_4.bin
a2b < offsets\_5.txt n1=1 > \setminus
offsets_5.bin
## Plot.
suaddhead < infile ns = 2501 | \
sushw key = dt a = 20000 > \
outfile.su
sushw < infile.su \setminus\\
infile = offsets_1.bin key = offset > \
outfile.su
suop < infile.su op = norm | \
supswigp xcur = 1 \text{ wbox} = 8 \text{ hbox} = 11 \text{ style} = seismic \setminus
nbpi = 300 linewidth = 0 \setminus
title = "decon_line_E.statout.windowed_sub_section_1" \
```

```
label1 = "Time (s)" labelsize = 9 \text{ n2tic} = 2 \text{ xbeg} = -0.2 \setminus
xend = 1 interp = 1 n1tic = 5 titlesize = 8 key = offset > \
outfile.su.ps
suaddhead < infile ns = 2501 | \
sushw key = dt a = 20000 > \
outfile.su
sushw < infile.su \
infile = offsets_2.bin key = offset > \
outfile.su
suop < infile.su op = norm | \
supswigp xcur = 1 \text{ wbox} = 8 \text{ hbox} = 11 \text{ style} = \text{seismic} \setminus
nbpi = 300 linewidth = 0 \setminus
title = "decon_line_E.statout.windowed_sub_section_2" \
label1 = "Time (s)" labelsize = 9 \text{ n2tic} = 2 \text{ xbeg} = -0.2 \setminus
xend = 1 interp = 1 n1tic = 5 titlesize = 8 key = offset > \
outfile.su.ps
suaddhead < infile ns = 2501 | \
sushw key = dt a = 20000 > \
outfile.su
```

```
sushw < infile.su \
infile = offsets\_3.bin key = offset > \
outfile.su
suop < infile.su op = norm | \
supswigp xcur = 1 \text{ wbox} = 8 \text{ hbox} = 11 \text{ style} = \text{seismic} \setminus
nbpi = 300 linewidth = 0 \setminus
title = "decon_line_E.statout.windowed_sub_section_3" \
label1 = "Time (s)" labelsize = 9 \text{ n2tic} = 2 \text{ xbeg} = -0.2 \setminus
xend = 1 interp = 1 n1tic = 5 titlesize = 8 key = offset > 
outfile.su.ps
suaddhead < infile ns = 2501 \mid \ 
sushw key = dt a = 20000 > \
outfile.su
sushw < infile.su \
infile = offsets_4.bin key = offset > \
outfile.su
suop < infile.su op = norm | \
supswigp xcur = 1 \text{ wbox} = 8 \text{ hbox} = 11 \text{ style} = seismic \setminus
```

```
nbpi = 300 linewidth = 0 \setminus
title = "decon line E.statout.windowed sub section 4" \
label1 = "Time (s)" labelsize = 9 \text{ n2tic} = 2 \text{ xbeg} = -0.2 \setminus
xend = 1 interp = 1 n1tic = 5 titlesize = 8 key = offset > 
outfile.su.ps
suaddhead < infile ns = 2501 | \
sushw key = dt a = 20000 > \
outfile.su
sushw < infile.su \
infile = offsets\_5.bin key = offset > \
outfile.su
suop < infile.su op = norm | \
supswigp xcur = 1 \text{ wbox} = 8 \text{ hbox} = 11 \text{ style} = \text{seismic} \setminus
nbpi = 300 linewidth = 0 \setminus
title = "decon_line_E.statout.windowed_sub_section_5" \
label1 = "Time (s)" labelsize = 9 \text{ n2tic} = 2 \text{ xbeg} = -0.2 \setminus
xend = 1 interp = 1 n1tic = 5 titlesize = 8 key = offset > \
outfile.su.ps
```

In order to avoid redundancy we demonstrate offsets_1.txt only, excluding offsets_2.txt offsets_5.txt. **Shell Name:** offsets_1.txt **Shell:** ## Establish station offsets (km from furthest north station at 100 km). 100 132.2501 154.9841 172.1616 **Shell Name:** taper_slantstack_coherency_filter.txt **Shell:** ## Taper the seismic section. windowstacktaper in = infile out = outfile nx = 4 nt = 2501 nx1 = 0 nx2 = 5 t0 = 0 t1 = 0 t2 = 50dt = 0.02 nxtap = 0 nttap = 0## Plot. suaddhead < infile ns = 2501 | \ sushw key = $dt a = 20000 > \$ outfile.su $suop < infile.su op = norm | \ \$

supswigp $xcur = 1.0 \text{ wbox} = 6 \text{ hbox} = 8.5 \text{ style} = seismic \setminus$

```
nbpi = 300 linewidth = 0 \setminus
title = "tapereddecon line E.statout.windowed sub section 1" \
label1 = "Time (s)" labelsize = 9 \text{ n2tic} = 2 \text{ xbeg} = -0.2 \setminus
xend = 1 interp = 1 n1tic = 5 titlesize = 8 key = offset > \
outfile.su.ps
## Forward slant stack.
slantstackforward in = infile outstack = outfile outsemb = outfile.semb mode = 2 nx = 4 dt =
0.02 \text{ nt} = 2501 \text{ t0} = 0.0 \text{ taumin} = 0 \text{ ntau} = 2501 \text{ dp} = 0.000375 \text{ pmin} = -0.075 \text{ np} = 400 \text{ para} = -0.075 \text{ np} = 400 \text{ para} = -0.075 \text{ np} = -0
offsets_1.txt
## Plot.
suaddhead < infile ns = 2501 \mid \ 
sushw key = dt a = 20000 > \
outfile.su
suop < infile.su | \
supswigp xcur = 1.0 \text{ wbox} = 6 \text{ hbox} = 8.5 \text{ style} = \text{seismic} \setminus
nbpi = 300 linewidth = 0 \setminus
title = "slantstack decon line E sub section 1" \
label1 = "Time (s)" labelsize = 9 \text{ n2tic} = 2 \text{ xbeg} = -0.2 \setminus
xend = 1 interp = 1 n1tic = 5 titlesize = 8 key = offset > \
outfile.su.ps
```

```
suaddhead < infile ns = 2501 | \
sushw key = dt a = 20000 > \
outfile.su
suop < infile.su | \
supswigp xcur = 1.0 \text{ wbox} = 6 \text{ hbox} = 8.5 \text{ style} = \text{seismic} \setminus
nbpi = 300 linewidth = 0 \setminus
title = "semblance1" \
label1 = "Time (s)" labelsize = 9 \text{ n2tic} = 2 \text{ xbeg} = -0.2 \setminus
xend = 1 interp = 1 n1tic = 5 titlesize = 8 key = offset > 
outfile.su.ps
## Filter the semblance spectra.
sufilter < infile.su f = 0.25, 0.5, 0.75, 1, 1.25, 1.5, 1.75, 2, 2.25 amps=1, 1, 1, 1, 0.75, 0.5, 0.25,
0, 0 > \text{outfile.su}
## Plot.
suop < infile.su | \
supswigp xcur = 1.0 \text{ wbox} = 6 \text{ hbox} = 8.5 \text{ style} = \text{seismic} \setminus
nbpi = 300 linewidth = 0 \setminus
title = "semblance1.su.filtered" \
label1 = "Time (s)" labelsize = 9 \text{ n2tic} = 2 \text{ xbeg} = -0.2 \setminus
```

```
xend = 1 interp = 1 n1tic = 5 titlesize = 8 key = offset > \
outfile.su.ps
## Strip the file header.
sustrip < infile.su > outfile
## Create a semblance matrix of ones and zeros using semblance spectra calculated during
forward slantstack.
sembmutebelowmac in = infile.semb out = outfile ntr = 400 nt = 2501 max orig = 1 thresh = 0.65
## Multiply matrix by forward slant stacked section.
tracemultmac in1 = infile1 in2 = infile2 out = outfile ntr = 400 nt = 2501
## Plot.
suaddhead < infile ns = 2501 | \
sushw key = dt a = 20000 > \
outfile.su
suop < infile.su | \
supswigp xcur = 1.0 \text{ wbox} = 6 \text{ hbox} = 8.5 \text{ style} = \text{seismic} \setminus
nbpi = 300 linewidth = 0 \setminus
title = "semblance_filtered_slantstack_decon_line_E_sub_section_1" \
label1 = "Time (s)" labelsize = 9 \text{ n2tic} = 2 \text{ xbeg} = -0.2 \setminus
```

```
xend = 1 interp = 1 n1tic = 5 titlesize = 8 key = offset > \
outfile.su.ps
Shell Name: offsets_1.txt
Shell:
## Establish station offsets (km from furthest north station at 100 km).
100
132.2501
154.9841
172.1616
Shell Name: remove_interfering_arrivals_inverse_slantstack.txt
Shell:
## Isolate PKP 1.
windowstacktaper in = infile out = outfile nx = 400 nt = 2501 nx1 = 175 nx2 = 250 t0 = 0 t1 = 100 nt
```

```
## Isolate PKP 1.

windowstacktaper in = infile out = outfile in 27 t2 = 29 dt = 0.02 nxtap = 0 nttap = 0

## Plot.

suaddhead < infile ns = 2501 | \

sushw key = dt a = 20000 > \

outfile.su

suop < infile.su op = norm | \
```

```
supswigp xcur = 1.0 \text{ wbox} = 6 \text{ hbox} = 8.5 \text{ style} = \text{seismic} \setminus
nbpi = 300 linewidth = 0 \setminus
title = "semblance filtered slantstack 1 PKP 1" \
label1 = "Time (s)" labelsize = 9 \text{ n2tic} = 2 \text{ xbeg} = -0.2 \setminus
xend = 1 interp = 1 n1tic = 5 titlesize = 8 key = offset > \
outfile.su.ps
## Isolate PKP 2.
windowstacktaper in = infile1 out = outfile nx = 400 nt = 2501 nx1 = 225 nx2 = 300 t0 = 0 t1 = 2501 nx1 = 2501 nx1 = 2501 nx2 = 300 t0 = 0 t1 = 2501 nx1 = 2501 nx1
39 t2 = 42 dt = 0.02 nxtap = 0 nttap = 0
## Plot.
suaddhead < infile ns = 2501 | \
sushw key = dt a = 20000 > \
outfile.su
suop < infile.su op = norm | \
supswigp xcur = 1.0 \text{ wbox} = 6 \text{ hbox} = 8.5 \text{ style} = \text{seismic} \setminus
nbpi = 300 linewidth = 0 \setminus
title = "semblance filtered slantstack 1 PKP 2" \
label1 = "Time (s)" labelsize = 9 \text{ n2tic} = 2 \text{ xbeg} = -0.2 \setminus
xend = 1 interp = 1 n1tic = 5 titlesize = 8 key = offset > \
outfile.su.ps
```

```
## Add extracted PKP arrivals.
tracescaleaddmac in1 = infile1 in2 = infile2 out = outfile ntr = 400 nt = 2501 ratio12 = 1
## Plot.
suaddhead < infile ns = 2501 | \
sushw key = dt a=20000 > \
outfile.su
suop < infile.su |\
supswigp xcur = 1.0 \text{ wbox} = 6 \text{ hbox} = 8.5 \text{ style} = \text{seismic} \setminus
nbpi = 300 linewidth = 0 \setminus
title = "summedslantstackextract" \
label1 = "Time (s)" labelsize = 9 \text{ n2tic} = 2 \text{ xbeg} = -0.2 \setminus
xend = 1 interp = 1 n1tic = 5 titlesize = 8 key = offset > \
outfile.su.ps
## Subtract PKP arrivals from the slantstack.
suop2 infile1.su infile2.su op = diff > outfile.su
suop2 infile1.su infile2.su op = diff > outfile.su
## Plot.
suop < infile.su | \
```

```
supswigp xcur = 1.0 \text{ wbox} = 6 \text{ hbox} = 8.5 \text{ style} = \text{seismic} \setminus
nbpi = 300 linewidth = 0 \setminus
title = "slantstack_PKP_removed_1" \
label1 = "Time (s)" labelsize = 9 \text{ n2tic} = 2 \text{ xbeg} = -0.2 \setminus
xend = 1 interp = 1 n1tic = 5 titlesize = 8 key = offset > \
outfile.su.ps
## Strip the file header.
sustrip < infile.su > outfile
## Inverse slant stack.
slantstackinverse in = infile out = outfile para = offsets_1.txt ireduce = 0 mode = 2 pmin = -
0.075 \text{ np} = 400 \text{ dp} = 0.000375 \text{ tau} = 0 \text{ ntau} = 2501 \text{ dt} = 0.02 \text{ nx} = 4 \text{ tmin} = 0.0 \text{ nt} = 2501 \text{ dt} = 0.02 \text{ nx} = 4 \text{ tmin} = 0.0 \text{ nt} = 2501 \text{ dt} = 0.02 \text{ nx} = 4 \text{ tmin} = 0.0 \text{ nt} = 2501 \text{ dt} = 0.02 \text{ nx} = 4 \text{ tmin} = 0.0 \text{ nt} = 2501 \text{ dt} = 0.02 \text{ nx} = 4 \text{ tmin} = 0.0 \text{ nt} = 2501 \text{ dt} = 0.02 \text{ nx} = 4 \text{ tmin} = 0.0 \text{ nt} = 2501 \text{ dt} = 0.02 \text{ nx} = 4 \text{ tmin} = 0.0 \text{ nt} = 2501 \text{ dt} = 0.02 \text{ nx} = 4 \text{ tmin} = 0.0 \text{ nt} = 2501 \text{ dt} = 0.02 \text{ nx} = 4 \text{ tmin} = 0.0 \text{ nt} = 2501 \text{ dt} = 0.02 \text{ nx} = 4 \text{ tmin} = 0.0 \text{ nt} = 2501 \text{ dt} = 0.02 \text{ nx} = 4 \text{ tmin} = 0.0 \text{ nt} = 2501 \text{ dt} = 0.02 \text{ nx} = 4 \text{ tmin} = 0.0 \text{ nt} = 2501 \text{ dt} = 0.02 \text{ nx} = 4 \text{ tmin} = 0.0 \text{ nt} = 2501 \text{ dt} = 0.02 \text{ nx} = 4 \text{ tmin} = 0.0 \text{ nt} = 2501 \text{ dt} = 0.02 \text{ nx} = 4 \text{ tmin} = 0.0 \text{ nt} = 2501 \text{ dt} = 0.02 \text{ nx} = 4 \text{ tmin} = 0.0 \text{ nt} = 2501 \text{ dt} = 0.02 \text{ nx} = 4 \text{ tmin} = 0.0 \text{ nt} = 2501 \text{ dt} = 0.02 \text{ nx} = 4 \text{ tmin} = 0.0 \text{ nt} = 2501 \text{ dt} = 0.02 \text{ nx} = 4 \text{ tmin} = 0.0 \text{ nt} = 2501 \text{ dt} = 0.02 \text{ nx} = 4 \text{ tmin} = 0.0 \text{ nt} = 2501 \text{ dt} = 0.02 \text{ nx} = 4 \text{ tmin} = 0.0 \text{ nt} = 2501 \text{ dt} = 0.02 \text{ nx} = 4 \text{ tmin} = 0.02 \text{ tmin} = 0.02 \text{ nx} = 4 \text{ tmin} = 0.02 \text{ tmin} = 0.0
## Apply the first derivative of the Hilbert Transform.
envelopehilbderivmac in = infile out = outfile nt = 2501 ntr = 4 hbt = 1 mode = 3
## Convert to binary.
a2b < offsets_1.txt \ n1 = 1 > \setminus
offsets_1.bin
## Plot.
suaddhead < infile ns = 2501 \mid \
```

```
sushw key = dt a = 20000 > \
outfile.su
sushw < infile.su \setminus
infile = offsets_1.bin key = offset > \
outfile.su
suop < infile.su op = norm | \
supswigp xcur = 1.0 \text{ wbox} = 6 \text{ hbox} = 8.5 \text{ style} = seismic \setminus
nbpi = 300 linewidth = 0 \setminus
title = "hilber\_inverseslantstack\_PKP\_Removed\_1" \setminus
label1 = "Time (s)" labelsize = 9 \text{ n2tic} = 2 \text{ xbeg} = -0.2 \setminus
xend = 1 interp = 1 n1tic = 5 titlesize = 8 key = offset > 
outfile.su.ps
suaddhead < infile ns = 2501 | \
sushw key = dt a = 20000 > \
outfile.su
sushw < infile.su \setminus
infile = offsets\_1.bin key = offset > \
outfile.su
```

```
suop < infile.su op = norm | \
supswigp xcur = 1.0 \text{ wbox} = 6 \text{ hbox} = 8.5 \text{ style} = \text{seismic} \setminus
nbpi = 300 linewidth = 0 \setminus
title = "inverseslantstack PKP Removed 1" \
label1 = "Time (s)" labelsize = 9 \text{ n2tic} = 2 \text{ xbeg} = -0.2 \setminus
xend = 1 interp = 1 n1tic = 5 titlesize = 8 key = offset > \
outfile.su.ps
## Filter the gather.
sufilter < infile.su f = 0.25, 0.5, 0.75, 1, 1.25, 1.5, 1.75, 2, 2.25 amps = 1, 1, 1, 1, 0.75, 0.5, 0.25,
0, 0 > outfile.su
## Plot.
sushw < infile.su \
infile = offsets_1.bin key = offset > \
outfile.su
suop < infile.su op = norm | \
supswigp xcur = 1.0 \text{ wbox} = 6 \text{ hbox} = 8.5 \text{ style} = \text{seismic} \setminus
nbpi = 300 linewidth = 0 \setminus
title = "filter output" \
label1 = "Time (s)" labelsize = 9 \text{ n2tic} = 2 \text{ xbeg} = -0.2 \setminus
xend = 1 interp = 1 n1tic = 5 titlesize = 8 key = offset > 1 titlesize = 1 titlesize = 8 key = offset > 1 titlesize = 8 key = 0 titlesize = 1 titles
```

```
outfile.su.ps
## Strip the file header.
sustrip < infile.su > outfile
Shell Name: offsets_1.txt
Shell:
## Establish station offsets (km from furthest north station at 100 km).
100
132.2501
154.9841
172.1616
Shell Name: sum_recovered_time_sections.txt
Shell:
## Add recovered time sub-sections.
cp infile1 outfile
dd if = infile2 >> outfile
dd if = infile3 >> outfile
dd if = infile4 >> outfile
dd if = infile5 >> outfile
```

Convert to binary.

```
a2b < station\_offsets.txt \ n1 = 1 > \setminus
station_offsets.bin
## Plot.
suaddhead < infile ns = 2501 | \
sushw key = dt a = 20000 > \
outfile.su
sushw < infile.su \
infile = station\_offsets.bin key = offset > \
outfile.su
suop < infile.su op = norm | \
supswigp xcur = 1 wbox = 8 hbox = 11 style = seismic \
nbpi = 300 linewidth = 0 \setminus
title = "line_E_time" \setminus
label1 = "Time (s)" labelsize = 9 \text{ n2tic} = 2 \text{ xbeg} = -0.2 \setminus
xend = 1 interp = 1 n1tic = 5 titlesize = 8 key = offset > \
outfile.su.ps
Shell Name: station_offsets_1.txt
Shell:
## Establish station offsets (km from furthest north station at 100 km).
```

100
132.2501
154.9841
172.1616
210.3187
215.5636
226.2973
243.0407
251.8002
257.4773
270.3391
280.0187
295.5633
312.8261
322.0726
338.1595
351.5521
391.0521
438.1444

Shell Name: migration.txt

Shell:

450.0378

```
## Migrate the sub-sectioned slant stack.
migslantzeroffset stack = infile nlayer = 12 model = vel.txt para = station_offsets_1.txt filt =
infile.semb out = outfile dt = 0.02 nxorig = 4 dporig = 0.000375 pminorig = -0.075 nporig = 400
taumin = -20 ntau = 2501 arrayelev = 1 arrayvel = 1 datum = 1 dx = 1 dz = 0.02 nx = 800 nz = 1
5501 \text{ tmin} = 0 \text{ tmax} = 30 \text{ pmin} = -0.025 \text{ pmax} = 0.025 \text{ maxgap} = 10 \text{ fmult} = 0.1 \text{ fresnelyesno} = 0.025 \text{ maxgap} = 10 \text{ fmult} = 0.1 \text{ fresnelyesno} = 0.025 \text{ maxgap} = 10 \text{ fmult} = 0.1 \text{ fresnelyesno} = 0.025 \text{ maxgap} = 10 \text{ fmult} = 0.1 \text{ fresnelyesno} = 0.025 \text{ maxgap} = 10 \text{ fmult} = 0.1 \text{ fresnelyesno} = 0.025 \text{ maxgap} = 10 \text{ fmult} = 0.1 \text{ fresnelyesno} = 0.025 \text{ maxgap} = 10 \text{ fmult} = 0.1 \text{ fresnelyesno} = 0.025 \text{ maxgap} = 10 \text{ fmult} = 0.1 \text{ fresnelyesno} = 0.025 \text{ maxgap} = 0.025 \text
1 \text{ vavg} = 7.4 \text{ freq} = 2
## Plot.
suaddhead < infile ns = 5501 \mid \ 
sushw key = dt a = 20000 > \
outfile.su
suop < infile.su | \
supswigp xcur = 1.0 \text{ wbox} = 16 \text{ hbox} = 2 \text{ style} = \text{seismic} \setminus
nbpi = 300 linewidth = 0 \setminus
title = "sub section line E 1 migrated" \
label1 = "Z" labelsize = 9 \text{ n2tic} = 2 \text{ xbeg} = -0.2 \setminus
xend = 1 interp = 1 n1tic = 5 titlesize = 8 key = offset > \
outfile.su.ps
Shell Name: station_offsets_1.txt
```

Shell:

Establish station offsets (km from furthest north station at 100 km). First column includes station identifier and second column includes station offset.

E31 100

E30 132.2501

E29 154.9841

E28 172.1616

Shell Name: Vel.txt

Shell:

Establish layer velocities (first column is slowness s/km, second column is depth to the base of the layer).

0.416667 1.2

0.166667 4.18

0.163676 7.16

0.160791 10.14

0.158006 13.12

0.155316 16.10

0.152716 19.08

0.150201 22.06

0.147768 25.04

0.145413 28.02

0.143131 31.00

0.123457 200.00

```
Shell Name: sum_migrated_sub-sections_global_norm.txt
Shell:
## Apply global normalization.
maxglobalnorm in = infile1 out = outfile1 out2 = junk ntr = 800 nt = 5501
maxglobalnorm in = infile2 out = outfile2 out2 = junk ntr = 800 nt = 5501
maxglobalnorm in = infile3 out = outfile3 out2 = junk ntr = 800 nt = 5501
maxglobalnorm in = infile4 out = outfile4 out2 = junk ntr = 800 nt = 5501
## Add migrated sub-sections.
tracescaleaddmac in1 = infile1 in2 = infile2 out = outfile ntr = 800 nt = 5501 ratio12 = 1
tracescaleaddmac in 1 = infile 1 in 2 = infile 2 out = outfile ntr = 800 nt = 5501 ratio 12 = 1
tracescaleaddmac in 1 = infile 1 in 2 = infile 2 out = outfile ntr = 800 nt = 5501 ratio 12 = 1
## Drop extra section (un-used).
seispickalt_2015 in = infile nx = 800 nx1 = 80 nx2 = 400 nt = 5501 nt1 = 1 nt2 = 5501
## Plot.
suaddhead < infile ns = 5501 \mid \ 
sushw key = dt a = 20000 > \
outfile.su
```

suop < infile.su | \

```
supswigp xcur = 1 wbox = 25 hbox = 5 style = seismic \
nbpi = 300 linewidth = 0 \
title = "Line_E_migrated" \
label1 = "Time (s)" labelsize = 9 n2tic = 2 xbeg = -0.2 \
xend = 1 interp = 1 n1tic = 5 titlesize = 8 key = offset > \
outfile.su.ps
```

APPENDIX C

SUPPLEMENTAL MATERIAL

SESAME Station Locations / Offsets

Line-D

Station #	Latitude (degrees)	Longitude (degrees)	Cumulative distance (km) from furthest west station (plus 100 km)
22	35.4629	-84.4588	100
21	35.1997	-84.1369	129.2011621
20	35.074	-83.9803	143.1467088
19	34.8721	-83.7338	165.5455132
18	34.7342	-83.6121	180.8437233
17	34.6044	-83.4507	195.2430269
15	34.4498	-83.2799	212.3931067
14	34.3765	-83.1811	220.5242669
13	34.2943	-83.1662	229.642587
12	34.2462	-83.0333	234.9781895
11	34.1565	-82.9731	244.9282551
10	34.0917	-82.9032	252.1161717
9	34.0448	-82.8278	257.3184899
8	33.9938	-82.7566	262.9755499
7	33.9376	-82.6864	269.2093537
6	33.859	-82.6304	277.9277098
5	33.7915	-82.5159	285.4147587
4	33.7301	-82.4518	292.225129
3	33.6594	-82.3884	300.0669535
2	33.6041	-82.2828	306.2005951

Line-W

Station #	Latitude (degrees)	Longitude (degrees)	Cumulative distance (km) from furthest north station (plus 100 km)	
35	34.9762	-83.9438	100	
34	34.8376	-83.9204	115.3761288	
33	34.6547	-83.886	135.666313	
32	34.4657	-83.8658	156.6325659	
315	34.1779	-83.8531	188.5577087	
31	33.9722	-83.7385	211.3747248	
30	33.7318	-83.9128	238.0398273	
29	33.4568	-83.7288	268.5414777	
28	33.1856	-83.8999	298.6203237	
27	32.9174	-83.9234	328.3651484	
23N	32.5234	-83.886	372.0595553	
22	32.4492	-83.8973	380.2879915	
21	32.404	-83.8587	385.3004144	
20	32.3665	-83.9198	389.4589238	
19	32.3132	-83.9064	395.3695093	
18	32.2725	-83.9017	399.882812	
16	32.1794	-83.8841	410.2067439	
15A	32.138	-83.8985	414.7975734	
14N	32.0938	-83.8987	419.6988606	
13	32.055	-83.8933	424.0013198	
12	32.0095	-83.8885	429.0466958	
11N	31.9587	-83.9083	434.6797322	
10N	31.9025	-83.8937	440.9115033	
9	31.8051	-83.8981	451.7116308	
8	31.7165	-83.886	461.5358331	
7	31.611	-83.911	473.2337738	
6	31.4486	-83.895	491.2404629	
5	31.2724	-83.8978	510.7767602	
4	31.0831	-83.8952	531.7649316	
3	30.8635	-83.8864	556.1117683	
2	30.5774	-83.8902	587.8301556	
1	30.2017	-83.9109	629.4799015	

Line-E

Station # Latitude (degrees) Longitude (degrees) Cumulative distance (km) from furthest north station (plus 100 km) 31 32.9866 -82.107 100 30 32.6958 -82.1091 132.2501995 29 32.4908 -82.1032 154.9841372 28 32.3359 -82.0967 172.1616303 27 32.2362 -82.1091 183.2175466 26 32.0979 -82.0991 198.5535989 25 31.9918 -82.1135 210.3187739 24 31.9445 -82.097 215.5636942 23 31.8887 -82.0737 221.7510974 22R 31.4477 -82.0899 226.2973626 21 31.738 -82.071 238.46125 20 31.6967 -82.0796 243.0406719 19 31.6177 82.1113 251.8002583 18 31.5665 -82.0996 257.4772994 17 31.5016 -82.0986 264.673327 15 31.3632 -82.0				Cumulative distance		
Closeries Closeries Station (plus 100 km)	Station #		_			
31 32.9866 -82.107 100 30 32.6958 -82.1091 132.2501995 29 32.4908 -82.1032 154.9841372 28 32.3359 -82.0967 172.1616303 27 32.2362 -82.1091 183.2175466 26 32.0979 -82.0991 198.5535989 25 31.9918 -82.1135 210.3187739 24 31.9445 -82.097 215.5636942 23 31.8887 -82.0737 221.7510974 22R 31.8477 -82.0899 226.2973626 21 31.738 -82.071 238.46125 20 31.6967 -82.0796 243.0406719 19 31.6177 82.1113 251.8002583 18 31.5665 -82.0996 257.4772994 17 31.5016 -82.0986 264.673327 15 31.3632 -82.0999 280.0186953 13 31.223 -82.0999 280.0186953 13			(degrees)			
30 32.6958 -82.1091 132.2501995 29 32.4908 -82.1032 154.9841372 28 32.3359 -82.0967 172.1616303 27 32.2362 -82.1091 183.2175466 26 32.0979 -82.0991 198.5535989 25 31.9918 -82.1135 210.3187739 24 31.9445 -82.097 215.5636942 23 31.8887 -82.0737 221.7510974 22R 31.8477 -82.0899 226.2973626 21 31.738 -82.071 238.46125 20 31.6967 -82.0796 243.0406719 19 31.6177 82.1113 251.8002583 18 31.5665 -82.0996 257.4772994 17 31.5016 -82.0986 264.673327 16 31.4505 -82.1299 270.3391772 15 31.3632 -82.0969 280.0186953 13 31.223 -82.088 301.0736867 11	31	32.9866	-82.107	*		
29 32.4908 -82.1032 154.9841372 28 32.3359 -82.0967 172.1616303 27 32.2362 -82.1091 183.2175466 26 32.0979 -82.0991 198.5535989 25 31.9918 -82.1135 210.3187739 24 31.9445 -82.097 215.5636942 23 31.8887 -82.0737 221.7510974 22R 31.8477 -82.0899 226.2973626 21 31.738 -82.071 238.46125 20 31.6967 -82.0796 243.0406719 19 31.6177 82.1113 251.8002583 18 31.5665 -82.0996 257.4772994 17 31.5016 -82.0986 264.673327 16 31.4505 -82.1299 270.3391772 15 31.3632 -82.0969 280.0186953 13 31.223 -82.0919 295.5633041 12 31.1733 -82.088 301.0736867 11						
28 32.3359 -82.0967 172.1616303 27 32.2362 -82.1091 183.2175466 26 32.0979 -82.0991 198.5535989 25 31.9918 -82.1135 210.3187739 24 31.9445 -82.097 215.5636942 23 31.8887 -82.0737 221.7510974 22R 31.8477 -82.0899 226.2973626 21 31.738 -82.071 238.46125 20 31.6967 -82.0796 243.0406719 19 31.6177 82.1113 251.8002583 18 31.5665 -82.0996 257.4772994 17 31.5016 -82.0986 264.673327 16 31.4505 -82.1299 270.3391772 15 31.3632 -82.0969 280.0186953 13 31.223 -82.0919 295.5633041 12 31.1733 -82.088 301.0736867 11 31.0673 -82.1019 308.3801443 10						
27 32.2362 -82.1091 183.2175466 26 32.0979 -82.0991 198.5535989 25 31.9918 -82.1135 210.3187739 24 31.9445 -82.097 215.5636942 23 31.8887 -82.0737 221.7510974 22R 31.8477 -82.0899 226.2973626 21 31.738 -82.071 238.46125 20 31.6967 -82.0796 243.0406719 19 31.6177 82.1113 251.8002583 18 31.5665 -82.0996 257.4772994 17 31.5016 -82.0986 264.673327 16 31.4505 -82.1299 270.3391772 15 31.3632 -82.0969 280.0186953 13 31.223 -82.0919 295.5633041 12 31.1733 -82.088 301.0736867 11 31.0673 -82.1019 308.3801443 10 31.0673 -82.1013 312.8260706 9						
26 32.0979 -82.0991 198.5535989 25 31.9918 -82.1135 210.3187739 24 31.9445 -82.097 215.5636942 23 31.8887 -82.0737 221.7510974 22R 31.8477 -82.0899 226.2973626 21 31.738 -82.071 238.46125 20 31.6967 -82.0796 243.0406719 19 31.6177 82.1113 251.8002583 18 31.5665 -82.0996 257.4772994 17 31.5016 -82.0986 264.673327 16 31.4505 -82.1299 270.3391772 15 31.3632 -82.0969 280.0186953 13 31.223 -82.0919 295.5633041 12 31.1733 -82.088 301.0736867 11 31.1074 -82.1019 308.3801443 10 31.0673 -82.1013 312.8260706 9 30.9839 -82.0717 338.1595619 7						
25 31.9918 -82.1135 210.3187739 24 31.9445 -82.097 215.5636942 23 31.8887 -82.0737 221.7510974 22R 31.8477 -82.0899 226.2973626 21 31.738 -82.071 238.46125 20 31.6967 -82.0796 243.0406719 19 31.6177 82.1113 251.8002583 18 31.5665 -82.0996 257.4772994 17 31.5016 -82.0986 264.673327 16 31.4505 -82.1299 270.3391772 15 31.3632 -82.0969 280.0186953 13 31.223 -82.0919 295.5633041 12 31.1733 -82.088 301.0736867 11 31.1074 -82.1019 308.3801443 10 31.0673 -82.1013 312.8260706 9 30.9839 -82.0717 338.1595619 7 30.718 -82.0979 351.5521357 6						
24 31.9445 -82.097 215.5636942 23 31.8887 -82.0737 221.7510974 22R 31.8477 -82.0899 226.2973626 21 31.738 -82.071 238.46125 20 31.6967 -82.0796 243.0406719 19 31.6177 82.1113 251.8002583 18 31.5665 -82.0996 257.4772994 17 31.5016 -82.0986 264.673327 16 31.4505 -82.1299 270.3391772 15 31.3632 -82.0969 280.0186953 13 31.223 -82.0919 295.5633041 12 31.1733 -82.088 301.0736867 11 31.1074 -82.1019 308.3801443 10 31.0673 -82.1013 312.8260706 9 30.9839 -82.0742 322.0726217 8 30.8388 -82.0717 338.1595619 7 30.718 -82.0979 351.5521357 6	25	31.9918				
23 31.8887 -82.0737 221.7510974 22R 31.8477 -82.0899 226.2973626 21 31.738 -82.071 238.46125 20 31.6967 -82.0796 243.0406719 19 31.6177 82.1113 251.8002583 18 31.5665 -82.0996 257.4772994 17 31.5016 -82.0986 264.673327 16 31.4505 -82.1299 270.3391772 15 31.3632 -82.0969 280.0186953 13 31.223 -82.0919 295.5633041 12 31.1733 -82.088 301.0736867 11 31.1074 -82.1019 308.3801443 10 31.0673 -82.1013 312.8260706 9 30.9839 -82.0742 322.0726217 8 30.8388 -82.0717 338.1595619 7 30.718 -82.0979 351.5521357 6 30.5853 -82.0999 366.2637235 5	24	31.9445	-82.097			
21 31.738 -82.071 238.46125 20 31.6967 -82.0796 243.0406719 19 31.6177 82.1113 251.8002583 18 31.5665 -82.0996 257.4772994 17 31.5016 -82.0986 264.673327 16 31.4505 -82.1299 270.3391772 15 31.3632 -82.0969 280.0186953 13 31.223 -82.0919 295.5633041 12 31.1733 -82.088 301.0736867 11 31.1074 -82.1019 308.3801443 10 31.0673 -82.1013 312.8260706 9 30.9839 -82.0742 322.0726217 8 30.8388 -82.0717 338.1595619 7 30.718 -82.0979 351.5521357 6 30.5853 -82.0999 366.2637235 5 30.3617 -82.1176 391.0521258 4 30.0271 -82.1095 428.1444573 3	23	31.8887	-82.0737			
20 31.6967 -82.0796 243.0406719 19 31.6177 82.1113 251.8002583 18 31.5665 -82.0996 257.4772994 17 31.5016 -82.0986 264.673327 16 31.4505 -82.1299 270.3391772 15 31.3632 -82.0969 280.0186953 13 31.223 -82.0919 295.5633041 12 31.1733 -82.088 301.0736867 11 31.1074 -82.1019 308.3801443 10 31.0673 -82.1013 312.8260706 9 30.9839 -82.0742 322.0726217 8 30.8388 -82.0717 338.1595619 7 30.718 -82.0979 351.5521357 6 30.5853 -82.0999 366.2637235 5 30.3617 -82.1176 391.0521258 4 30.0271 -82.1095 428.1444573 3 29.8296 -82.1318 450.0375793 2	22R	31.8477	-82.0899	226.2973626		
19 31.6177 82.1113 251.8002583 18 31.5665 -82.0996 257.4772994 17 31.5016 -82.0986 264.673327 16 31.4505 -82.1299 270.3391772 15 31.3632 -82.0969 280.0186953 13 31.223 -82.0919 295.5633041 12 31.1733 -82.088 301.0736867 11 31.1074 -82.1019 308.3801443 10 31.0673 -82.1013 312.8260706 9 30.9839 -82.0742 322.0726217 8 30.8388 -82.0717 338.1595619 7 30.718 -82.0979 351.5521357 6 30.5853 -82.0999 366.2637235 5 30.3617 -82.1176 391.0521258 4 30.0271 -82.1095 428.1444573 3 29.8296 -82.1318 450.0375793 2 29.443 -82.0674 492.8907804	21	31.738	-82.071	238.46125		
18 31.5665 -82.0996 257.4772994 17 31.5016 -82.0986 264.673327 16 31.4505 -82.1299 270.3391772 15 31.3632 -82.0969 280.0186953 13 31.223 -82.0919 295.5633041 12 31.1733 -82.088 301.0736867 11 31.1074 -82.1019 308.3801443 10 31.0673 -82.1013 312.8260706 9 30.9839 -82.0742 322.0726217 8 30.8388 -82.0717 338.1595619 7 30.718 -82.0979 351.5521357 6 30.5853 -82.0999 366.2637235 5 30.3617 -82.1176 391.0521258 4 30.0271 -82.1095 428.1444573 3 29.8296 -82.1318 450.0375793 2 29.443 -82.0674 492.8907804	20	31.6967	-82.0796	243.0406719		
17 31.5016 -82.0986 264.673327 16 31.4505 -82.1299 270.3391772 15 31.3632 -82.0969 280.0186953 13 31.223 -82.0919 295.5633041 12 31.1733 -82.088 301.0736867 11 31.1074 -82.1019 308.3801443 10 31.0673 -82.1013 312.8260706 9 30.9839 -82.0742 322.0726217 8 30.8388 -82.0717 338.1595619 7 30.718 -82.0979 351.5521357 6 30.5853 -82.0999 366.2637235 5 30.3617 -82.1176 391.0521258 4 30.0271 -82.1095 428.1444573 3 29.8296 -82.1318 450.0375793 2 29.443 -82.0674 492.8907804	19	31.6177	82.1113	251.8002583		
16 31.4505 -82.1299 270.3391772 15 31.3632 -82.0969 280.0186953 13 31.223 -82.0919 295.5633041 12 31.1733 -82.088 301.0736867 11 31.1074 -82.1019 308.3801443 10 31.0673 -82.1013 312.8260706 9 30.9839 -82.0742 322.0726217 8 30.8388 -82.0717 338.1595619 7 30.718 -82.0979 351.5521357 6 30.5853 -82.0999 366.2637235 5 30.3617 -82.1176 391.0521258 4 30.0271 -82.1095 428.1444573 3 29.8296 -82.1318 450.0375793 2 29.443 -82.0674 492.8907804	18	31.5665	-82.0996	257.4772994		
15 31.3632 -82.0969 280.0186953 13 31.223 -82.0919 295.5633041 12 31.1733 -82.088 301.0736867 11 31.1074 -82.1019 308.3801443 10 31.0673 -82.1013 312.8260706 9 30.9839 -82.0742 322.0726217 8 30.8388 -82.0717 338.1595619 7 30.718 -82.0979 351.5521357 6 30.5853 -82.0999 366.2637235 5 30.3617 -82.1176 391.0521258 4 30.0271 -82.1095 428.1444573 3 29.8296 -82.1318 450.0375793 2 29.443 -82.0674 492.8907804	17	31.5016	-82.0986	264.673327		
13 31.223 -82.0919 295.5633041 12 31.1733 -82.088 301.0736867 11 31.1074 -82.1019 308.3801443 10 31.0673 -82.1013 312.8260706 9 30.9839 -82.0742 322.0726217 8 30.8388 -82.0717 338.1595619 7 30.718 -82.0979 351.5521357 6 30.5853 -82.0999 366.2637235 5 30.3617 -82.1176 391.0521258 4 30.0271 -82.1095 428.1444573 3 29.8296 -82.1318 450.0375793 2 29.443 -82.0674 492.8907804	16	31.4505	-82.1299	270.3391772		
12 31.1733 -82.088 301.0736867 11 31.1074 -82.1019 308.3801443 10 31.0673 -82.1013 312.8260706 9 30.9839 -82.0742 322.0726217 8 30.8388 -82.0717 338.1595619 7 30.718 -82.0979 351.5521357 6 30.5853 -82.0999 366.2637235 5 30.3617 -82.1176 391.0521258 4 30.0271 -82.1095 428.1444573 3 29.8296 -82.1318 450.0375793 2 29.443 -82.0674 492.8907804	15	31.3632	-82.0969	280.0186953		
11 31.1074 -82.1019 308.3801443 10 31.0673 -82.1013 312.8260706 9 30.9839 -82.0742 322.0726217 8 30.8388 -82.0717 338.1595619 7 30.718 -82.0979 351.5521357 6 30.5853 -82.0999 366.2637235 5 30.3617 -82.1176 391.0521258 4 30.0271 -82.1095 428.1444573 3 29.8296 -82.1318 450.0375793 2 29.443 -82.0674 492.8907804	13	31.223	-82.0919	295.5633041		
10 31.0673 -82.1013 312.8260706 9 30.9839 -82.0742 322.0726217 8 30.8388 -82.0717 338.1595619 7 30.718 -82.0979 351.5521357 6 30.5853 -82.0999 366.2637235 5 30.3617 -82.1176 391.0521258 4 30.0271 -82.1095 428.1444573 3 29.8296 -82.1318 450.0375793 2 29.443 -82.0674 492.8907804	12	31.1733	-82.088	301.0736867		
9 30.9839 -82.0742 322.0726217 8 30.8388 -82.0717 338.1595619 7 30.718 -82.0979 351.5521357 6 30.5853 -82.0999 366.2637235 5 30.3617 -82.1176 391.0521258 4 30.0271 -82.1095 428.1444573 3 29.8296 -82.1318 450.0375793 2 29.443 -82.0674 492.8907804	11	31.1074	-82.1019	308.3801443		
8 30.8388 -82.0717 338.1595619 7 30.718 -82.0979 351.5521357 6 30.5853 -82.0999 366.2637235 5 30.3617 -82.1176 391.0521258 4 30.0271 -82.1095 428.1444573 3 29.8296 -82.1318 450.0375793 2 29.443 -82.0674 492.8907804	10	31.0673	-82.1013	312.8260706		
7 30.718 -82.0979 351.5521357 6 30.5853 -82.0999 366.2637235 5 30.3617 -82.1176 391.0521258 4 30.0271 -82.1095 428.1444573 3 29.8296 -82.1318 450.0375793 2 29.443 -82.0674 492.8907804	9	30.9839	-82.0742	322.0726217		
6 30.5853 -82.0999 366.2637235 5 30.3617 -82.1176 391.0521258 4 30.0271 -82.1095 428.1444573 3 29.8296 -82.1318 450.0375793 2 29.443 -82.0674 492.8907804	8	30.8388	-82.0717	338.1595619		
5 30.3617 -82.1176 391.0521258 4 30.0271 -82.1095 428.1444573 3 29.8296 -82.1318 450.0375793 2 29.443 -82.0674 492.8907804		30.718	-82.0979	351.5521357		
4 30.0271 -82.1095 428.1444573 3 29.8296 -82.1318 450.0375793 2 29.443 -82.0674 492.8907804	6	30.5853	-82.0999			
3 29.8296 -82.1318 450.0375793 2 29.443 -82.0674 492.8907804	5	30.3617	-82.1176	391.0521258		
2 29.443 -82.0674 492.8907804	4	30.0271	-82.1095	428.1444573		
	3	29.8296	-82.1318	450.0375793		
1 29.2116 -82.0545 518.5394341	2	29.443	-82.0674	492.8907804		
	1	29.2116	-82.0545	518.5394341		

2-D Slant Stack Depth Migration Velocity Models

Line-W

Layer #	Slowness (s/km)	Depth to bottom of layer (km)
1	0.416667	1.2
2	0.25	5.2
3	0.166667	8.18
4	0.163676	11.16
5	0.160791	14.14
6	0.158006	17.12
7	0.155316	20.1
8	0.152716	23.08
9	0.150201	26.06
10	0.147768	29.04
11	0.145413	32.02
12	0.143131	35
13	0.120482	200

Line-E

Layer #	Slowness (s/km)	Depth to bottom of layer (km	
1	0.416667	1.2	
2	0.166667	4.18	
3	0.163676	7.16	
4	0.160791	10.14	
5	0.158006	13.12	
6	0.155316	16.1	
7	0.152716	19.08	
8	0.150201	22.06	
9	0.147768	25.04	
10	0.145413	28.02	
11	0.143131	31	
12	0.120482	200	

Earthquake Event Information

<u>2014-01-25</u>

Origin Time (UT)	Latitude (degrees)	Longitude (degrees)	Depth (km)	Magnitude (Mw)	Back-Azimuth (degrees)	Distance (degrees)	Ray Parameter (PKIKP in s/km)
05:09:16.25	-7.9855	109.2653	66	6.1	Line-D (d03-d22):	Line-D (d03-d22):	Line-D (d03-d22):
03.09.10.23	-7.3633	109.2033	00	0.1	332.061 - 334.531	149.89 - 152.27	0.0141 - 0.0131
					Line-E (e01-e31):	Line-E (e01-e31):	Line-E (e01-e31):
					331.012 - 334.539	156.35 - 152.98	0.0131 - 0.0124
					Line-W (w01-w35):	Line-W (w01-w35):	Line-W (w01-w35):
					328.135 - 332.616	154.68 - 150.53	0.0131 - 0.0124